의학박사 학위논문

Fructose promotes breast cancer metastasis by inducing the KHK-A phosphorylation of YWHAH

과당에 의해 활성화되는 YWHAH에 대한 KHK-A의 인산화 기능이 유방암 전이를 촉진시키는 기전에 관한 연구

2021 년 2 월

서울대학교 대학원

의과학과 약리학전공

김 지 영

A thesis of the Degree of Doctor of Philosophy

Fructose promotes breast cancer metastasis by inducing the KHK-A phosphorylation of YWHAH

과당에 의해 활성화되는 YWHAH에 대한 KHK-A의 인산화 기능이 유방암 전이를 촉진시키는 기전에 관한 연구

February 2021

The Department of Biomedical Sciences,

Seoul National University

College of Medicine

Jiyoung Kim

Fructose promotes breast cancer metastasis by inducing the KHK-A phosphorylation of YWHAH

과당에 의해 활성화되는 YWHAH에 대한
KHK-A의 인산화 기능이 유방암 전이를 촉진
시키는 기전에 관한 연구

지도교수 박 종 완

이 논문을 의학박사 학위논문으로 제출함

2020년 10월

서울대학교 대학원
의과학과 약리학전공
김 지 영

김지영의 의학박사 학위논문을 인준함

2021년 1월

위 원 장 윤 홍 덕 (인)
부위원장 박 종 완 (인)
위 원 신 현 우 (인)
위 원 이 창 한 (인)
위 원 강 인 산 (인)

Fructose promotes breast cancer metastasis by inducing the KHK-A phosphorylation of YWHAH

by

Jiyoung Kim

A thesis submitted to the Department of Biomedical Science in partial fulfillment of the requirements for the Degree of Doctor of Philosophy in Biomedical Science at Seoul National University College of Medicine

October 2020

Approved by Thesis Committee:

January 2021

Professor Hong-Duk Youn Chairman

Professor Sang-Nam Park Vice chairman

Professor Hyun-Woo Shin

Professor Chang Han Lee

Professor In-San Kim

Abstract

Fructose promotes breast cancer metastasis by inducing the KHK-A phosphorylation of YWHAH

Jiyoung Kim

The Department of Biomedical Sciences

The graduate School

Seoul National University

Harmful effects of high fructose intake on health have been widely reported in epidemiological and laboratory studies. Although it has been reported that fructose promotes cancer development and progression, little is known about the underlying molecular mechanisms. Here, I found that fructose triggers breast cancer metastasis through the ketohexokinase-A signaling pathway. Molecular experiments showed that ketohexokinase-A, rather than ketohexokinase-C, is necessary and sufficient for fructose-induced cell invasion. An orthotopic xenograft experiment revealed that ketohexokinase-A-overexpressing breast cancer is highly metastatic in fructose-fed mice. Mechanistically, ketohexokinase-A moves from the cytoplasm to the nucleus during fructose stimulation, which is mediated by the nuclear importers

LRRC59 and KPNB1. In the nucleus, ketohexokinase-A phosphorylates YWHAH at Ser25 and, in turn, YWHAH recruits SLUG to the *CDH1* promoter, which weakens cell adhesion and triggers cell migration. This study provides a new insight into the effect of nutrition on breast cancer metastasis. High intake of fructose should be restricted in cancer patients to reduce the risk of metastasis. From a therapeutic perspective, the ketohexokinase-A signaling pathway could be a potential target to prevent cancer metastasis.

.....

Key words: Breast cancer metastasis; fructose; ketohexokinase-A; nuclear translocation; serine kinase

Student number: 2014-25057

Contents

List of tables and figures

List of abbreviations

ALDOB: Aldolase B

ALOX12: 12-Lipoxygenase

CDH1: Cadherin-1

ChIP: Chromatin immunoprecipitation

EMT: Epithelial-mesenchymal transition

GFP: Green fluorescent protein

GLOD4: Glyoxalase domain-containing protein 4

H&E: Hematoxylin and Eosin

HIF: Hypoxia inducible factor

IHC: Immunohistochemistry

IP: Immunoprecipitation

IRES: Internal ribosome entry site

KHK: Ketohexokinase

KPNB1: Karyopherin subunit beta 1

LRRC59: Leucine-rich repeat-containing protein 59

Luc: Luciferase

MD: Molecular dynamics

ODDD: Oxygen-dependent degradation domain

PCR: Polymerase chain reaction

PMF: Potential mean force

PRIDE: Proteomics Identifications database

PRPS1: Phosphoribosyl pyrophosphate synthetase 1

Pypy: Pyrimidinopyrimidine

ROI: Region of interest

ROS: Reactive oxygen species

SDs: Standard deviations

TCGA: The cancer genome atlas

YWHAH: Tyrosine 3-Monooxygenase/Tryptophan 5-monooxygenase activation protein Eta

INTRODUCTION

Fructose naturally occurs in fruits and is a popular sweetener for cooking and baking[1]. Many reports have warned against excessive intake of fructose because it aggravates obesity, diabetes, and hepatic steatosis[2, 3, 4]. Aside from metabolic disorders, high consumption of fructose is associated with high risks of endometrial[5], breast[6], esophageal[7], small intestine[7], pleural[7], and colorectal cancers[8]. Fructose-induced carcinogenesis is considered to be attributed to altered energy metabolism, increased oxidative stress, and inflammation[9, 10, 11].

Glucose provides energy and intermediate metabolites required for amino acid and nucleic acid syntheses. The metabolism of cancer cells is reprogrammed to consume large quantities of glucose, resulting in glucose depletion in tumor microenvironments. To compensate for insufficient glucose, cancer cells use fructose as an alternative energy source. For instance, the fructose flux is increased in pancreatic cancer cells, which accelerates nucleic acid synthesis through the non-oxidative pentose phosphate pathway[12]. Besides cell proliferation, fructose is also associated with cancer metastasis. Fructose promotes colon cancer metastasis toward the liver via the ketohexokinase–aldolase B pathway[9]. In other cancers, fructose has been also reported to increase metastatic potential[13, 14, 15, 16]. However, the precise mechanism underlying the metastogenic action of fructose remains unclear.

Ketohexokinase (KHK) is the enzyme that converts fructose to fructose-1-phosphate at the rate-limiting first step of fructose metabolism. The *KHK* gene expresses two isoforms, KHK-A and KHK-C, resulting from alternative splicing of exon 3 (Figure 1). KHK-C, which is exclusively expressed in a few tissues, including the liver, drives the aforementioned metabolism. Conversely, KHK-A is not believed to contribute to this metabolism because its enzymatic function is very low at the physiological level of fructose.

The overall structure of the KHK-A is similar to the KHK-C subunit. Superposition of the exon 3a or -3c corresponding structural domains (the central α/β-fold or the extended four-stranded β-sheet) between two isoforms shows similar conformation in main chains except relative orientation of the exon 3 specific secondary structure (Figure 2)[17]. It is known that the enzyme activity against fructose differs depending on the isoforms (KHK-C Km = 0.8 Mm; KHK-A Km = 8 Mm). However, fructose binding sites are independent of the exon3.

The KHK-C-driven fructose metabolism has been strongly suggested as a pathologic pathway that exacerbates obesity, diabetes, metabolic disorders or even in cancer. On the contrary, KHK-A suggested as slow metabolizer of fructose in tissues that do not express KHK-C. The KHK-A knock-out mice showed severe metabolic syndrome compare to WT mice[18], also in AldoB knock-out mice[19], suggesting that KHK-A plays a protective role in the fructose-mediated metabolic disorders. However, KHK-A is ubiquitously

expressed in most tissues, KHK-A is believed to have some biological functions other than energy metabolism[20, 21].

Recently, an interesting role of KHK-A was reported in hepatocellular carcinoma. c-Myc-induced KHK-A facilitates nucleic acid synthesis by directly phosphorylating phosphoribosyl pyrophosphate synthetase 1 (PRPS1), thereby promoting cell proliferation[22]. Considering its role as a protein kinase, KHK-A is expected to participate in diverse signaling pathways, which remain to be explored.

Breast cancer cells highly express the fructose transporter GLUT5[23], and metastasize in response to high fructose[16]. However, little is known about the molecular mechanism underlying fructose-induced metastasis in breast cancer. Herein, I tested the possibility that KHK-A mediates breast cancer metastasis in response to fructose. Upon fructose stimulation, LRRC59, in concert with KPNB1, transported KHK-A to the nucleus, where KHK-A phosphorylated YWHAH at Ser25. Phosphorylated YWHAH promoted SLUG to repress the *CDH1* gene, thereby leading to cell invasion in breast cancer. This work provides the molecular mechanism underlying fructose-induced cancer metastasis.

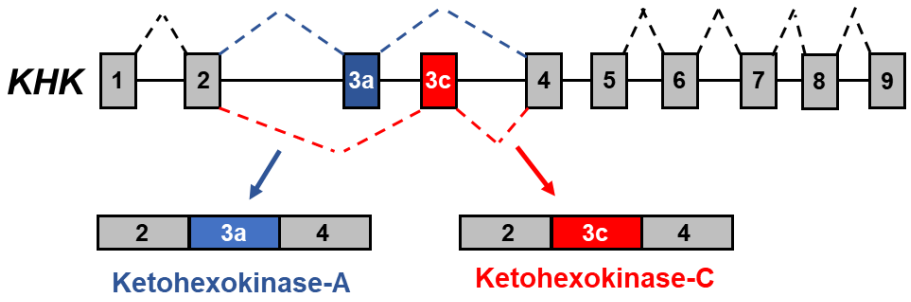

Figure 1. Schematic diagram of alternative splicing of *KHK*

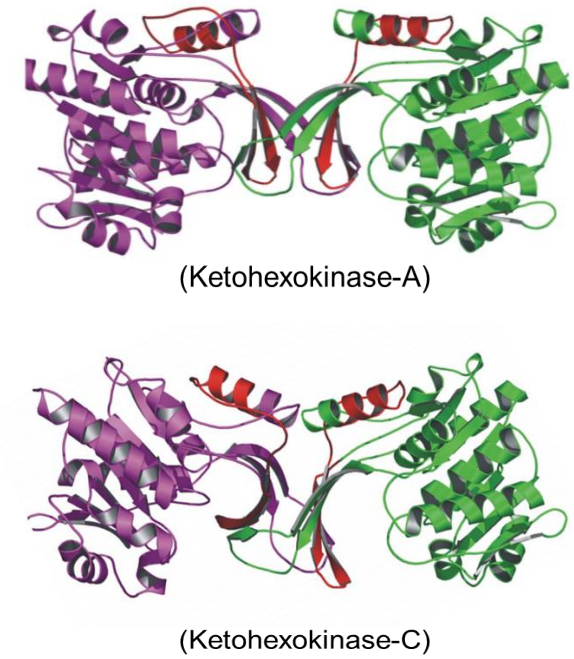

Figure 2. Structure of Ketohexokinase-A and -C. Ribbon diagrams of KHK-A (upper panel), and KHK-C (lower panel). Exon 3-specific secondary structure (aa 72 to 115) shown in red.

MATERIALS AND METHODS

Cell lines and Cell culture

Human breast cancer (MDA-MB-231 and MCF-7), embryonic kidney (HEK293T), glioblastoma (U87 and U251), lung adenocarcinoma (H1299 and A549), colon cancer (HCT116, and DLD-1), renal cancer (786O and RCC4), cervical cancer (SiHa and HeLa), ovarian cancer (SKOV3), bone cancer (U2OS), hepatocellular carcinoma (HepG2, and Hep3B) cell lines were obtained from American Type Culture Collection (ATCC; Manassas, VA); human pancreatic cancer (MIApaca2 and PanC1), human prostate cancer (PC3 and DU145) and mouse breast cancer (MTV-TM-011) cell lines from Korean Cell Line Bank (Seoul, Korea). MDA-MB-231, MCF-7, MTV-TM-011, U251, H1299, A549, DU145, PC3, 786O, RCC4, HeLa, SKOV3, U2OS, and Hep3B were cultured in RPMI1640; U87 and HepG2 in MEM; HEK293T, MIApaca2, PanC1, DLD-1, HCT116, and SiHa in DMEM, which were supplemented with 10% heat-inactivated FBS. Mycoplasma contamination was routinely checked when cell growth or shape was altered. After thawing, cells were usually cultured for no more than 3 months. Cells were grown in a humidified atmosphere containing 5% CO_2 at 37^{o}C. Luciferase-expressing, luciferase/KHK-A, and luciferase/KHK-C-co-expressing MCF-7, MDA-MB-231, and MTV-TM-011 stable cell lines were established from G418-resistant clones for each one.

Antibodies and reagents

A ketohexokinase inhibitor Pypy (420640) was purchased from Millipore (Burlington, MA). Culture media, FBS, D-fructose (F3510), D-glucose (G7021), and anti-FLAG antibody (F7425, 1:5000 dilution) were purchased from Sigma-Aldrich (St. Louis, MO). Antibodies against KHK (sc-377411, 1:500), Slug (sc-166476, 1:1000), N-cadherin (sc-7939, 1:1000), Vimentin (sc-7558, 1:1000), ZEB-1 (sc-25388, 1:1000), β-tubulin (sc-9104, 1:5000), GST-tag (sc-138, 1:1000), PRPS1/2 (sc100288, 1:1000), Aldolase B (sc393278, 1:1000) and Lamin-B (sc-6216, 1:1000) were purchased from Santa Cruz Biotechnology (Santa Cruz, CA); antibodies against Importin-β (ab2811, 1:1000), α-SMA (ab7817, 1:1000), TWIST (ab50581, 1:1000) and Snail (ab53519, 1:1000) from Abcam (Cambridge, UK); antibodies against YWHAH (9640, 1:1000), Myc-tag (2278, 1:1000), GFP (2555,1:1000), and SQSTM1/p62 (5114T, 1:1000) from Cell Signaling Technology (Danvers, MA); antibodies against phosphor-serine/threonine (PP2551, 1:1000) and phosphor-tyrosine (PP2221, 1:1000) from ECM biosciences (Versailles, KY); antibodies against LRRC59 (NBP1-93953, 1:1000) and 12-lipoxygenase (NBP1-90338, 1:1000) were from Novus Biologicals (Littleton, CO); isotype-specific antibodies against KHK-A (21708-2, 1:1000) and KHK-C (21709-2, 1:1000) from Signalway Antibody LLC (Pearland, TX, USA); antibodies against His(6)-tag (PM032, 1:1,000) from MBL (Nagoya, Japan). HRP-conjugated rabbit anti-goat (81-1620, 1:5000), anti-E-cadherin (131700,

1:1000), and SQSTM1/p62 phospho-Ser28 (PA5-35409, 1:1000) antibodies from Thermo Fisher Scientific (Waltham,MA); HRP-conjugated goat anti-rabbit (G21234, 1:5,000) and HRP-conjugated goat anti-mouse (G21040, 1:5,000) from Invitrogen (Carlsbad, CA); anti-GLOD4 (GTX104484, 1:1000) from Genetex (San Antonio, TX). Anti-HIF-1α antibody (1:1000) was raised in rabbits against the ODDD peptide (aa. 418-698) of human HIF-1α[24].

. A monoclonal antibody against S25-phosphorylated YWHAH was raised using a phage display technology through a commercial facility (Bioneer, Daejoen, South Korea). The synthetic peptides (RYDDMASAMKAVTE and RYDDMA(p)SAMKAVTE) were purchased from GL Biochem (Shanghai, China) and conjugated with bovine serum albumin to be used as antigens.

Preparation of plasmids, siRNAs and transfection

The cDNAs for human *KHK-A* (NM_000221), human *KHK-C* (NM_006488), human *LRRC59* (NM_018509) and human *YWHAH* (also known as 14-3-3η; NM_003405) were cloned by RT-PCR using Pfu DNA polymerase and inserted into pcDNA-Myc, pcDNA-FLAG, pcDNA-GFP, pcDNA-His(6), CMV-luciferase/IRES, or pGEX plasmids using blunt-end ligation. The mutations of KHK-A and YWHAH were performed using PCR-based mutagenesis. The kinase-defective KHK-A (KHK-A-dATP) was constructed by deleting a.a. 255-260. The E-cadherin plasmid was purchased from Addgene

(#47502; Cambridge, MA). For transient transfection of plasmids or siRNAs, cells at ~70% confluence were transfected using Lipofectamine 3000 (for plasmid) or Lipofectamine RNAiMAX (for siRNA), respectively. The transfected cells were stabilized for 48 hr before being used in experiments. Nucleotide sequences of siRNAs are summarized in Table 1.

Table 1. Nucleotide sequences of siRNAs

siRNA		Sequence
Pan	Control	5'- AUGAACGUGAAUUGCUCAATT -3'
human	KHK-A	5'- GUCAUCAUCAACGAGGCCAGUGGTA -3'
human	KHK-C	5'- CCAAUGGCAACCGUACCAUUGUGCT -3'
human	PRPS1	5'- CAAUGGAGAAUCCGUUUCUUACCTA -3'
human	ALDOB	5'- CUUGCUAGUCAUUGGAAUCAAGCCG -3'
human	ALOX12	5'- GAUCCAGUAUCACUUGCUGAACACT -3'
human	GLOD4	5'- GACUACAAGCUUGGCAAUGACUUTA -3'
human	YWHAH	5'- ACAGUGUGGUCGAAGCUUCUGAAGC -3'
human	YWHAH (3'UTR)	5'- GUUUUGGAAUUCAAUGGGUAAAUAA -3'
mouse	Ywhah	5'- CAAGAACUGCAAUGAUUUUCAGUAT -3'
mouse	Ywhah (3'UTR)	5'- GCAGUUUCAGAUAAACCUUCAUGGG -3'
human	LRRC59	5'- AAGCUAGACCUGAGUAAGAACAAGC -3'
human	KPNB1	5'- GAGGUGGCUUUACAAGGGAUAGAAT -3'
human	SNAI1	5'- CAACUGCAAAUACUGCAACAAGGAA -3'
mouse	Snai1	5'- ACAGUUUAUUGAUAUUCAAUAAAAT -3'
human	SNAI2	5'- ACUGAGUGACGCAAUCAAUGUUUAC -3'
mouse	Snai2	5'- UAUAUUUACUGACAGCUAGAUUGAA -3'

Establishment of stable cell lines with lentiviral vectors

Lentiviral vectors containing mouse *Khk-a*-silencing shRNAs were generated by GenePharma (Shanghai, China). Oligonucleotides were annealed and inserted into the shRNA expresseion vector pGLVU6/Puro. The shRNA sequences (Supplementary table 2) were designed to target the coding region of the mouse *Khk-a* (NM_001349066). The virus containing supernatant was harvested form HEK293T cells, centrifuged at 800x*g*, and filtered. The filtrates were incubated with Lentivuris Concentrator Solution containing PEG-8000 overnight at 4^{o}C. The filtrates were centrifuged at 1600x*g* for 60 min, and the viral pellet was re-suspended in PBS to be applied to MTV-TM/011 cells. The transfected cells were selected with 1 μg/mL of puromycin. To get stable cell lines for tumor grafting, several colonies of MTV-TM/011 were pooled. Nucleotide sequences of shRNAs are summarized in Table 2.

Table 2. Nucleotide sequences of shRNAs

shRNA	Sequence
Control	5'- TTCTCCGAACGTGTCACGT -3'
Khk-a	5'- GGACTTACGATATGTGGTCCT -3'

Breast cancer xenografts

All animal experiments were carried out with an approved protocol proposal from the Seoul University Institutional Animal Care and Use Committee (approval No. SNU-170721-1-5; 190712-2-1; 190819-1). MTV-TM-011 cell lines harboring the CMV luciferase-IRES-GFP plasmid or the CMV luciferase-IRES-KHK-A plasmid were selected with G418; CMV luciferase-IRES-GFP plasmid with sh-*Khk-a* (or sh-control), or the CMV luciferase-IRES-KHK-C plasmid with sh-*Khk-a* were selected with G418 and puromycin; CMV luciferase-IRES-GFP plasmid with His-YWHAH_WT or His-YWHAH_S25A were selected with G418 and Zeocin. These cells were implanted into lower right mammary fat pads of female mice (8 weeks old, Balb/cSlc-nu/nu). Tab water or 15% fructose (or glucose)-containing water was provided *ad libitum*. To get live images of tumors, mice were anaesthetized with isoflurane and injected intraperitoneally with 100 μL of the VivoGlo luciferin (40 mg/mL) solution (Promega, Madison, WI). After 10 min, images were acquired with the Xenogen IVIS 100 and analyzed using the LivingImage 2.50.1 software (Xenogen, Alameda, CA). Two weeks after implantation, the primary tumor growth was monitored thrice a week. When average primary tumor volumes were reached 500-600 mm^3, the primary tumors were removed and tumor metastasis was monitored for 3 weeks. Major vital organs (lung, liver, heart, spleen, brain, kidney, hind leg, and GI tract) were collected to identify tumor metastasis.

Cell invasion assay

To assess cell invasion, the Transwell chambers partitioned by a Matrigel-coated membrane with 8 μm pore size was used. Cells were seeded onto upper chambers in serum-free medium at a density of 2×10^4 (H1299, A549, and MDA-MB-231), 3×10^4 (U87, U251, DU145, DLD-1, HCT116, 786O, RCC4, SiHa, and HeLa), 4×10^4 (MCF7 and U2OS), 6×10^4 (MIApaca2, PanC1, and MTV-TM-011), or 7×10^4 (PC3 and HepG2) cells/well, an FBS-containing medium was placed in the lower chamber. After incubated for 18 hr, cells were fixed with 4% paraformaldehyde and stained with Hematoxylin and Eosin. Cells on upper side of the filters were removed with cotton-tipped swabs and invaded cells on the down side were viewed and photographed under BX53-P polarizing microscope (Olympus; Tokyo, Japan). The invaded cells were counted using the ImageJ software (NIH, Bethesda, MD).

Preparation of recombinant proteins

Recombinant GST-KHK-A, GST-YWHAH, and free GST proteins were expressed in *Escherichia coli* BL21 cells, pulled down using glutathione-affinity beads (GE Healthcare; Chicago, IL) at 4°C for 1 hr, and eluted with 10 mM reduced glutathione (Sigma-Aldrich). FLAG-LRRC59 and His(6)-KHK-A proteins were expressed in HEK293T cells, pulled down using EZview Red

anti-FLAG (Sigma-Aldrich) and nickel-NTA (Qiagen; Hilden, Germany) affinity beads at 4°C for 4 hr, and eluted with 500 ng/μL of FLAG peptide and 250 mM imidazole, respectively. The amounts and purities of proteins were checked by SDS-PAGE and Coomassie Brilliant Blue R-250 staining.

In vitro binding assay

The mixtures of purified His-KHK-A and FLAG-LRRC59 or GST-YWHAH were incubated in a binding buffer (25 mM HEPES/pH 7.5, 150 mM KCl, 12.5 mM $MgCl_2$, 0.5 mM DTT, 0.1% NP-40, and 10% glycerol) at 4°C for 1 hr with or without 1 mM fructose, and further incubated with nickel-NTA affinity beads at 4°C for 1 hr. After the beads were washed with the binding buffer, bound proteins were eluted in the denaturing SDS sample buffer and subjected to Western blotting.

In vitro kinase assay

Recombinant His-KHK-A (10 ng) or His-KHK-C (10 ng) and GST-YWHAH (500 ng) in 30 μL of the kinase buffer containing 50 mM Tris-HCl/pH 7.5, 100 mM KCl, 50 mM $MgCl_2$, 1 mM sodium orthovanadate, 1 mM DTT, 10% glycerol, and 2 mM ATP. The reactions were incubated at 37°C for 1 hr,

terminated by heating the samples in an SDS buffer. The protein phosphorylation was evaluated by Western blotting

Quantitative RT-PCR

Total RNAs were extracted using TRIZOL (Invitrogen; Carlsbad, CA), and reverse-transcribed at 42℃ for 60 min in a reaction mixture containing M-MLV Reverse Transcriptase (Enzynomics, Daejeon, Korea), RNase inhibitor, dNTP, and random primers. Real-time PCR was performed in the qPCR Mastermix (Enzynomics), and fluorescence emitting from dye-DNA complex was monitored in CFX Connect Real-Time Cycler (BIO-RAD, Hercules, CA). The mRNA values of targeted genes were normalized to GAPDH expression for each sample. All reactions were performed as triplicates. Primers used in real-time quantitative PCR were summarized in Table 3.

Table 3. Primers used in real-time quantitative PCR

Gene		Forward	Reverse
human	KHK-A_1	5'- TCATGGAAGAGAAGCAGATC -3'	5'- GGAGGTCATCCAGGACAAAA -3'
human	KHK-A_2	5'- TATTCTGTGGACCTACGCTA-3'	5'- CATAGTATAGGATGGTGCGG-3'
human	KHK-C_1	5'- TCATGGAAGAGAAGCAGATC -3'	5'- TGAAGTCGGCCACCAGGAAG -3'
human	KHK-C_2	5'- CATGTTGCTGACTTCCTGG-3'	5'- TTGGAGTTGTTGATGATGCA-3'
human	CDH1	5'- TCTGGATAGAGAACGCATTG -3'	5'- TGTTGTCATTCTGATCGGTT -3'
human	GAPDH	5'- GAGTCAACGGATTTGGTCGT -3'	5'- TTGATTTTGGAGGGATCTCG -3'
mouse	Cdh1	5'-AAGCAGCAATACATCCTTCA -3'	5- CTCTCGAGCGGTATAAGATG -3'
mouse	18S rRNA	5'- GTTAATTCCGATAACGAACG -3'	5'- CACAGACCTGTTATTGCTCA -3'

Chromatin immunoprecipitation

Cells were fixed with 1% formaldehyde at 37℃ for 10 min, and washed with cold PBS containing protease inhibitors. After cells were lysed with 0.5% NP-40, the nuclear fraction was extracted with 1% SDS and sonicated to cut genomic DNAs into 300-500 bp fragments. Soluble chromatin complexes were precipitated with anti-FLAG, anti-SLUG, anti-SNAIL, or anti-YWHAH antibody overnight at 4℃. Immune complexes were precipitated with protein A/G beads (Santa Cruz Biotechnology) at 4℃ for 2 hr. The beads were sequentially washed with low salt, high salt, LiCl, and TE solutions. The bound chromatin complexes were eluted twice in a ChIP direct elution buffer for 15

min, and incubated overnight at 65°C to reverse cross-linking. DNAs were extracted by phenol–chloroform and precipitated with ethanol. The precipitated DNAs were resolved in distilled water and analyzed by qPCR (95°C/55°C/72°C, 20 sec at each phase). The nucleotide sequences (5′ to 3′) of PCR primers are; GCGCTGCTGATTGGCTGTG and GGCTGGAGTCTGAACTGAC for the *CDH1* promoter. ChIP-qPCR results were represented as the percentages of the input signal (% input). All reactions were performed as triplicates.

Fractionation of cytoplasmic and nuclear components

Cells were centrifuged at 1000xg for 5 min, and homogenized in a lysis buffer containing 10 mM Tris/HCl (pH 7.4), 10 mM KCl, 1 mM EDTA, 1.5 mM $MgCl_2$, 0.2% NP-40, 0.5 mM DTT, 1 mM sodium orthovanadate, and 400 μM PMSF. The cell lysates were separated into pellet (for nuclear fraction) and supernatant (for cytosolic fraction) using centrifugation at 1000xg for 5 min. One packed volume of a nuclear extraction buffer (20 mM Tris/HCl, pH 7.4, 420 mM NaCl, 1 mM EDTA, 1.5 mM $MgCl_2$, 20% glycerol, 0.5 mM DTT, 1 mM sodium orthovanadate, and 400 μM PMSF) was added to the pellet, and vortexed intermittently at low speed on ice for 30 min. The nuclear and cytosolic factions were spun at 20,000xg for 10 min and stored at -70°C.

Immunoblotting and immunoprecipitation

Proteins were separated on SDS/PAGE and transferred to Immobilon-P membranes (Millipore; Bedford, MA). The membranes were blocked with 5% skim milk, incubated overnight at 4℃ with a primary antibody, incubated with a horseradish peroxidase (HRP)-conjugated secondary antibody for 1 hr, and visualized using the ECL-plus kit (Amersham Biosciences; Piscataway, NJ). To analyze protein interactions, cell lysates were incubated with anti-KHK, anti-YWHAH, or IgG overnight at 4℃, and the immune complexes were pulled down with protein A/G beads. Otherwise, cell lysates were incubated with EZview Red anti-Myc, or anti-FLAG affinity gel, or Nickel-NTA affinity beads at 4℃ for 4 hr. The bound proteins were eluted in a denaturing SDS sample buffer and loaded on SDS-PAGE. All Western blotting experiments were performed three or more times.

Immunofluorescence analysis

KHK-A and KHK-C cDNAs were fused to the C-terminus of GFP and observed using Carl Zeiss LSM510 META confocal microscope at 488 nm. To examine the subcellular localization of LRRC59 and YWHAH, cells were fixed with 3.7% formaldehyde for 10 min and permeabilized with 0.1% Triton X-100 for 30 min. Cells were incubated in PBS containing 0.05% Tween-20 and 3% BSA for 1

hr, and further incubated overnight at 4°C with a primary antibody. Cells were incubated with Alexa Fluor 594-conjugated secondary antibodies for 1 hr. To stain F-actin, cells were incubated with Alexa Fluor 633 phalloidin (Invitrogen) for 30 min, stained with DAPI (Sigma-Aldrich) for 30 min, mounted in Faramount aqueous mounting medium (Dako; Glostrup, Denmark), and examined under the confocal microscope.

Immunohistochemistry

Primary tumors and lungs from mice were fixed with 4% paraformaldehyde, paraffin-embedded, and cut into 4 μm section slices. The slides were incubated in dry oven at 60°C, de-paraffinized, re-hydrated, and incubated in a citrate buffer (Dako) at 121°C for 10 min to retrieve antigen. To block non-specific signals. the slides were incubated with 3% H_2O_2 for 15 min and with 2% horse serum in BSA solution for 1 hr. The slides were incubated overnight at 4°C with anti-KHK (1:100, Santa Cruz), anti-LRRC59 (1:100, Novus biologicals) or anti-E-cadherin (1:200, Thermo Fisher Scientific). The sections were biotinylated with a secondary antibody for 1 hr. The immune complexes were visualized using the Vectastatin ABC kit (Vector Laboratories) and the DAB detection kit (Dako). Finally, the slides were counterstained with hematoxylin for 15 min, and photographed at four high power fields in each slide.

Mass analysis to identify protein interactome

MCF7 and MDA-MB-231 cells were transfected with empty vector, His-KHK-A, or His-KHK-C, incubated with 5 mM fructose for 8 hr. To identify protein interactions, cell lysates were incubated with nickel-NTA beads at 4℃ for 4 hr. The bound proteins were eluted by 250 mM imidazole. Protein concentration of the elute was measured using the BCA kit (Thermo Fisher Scientific, Rockfold, IL). After the Filter Aid Sample Preparation procedure was performed using a 30K Amicon Ultra Centrifugal filter (Millipore, UK), peptides were separated on Nanoflow Easy-nLC1000 system (Proxeon Biosystems, Odense, Denmark), which was equipped with a packing column (100 Å, 1.8-um particle, 75 μm x 50 cm). A gradient that ranged from 5 to 30% acetonitrile with 0.1% formic acid was run at a fixed flow rate of 300 nL/min for 90 min. Ionized peptides were analyzed on a quadrupole-orbitrap mass spectrometer (Q-Exactive, Thermo Fisher Scientific, San Jose, CA). MS1 spectra were measured in DDA mode at a resolution of 70,000 with an *m/z* scan range of 300 to 1800. For MS2 spectra, peptides were fragmented by higher-energy collisional dissociation (HCD) with a normalized collision energy of 30 and a resolution of 17,500. Raw MS data files for the label-free quantification were processed using the Maxquant (ver.1.5.5.1), to match the spectra against the uniprotKB FASTA database (74,540 entries, version from June 2014). MS/MS peaks searches were performed with the following parameters: peptide length of at least six amino acids, fixed carbamidomethyl modification, variable

methionine oxidation, and variable N-terminal acetylation. The tolerance was set to the 6 ppm, and 20 ppm for main search and first search, respectively. A false discovery rate of 1% was applied to all proteins and peptide searches. The mass spectrometry proteomics data have been deposited to the ProteomeXchange Consortium via the PRIDE partner repository with the dataset identifier PXD021035.

Mass analysis to identify post-translational modifications

For LC-MS/MS analysis of intracellular YWHAH protein, MDA-MB-231 cells with KHK-A overexpression or knock-down were transfected with FLAG-YWHAH, and then were treated with 5 mM fructose for 24 hr. FLAG-YWHAH was purified using FLAG-affinity beads and subjected to SDS-PAGE. For LC-MS/MS analysis of YWHAH phosphorylated *in vitro*, recombinant GST-YWHAH, which was reacted with GST-KHK-A as described in the *in vitro* kinase assay, was separated by SDS-PAGE. Proteins in gel slices were digested with trypsin and loaded to Easy n-LC (Thermo Fisher; San Jose, CA). Samples were separated on a C18 nanobore column (150 mm × 0.1 mm, 3 μm pore size; Agilent). The mobile phase A for LC separation was 0.1% formic acid, 3% acetonitrile in deionized water and the mobile phase B was 0.1% formic acid in acetonitrile. The chromatography gradient was designed for a linear increase from 5% B to 55% B in 40 min, 52% B to 75% B in 4 min, 95% B in 4 min, and 3% B in 6 min. The flow rate was maintained at 1500 nL/min. Mass spectra

were analyzed using LTQ Orbitrap XL mass spectrometer (Thermo Fisher) equipped with a nano-electrospray source. Mass spectra were acquired using data-dependent acquisition with a full mass scan (350–1200 *m/z*) followed by 10 MS/MS scans. For MS1 full scans, the orbitrap resolution was 30,000 and the AGC was 2×10^5. For MS/MS in the LTQ, the AGC was 1×10^4. The phosphorylation was identified by the additional mass of 78 Dalton on digested peptides. To identify modified amino acid, proteome discoverer (V1.2.0.208 with SEQUEST algorithm) was used.

Mass analyses of fructose and fructose-1-phosphate

MCF-7 and MDA-MB-231 cells were incubated with or without 5 mM fructose for 4 hr. Cells were gently homogenized in a hypotonic solution with 0.6% NP40 on ice, and spun down at 1000xg, and the pellet was saved as the nuclear fraction. The supernatant was centrifuged at 10000xg and collected as the cytoplasmic fraction. The cytoplasmic and nuclear fractions were vortexed with an ice-cold extraction solvent (Acetonitril:Methanol:Water = 4:4:2, v/v/v) for 1 min and snap-frozen in liquid nitrogen for 1 min, followed by centrifugation at 10000xg for 15 min. The samples were evaporated using SpeedVac vacuum centrifugation. Dried samples were derivatized with 50 μL of methoxyamine hydrochloride in pyridine (20 mg/mL) at 30°C for 90 min, followed by trimethylsilylation with 70 μl of N-methyl-N-(trimethylsilyl)

trifluoroacetamide at 60°C for 30 min. The derivatized samples were applied to Leco LECO Pegasus® BT time-of-flight (TOF) MS (Leco Corporation, Edinburgh, UK) coupled with an Agilent 6890 GC (Agilent technologies) equipped with a 30 m-long 0.25 mm Rtx-5Sil MS column. The chromatographic condition was a constant flow of 1 mL/min and the temperature was increased from 50°C to 330°C at the rate of 20°C/min. The electron ionization and ion source temperature were set −70 eV and 250°C, respectively. To measure fructose-1-phosphate, cells were harvested in 500 μL of ice-cold ethanol, vigorously vortexed with 400 μL of chloroform, mixed with 150 μL of water, and centrifuged at 10000xg for 15 min. The upper phase containing polar metabolites was subjected to derivatization and applied to GC-MS analysis, as described above. Fructose-1-phosphate was quantified using the standard chemical (MF03840) provided by Carbosynth LTD (Berkshire, UK).

Kinetic parameters for the KHK-A-YWHAH reaction

Ten ng of recombinant GST-KHK-A and various amounts of GST-YWHAH were incubated with various concentrations of fructose in 51 μL of a kinase buffer containing 1 mM sodium orthovanadate, 2 mM ATP and 10 μCi of [γ-^{32}P]-ATP. The reactions were incubated at 37°C for 10 min, and terminated by adding the 10% ice-cold Trichloroacetic acid. Precipitated proteins were

spun down at 15,000 x *g*, and washed 3 times in ice-cold acetone. The radioactivity in the pellet was measured with a scintillation counter. The K_m of KHK-A for YWHAH was calculated from a plot of 1/c.p.m. versus 1/[YWHAH] according to the Lineweaver–Burk equation. The K_i of fructose for the KHK-A-mediated YWHAH phosphorylation was fitted with the competitive inhibition model from the data using the GraphPad Prism 5.0 software. Data represented the means from three independent experiments. To measure the IC_{50} of fructose against the KHK-A-YWHAH reaction, 10 ng of GST-KHK-A and 1 μg of GST-YWHAH were incubated with various concentrations of fructose in 51 μL of the reaction buffer at 37°C for 10 min. The IC_{50} was calculated from a plot of KHK-A enzyme activity versus log[fructose] using the GraphPad Prism 5.0 software. Data represented the means from three independent experiments.

Determination of K_d of KHK-A and KHK-C for fructose

Recombinant His-KHK-A or His-KHK-C (10 ng) and various concentrations of D-[^{14}C(U)]-fructose (ARC 0116A, American Radiolabeled Chemicals, St. Louis, MO) were mixed in 30 μL of 25 mM HEPES or 50 mM phosphate buffer solution (pH 7.5) containing 85 mM KCl, 17 mM NaCl, 1 mM $MgCl_2$, and 0.2 mM $CaCl_2$. The mixtures were incubated at 37°C for 10 min and the reactions

were terminated by adding the 10% ice-cold trichloroacetic acid. Precipitated proteins were spun down at 15,000 x *g*, and washed 3 times in ice-cold acetone. The radioactivity of protein-bound fructose in the pellet was measured with a scintillation counter, and the K_d for fructose was fitted using the GraphPad Prism 5.0 software.

Human Breast Cancer Tissue Microarray

Human breast cancer tissue microarrays, which contained 40 different breast cancer specimens, were purchased from SuperBioChips Lab (Seoul, South Korea). Clinical records, including sex, age, TNM stage, histologic grade, survival, and cause of death, were also provided by the company. Histologic grading was defined according to the Nottingham Modification of Bloom-Richard System. Clinical information is summarized in Supplementary table 5. To score protein expression in immunostained specimens, two examiners observed four high-power field on each slide. Protein expression was analyzed using histoscore, which reflects both the intensity of nuclear staining (graded as: 0, non-staining; 1, weak; 2, moderate; 3, strong) and the percentage of positive cells. The range of possible scores was from 0 to 300.

Table 4. Clinical information on breast cancer patients

No.	Age	Sex	Organ	Diagnosis	LM	Histologic grade
1	59	F	Breast	Infiltrating duct carcinoma	0/19	II
2	48	F	Breast	Infiltrating duct carcinoma	0/16	II
3	42	F	Breast	Infiltrating duct carcinoma	5/19	II
4	37	F	Breast	Infiltrating duct carcinoma	8/8	III
5	37	F	Breast	Infiltrating duct carcinoma	0/20	III
6	55	F	Breast	Infiltrating duct carcinoma	0/19	II
7	55	F	Breast	Infiltrating duct carcinoma	20/20	II
8	36	F	Breast	Infiltrating duct carcinoma	0/14	II
9	52	F	Breast	Infiltrating duct carcinoma	5/24	III
10	40	F	Breast	Infiltrating duct carcinoma	0/11	II
11	51	F	Breast	Infiltrating duct carcinoma	0/1	III
12	55	F	Breast	Infiltrating duct carcinoma	0/19	III
13	60	F	Breast	Infiltrating duct carcinoma	0/16	III
14	45	F	Breast	Sarcomatoid carcinoma	3/23	III
15	38	F	Breast	Infiltrating duct carcinoma	3/13	III
16	53	F	Breast	Infiltrating duct carcinoma	3/14	II
17	48	F	Breast	Infiltrating duct carcinoma	2/15	II
18*	46	F	Breast	Intraductal papillary carcinoma	0/15	uk
19	40	F	Breast	Infiltrating duct carcinoma	0/10	III
20*	51	F	Breast	Atypical medullary carcinoma	1/16	uk
21	56	F	Breast	Infiltrating duct carcinoma	0/14	III
22*	45	F	Breast	Metaplstic carcinoma	0/17	uk
23	42	F	Breast	Infiltrating duct carcinoma	12/26	II
24	27	F	Breast	Infiltrating duct carcinoma	1/11	II
25	39	F	Breast	Infiltrating duct carcinoma	2/17	III
26	51	F	Breast	Infiltrating duct carcinoma	1/13	III
27	49	F	Breast	Infiltrating duct carcinoma	0/20	III
28	57	F	Breast	Infiltrating duct carcinoma	3/7	II
29	52	F	Breast	Infiltrating duct carcinoma	1/22	II
30	41	F	Breast	Infiltrating duct carcinoma	7/9	II
31	48	F	Breast	Infiltrating duct carcinoma	35/35	III
32	34	F	Breast	Infiltrating duct carcinoma	2/11	III
33*	37	F	Breast	Infiltrating duct carcinoma	22/23	III
34	58	F	Breast	Infiltrating duct carcinoma	19/22	III
35	37	F	Breast	Infiltrating duct carcinoma	17/19	III
36	66	F	Breast	Infiltrating duct carcinoma	4/11	III
37	51	F	Breast	Infiltrating duct carcinoma	3/16	III
38	41	F	Breast	Infiltrating duct carcinoma	15/21	III
39	56	F	Breast	Infiltrating duct carcinoma	5/13	II
40	47	F	Breast	Infiltrating duct carcinoma	11/13	II

LM, Lymph-node metastasis; Histologic grade, Nottingham Modification of Bloom-Richard system; uk, unknown; *, denotes data were excluded from analysis.

ROS measurement

MCF-7 and MDA-MB-231 cells, which had been transfected with Myc-KHK-A, Myc-KHK-C plasmid or siRNA, were incubated 5 mM fructose with or without 400 nM of pyrimidinopyrimidine, 20 μM of H_2O_2 was used as positive control for ROS production. After incubation with fructose, DCF-DA (20 μM) was added to cells. After being incubated in the dark for 20 min, cells were washed twice in PBS, and applied to a TECAN infinite M200 pro (*Grödig*, Austria). DCF fluorescence was excited at 488 nm and detected at 524 nm.

Molecular dynamics simulation

All-atom atomistic molecular dynamics (MD) models were used to simulate ternary complex system of YWHAH-11/ATP/KHK-A. The KHK-A/ATP and YWHAH-11 as a receptor-ligand pair were prepared by modifying KHK-A/fructose/adenyl-50-yl imidodiphosphate and YWHAH obtained from PDB ID: 2hw1 and 2c63, respectively [17, 25]. Molecular docking was carried out using Hex package (version. 8.0.0)[26] which generates the ensemble of ligand (YWHAH-11)-receptor(KHK-A/ATP) conformations by updating randomly the coordinates of the ligand and receptor molecules via spherical polar Fourier algorithm[27]. During the docking process, the ligand and receptor molecules were kept rigid. Amog the produced ligand-receptor structures, the most favorable structure with the highest energy score was selected for initial

structure. The selected structure was then solvated by TIP3P water molecules with 100 mM NaCl in the simulation box with a periodic boundary condition. The solvated system was then equilibrated for 10 ns at 310 K and 1 bar by performing NPT-ensemble MD simulations using GROMACS package[28](version 5.1.2) with CHARMM36 force field[29]. The modified Berendsen thermostat[30] and Parrinello-Rahman barostat[31] were used for maintaining temperature and pressure. Following equilibration, starting from the end of the trajectory obtained from the previous equilibrium simulation, a steered MD simulation was performed by pulling the oxygen of S25-OH of YWHAH-11 toward the phosphorus of ATP-γPO_3 over 1 ns using spring constant of 1000 kJ mol^{-1} nm^{-2} and a pull rate of 0.001 nm ps^{-1} to get a trajectory of S25-OH approaching to ATP-γPO_3 where ATP was fixed as an immobile reference by position restraint algorithm. Using this trajectory from pulling simulation, configurations having different *d* with interval 0.1 nm were prepared as starting configurations for umbrella sampling where 10 ns of NPT-ensemble MD were subsequently performed. The PMF profile was finally obtained by the weighted histogram analysis method (WHAM)[32]. Analysis performed 5 fully independent sets of umbrella simulations for each of profiles to check the reproducibility. Furthermore, the uncertainties of the profiles were also estimated by resampling technique using Bayesian bootstrap analysis with 200 bootstraps. The whole simulation procedure described above was conducted also for YWHAH-11/ATP/KHK-C, PRPS1-11/ATP/KHK-A, and YWHAH-11_D21A/ATP/KHK-A to compute their PMFs.

KHK isoform analysis from TCGA dataset

KHK-A and KHK-C expressions in human cancers were analyzed by using data from The Cancer Genome Atlas (TCGA). Primary data (rnaseq V2 level 3 data for transcript isoforms normalized by RSEM) downloaded from the Broad Institute FireBrowse portal[44]. The UCSC isoform identifiers against the *KHK* gene were discriminated in the UCSC genome browser by the position of exon 3 (uc002ril.3 for KHK-A; uc002rim.3 for KHK-C).

Data availability

The mass spectrometry proteomics data have been deposited to the ProteomeXchange Consortium via the PRIDE partner repository with the dataset identifier PXD021035. The proteomics data referenced during the study are available in a public repository from the PRIDE website. All the other data supporting the findings of this study are available within the article and its supplementary information files and from the corresponding author upon reasonable request. A reporting summary for this article is available as a Supplementary Information file.

Statistical analysis and reproducibility

All data were analyzed using the Microsoft Excel 2013 or the GraphPad Prism

8.0 software. Results were presented as the means and standard deviation (S.D.). The unpaired, two-sided Student's *t*-test was used to analyze the results of cell number, RNA level, protein level, and Mass-based interactome data. A two-sided Mann-Whitney *U* test was used to analyze the results of histoscore, ROI flux, tumor volume, mouse body weight, and Spearman correlation analysis used to analyze the correlation coefficient between KHK-A and YWHAH-pS25 expression in breast cancer tissue arrays. The statistical significance was considered when $P < 0.05$. All immunoprecipitation, immunoblotting, immunohistochemistry and H&E staining, immunofluorescence, RT-qPCR, ChIP-assay, *in vitro* binding assay, *in vitro* kinase assay, invasion assay, and proteomics analyses were independently repeated at least three times. The results for significance tests are included in each panel.

RESULTS

Fructose stimulates cell invasion in breast cancer

First, I examined which cancer cells became more invasive in response to fructose. Compared with saline or glucose, fructose facilitated Matrigel invasion in cancer cell lines derived from the breast, brain, lung, pancreas, colon, prostate, and uterine cervix, but not in those from the ovary, kidney, bone, and liver (Figure 3). To examine the role of KHK in this process, I measured the cellular levels of two KHK isoforms in various cancer cell lines. Most cell lines except HepG2 predominantly expressed KHK-A (Figure 4). Informatics analyses using TCGA revealed that KHK-A, rather than KHK-C, is predominantly expressed in most human cancers, including breast cancer (Figure 5). Next, I explored the metastogenic role of KHK-A in breast cancer because cell invasion in response to fructose was strongly shown in all three breast cancer cell lines. As glucose as well as fructose could affect cell behavior[33, 34], I performed the invasion assay under the same concentration (finally 5 mM) of glucose or fructose. Fructose robustly stimulated cell invasion, but glucose at such a concentration showed a marginal effect on the invasion (Figure 6). To examine which isoform was responsible for fructose-induced cell invasion, I knocked down KHK-A or KHK-C using siRNAs that target isotype-specific sequences in exon 3. Consequently, fructose-induced invasion was attenuated by knockdown of KHK-A but not by knockdown of KHK-C.

Moreover, cell invasion was augmented by KHK-A overexpression (Figure 7). To examine the structure of intracellular cytoskeletons, F-actin was stained with phalloidin. During fructose incubation, MDA-MB-231 cells were morphologically altered with enhanced front–rear polarization and F-actin rearrangement (Figure 8A), which indicates that cells underwent the epithelial–mesenchymal transition (EMT). Of the representative EMT markers, the cell-adhesion molecule CDH1 (alternatively named E-cadherin) was substantially suppressed by fructose, and this effect was augmented by KHK-A overexpression (Figure 8B). Hence, the results suggest that fructose triggers EMT in breast cancer, which may be mediated by KHK-A. Given that KHK-A is known to be less active in fructose utilization, I needed to determine whether the fructose-induced invasion was attributable to the enzymatic function of KHK-A. Under fructose stimulation, both the cytoskeletal rearrangement and cell invasion in MDA-MB-231 cells were attenuated by a KHK-specific kinase inhibitor pyrimidinopyrimidine (Pypy) (Figure 9A, B). I also checked whether KHK-A participates in the fructose flux by measuring the cellular levels of fructose-1-phosphate and ROS. As expected, their levels were enhanced by KHK-C, but not by KHK-A (Figure 10A, B, C, and Figure 11A, B). These results suggest that KHK-A promotes cell invasion due to its kinase function regardless of the fructose metabolism.

On the other hand, ALDOB and ALOX12 were previously reported to play roles in fructose-induced metastasis in colon and breast cancers, respectively[9,

[13]. Therefore, I also investigated whether these proteins were involved in the fructose-stimulated invasion of breast cancer cells. However, the knockdown of either ALDOB or ALOX12 failed to attenuate cell invasion upon fructose stimulation (Figure 12A, B). About inconsistent results with previous reports, I concluded that it is because of using different types of cell line or experiment under different circumstances cause alteration of cellular metabolism. As mentioned, KHK-A was reported to promote hepatocellular carcinogenesis by phosphorylating PRPS1[22]. Therefore, I explored the possibility that PRPS1 mediates KHK-A action on cell invasion. Even while PRPS1 was knocked down, MDA-MB-231 cells showed good invasiveness in response to fructose (Figure 12C). Taken together, these data indicate that KHK-A seems to promote cell invasion.

KHK-A potentiates the fructose-induced metastasis in xenografted breast cancer

To evaluate whether the KHK-A promotes breast cancer metastasis *in vivo*, I implanted the murine MTV-TM-011 cell lines in the mammary fat pads of mice. The cell lines were established to stably express KHK-A or KHK-C/sh-*Khk-a* with luciferase. Luciferase activity, KHK-A, -C expressions and knock-down of mouse KHK-A were verified as shown in Figure 13A, and Figure 16A. Mice were randomly allocated to six groups (seven mice per group). The experimental schedules are summarized in Figure 13B, and 16B. I found that

the body weights of mice were severely reduced in group ‘f’ (KHK-A-overexpressing tumor in fructose-fed mice) (Figure 13C). Tumor growth was faster in three KHK-A-overexpressing groups than in three control groups. Fructose intake marginally enhanced tumor growth in the KHK-A groups, but not in the control groups (Figure 13D). However, when endogenous KHK-A was silenced or replaced with ectopic KHK-C, fructose intake showed no more effects on tumor growth and body weight (Figure 16C, and D). Because tumor volume can affect the chance of metastasis, the primary tumors were clearly resected when the tumor volume reached 500–600 mm^3. Two weeks later, chest metastasis was detected in six mice in group ‘f,’ whereas metastasis rarely developed in the other groups (Figure 14, and 17). To further evaluate lung metastasis, bioluminescence emission was measured in excised lung tissues. In most lungs from group ‘f,’ bioluminescence was strongly emitted over entire areas (Figure 15A). Weak emission was locally detected in two lungs from groups ‘c’ and ‘h’ (control tumors in fructose-fed mice, Figure 15A, and 18A), but not in other groups. Histological examination confirmed lung metastases in both fructose-feeding groups (Figure 15B, and 18B). In addition to the lung, tumor metastasis was detected in the liver, heart, hind leg, and GI tract in group ‘f’ (Figure 15C). However, when KHK-A was silenced or replaced with KHK-C, fructose intake failed to promote tumor metastasis (Figure 17, and 18A, B). Collectively, fructose feeding promotes breast cancer metastasis, which is exacerbated by KHK-A overexpression.

Fructose facilitates KHK-A binding to LRRC59 and YWHAH

Given that KHK-C has no effect on cell invasion, I hypothesized that KHK-A promotes cell invasion via some unique pathway irrespective of fructose metabolism. To identify the KHK-A pathway, I searched for proteins that interacted with KHK-A in a fructose-dependent manner. In both MCF-7 and MDA-MB-231 cells, three proteins, glyoxalase domain-containing protein 4 (GLOD4), Tyrosine 3-Monooxygenase/Tryptophan 5-Monooxygenase Activation Protein Eta (YWHAH), and leucine-rich repeat-containing protein 59 (LRRC59), were commonly identified as interacting with KHK-A in a fructose-dependent manner (Figure 19). To determine which of the three proteins participate in KHK-A-promoted cell invasion, I knocked down each candidate. The fructose-induced invasions of MCF-7 and MDA-MB-231 were attenuated by silencing YWHAH or LRRC59 but not by silencing GLOD4 (Figure 20A, and B). This result indicates that LRRC59 and YWHAH are involved in the KHK-A pathway for cell invasion. Immunoprecipitation analyses confirmed the fructose-dependent interaction of KHK-A, but not KHK-C, with the two proteins (Figure 21A, B). To examine where the proteins interact, I performed immunoprecipitation in subcellular fractions. KHK-A associated with LRRC59 in both the cytoplasm and the nucleus and with YWHAH in only the nucleus (Figure 22A, B). Interestingly, the input results showed that fructose induced the nuclear translocation of KHK-A and LRRC59, which encouraged us to test the possibility that the nuclear transporter LRRC59

aids KHK-A with entering the nucleus.

LRRC59 and KPNB1 transport KHK-A to the nucleus.

In the immunoblotting of subcellular fractions and immunofluorescence analyses, fructose induced nuclear translocation of KHK-A in dose- and time-dependent manners (Figure 23A, and C-E). By contrast, KHK-C stayed in the cytoplasm regardless of fructose treatment (Figure 23 B-E). Compared with KHK-C, KHK-A has a higher Km value for fructose on the enzyme kinetics[20]. Based on this enzymatic property, KHK-A has been regarded to have a lower affinity to fructose, so it was questioned how fructose triggers the nuclear translocation of KHK-A. Therefore, I measured a physical affinity for KHK-A or KHK-C binding to radioactive fructose. In HEPES and phosphate buffers, the Kd values (mM) of KHK-A for fructose were 0.53 and 0.55, and those of KHK-C were 0.40 and 0.47, respectively (Figure 24). These results suggest that KHK-A interacts with fructose as sensitively as KHK-C does but is ineffective in phosphorylating fructose. Given that the fructose-dependent nuclear translocation of KHK-A was attenuated by silencing LRRC59 (Figure 25A), LRRC59 might function as a nuclear importer for KHK-A. An *in vitro* binding assay showed that the existence of fructose is a prerequisite for the association of KHK-A and LRRC59 (Figure 25B). As LRRC59 is known to transport proteins in concert with KPNB1[35], I investigated the involvement of KPNB1 in the KHK-A translocation. Consequently, KPNB1 also joined to the fructose-

dependent complex of LRRC59 and KHK-A (Figure 25C); the association of KPNB1 also depended on LRRC59 (Figure 25D). Given that the nuclear translocations of KHK-A and LRRC59 were blocked by KPNB1 knockdown (Figure 25E), KPNB1 is also required for fructose-dependent nuclear translocation. Next, I examined whether the Leu83 residue in the hydrophobic motif of KHK-A was essential for the LRRC59 interaction, as it was for the PRPS1 interaction[22]. The KHK-A_L83A mutant cannot interact with the nuclear importers (Figure 26A). Furthermore, KHK-A_L83A neither enters the nucleus, even under fructose stimulation (Figure 26B), nor promotes fructose-dependent cell invasion (Figure 26C, and D). It should be noted that leucine 83 is present only in KHK-A because it is encoded by exon 3, which is spliced differently in KHK-A than in KHK-C. The isoform-specific exon 3 motif provides the unique action of KHK-A in response to fructose.

KHK-A functions as a serine kinase for YWHAH

First, I excluded the possibility that YWHAH participates in the fructose-induced nuclear translocation of KHK-A (Figure 27A). As the kinase KHK-A interacts with YWHAH in the nucleus, I hypothesized that KHK-A moonlights to phosphorylate YWHAH. An *in vitro* binding assay showed that KHK-A directly interacts with YWHAH (Figure 27B). Surprisingly, KHK-A was found to induce Ser/Thr-phosphorylation of YWHAH (Figure 27C). However, the kinase-dead mutant KHK-A_dATP, which lacked the ATP binding motif, failed

to induce phosphorylation of YWHAH, even though it entered the nucleus in response to fructose (Figure 27C, and D). Additionally, Pypy also attenuated YWHAH phosphorylation (Figure 27E). These results further support the notion that YWHAH phosphorylation is mediated by the kinase reaction of KHK-A. An *in vitro* kinase assay confirmed that KHK-A directly phosphorylates YWHAH but KHK-C does not (Figure 28A, and B). Unexpectedly, the YWHAH phosphorylation was inhibited by co-incubation with 1 mM fructose. The fructose binding to the catalytic site of KHK-A seems to interfere with the KHK-A action on YWHAH phosphorylation. I further examined the effect of fructose on the KHK-A phosphorylation of YWHAH. In an enzyme kinetics analysis, the Km value of KHK-A for YWHAH was identified to be 246 nM (Figure 29A). The IC_{50} and Ki values of fructose against the KHK-A phosphorylation of YWHAH was 0.91 mM and 0.72 mM, respectively (Figure 29B, and C). To test the possibility that fructose inhibits the YWHAH kinase activity of KHK-A in the nucleus, I quantified the nuclear concentration of fructose using a gas-chromatography mass analysis. When breast cancer cells were incubated with 5 mM fructose, a substantial concentration of fructose was detected in the cytoplasmic fraction, but not in the nuclear fraction (Figure 30). These results suggest that the fructose inhibition of YWHAH phosphorylation does not occur in the nucleus.

To specify the site of YWHAH phosphorylation, I performed the Orbitrap tandem mass analysis, which indicates that KHK-A phosphorylates YWHAH

at serine 25 in test tubes (Figure 31A, and B) and in cells (Figure 31C, and D). To verify the S25 phosphorylation, I expressed the YWHAH_S25A mutant and found that the mutant was not more phosphorylated by KHK-A (Figure 31E). This result also indicates that Ser25 is the only residue for KHK-A-dependent phosphorylation. To evaluate the involvement of YWHAH in cell invasion, first I checked the fructose-dependent F-actin rearrangement and found that YWHAH facilitates filopodia formation (Figure 32A). Next, I removed endogenous YWHAH in MDA-MB-231 cells using siRNA targeting the 3′-UTR and then restored wild-type YWHAH or YWHAH_S25A. Consequently, YWHAH promoted the fructose-dependent invasion of human (Figure 32B) breast cancer cells, but the YWHAH_S25A mutant did not. Taken together, these data indicate that KHK-A mediates fructose-dependent cell invasion by phosphorylating YWHAH at S25.

Since PRPS1 and p62 were previously reported as substrate of KHK-A in liver cancer[22, 36], I examined whether fructose facilitates the PRPS1 and p62 phosphorylation in liver and breast cancer cells. Fructose did not affect the phosphorylation of PRPS1 in Hep3B, but slightly reduced that in MCF7 and MDA-MB-231 (Figure 33A-C). As reported previously, p62 was found to be phosphorylated at Ser28 under hypoxia in liver and breast cancer cells, which verify the antibody used in this study. HIF-1α was detected as a marker for hypoxia. Consequently, fructose did not induce the p62 phosphorylation (Figure 33D-F). Therefore, it is suggested that fructose does not enhance the

protein kinase activity of KHK-A.

Phosphorylation of YWHAH promotes breast cancer metastasis.

For *in vivo* evaluation of breast cancer metastasis, I established the MTV-TM-011 cell lines that stably co-express luciferase and YWHAH or YWHAH_S25A (Figure 34A). Mice (7 per group) were randomly allocated to six groups and subjected to tumor graft (Figure 34B). The body weight was severely reduced in group 'd' (Figure 34C). Tumor growth was faster in the YWHAH-overexpressing groups than in the control or YWHAH_S25A groups (Figure 34D). After the resection of primary tumors, metastasizing tumors were detected at the chests of seven mice in group 'd' and at those of two mice in group 'b', whereas the metastasis rarely developed in the other groups (Figure 35). In group 'd', bioluminescence was strongly emitted over entire areas of the excised lungs (Figure 36A). Weak emission was locally detected in several lungs from groups 'b' and 'f', but no emission in other groups. Histological examination confirmed metastatic tumor nodules in the lung tissues from fructose-fed mice (Figure 36B). In group 'd', metastatic tumors were also detected in the livers, spleen, brain, and GI tracts (Figure 36C). Given these results, the KHK-A-mediated phosphorylation of YWHAH is critical for the fructose-induced metastasis of breast cancer.

Structural analysis for the KHK-A-mediated S25 phosphorylation of YWHAH.

Considering that KHK-C phosphorylates a small molecule (fructose), it seems strange that KHK-A phosphorylates amino acid resides in proteins, such as PRPS1 and YWHAH. To clarify this conflict, molecular dynamics (MD) simulation was analyzed with an 11-residue peptide model for the local fragment of YWHAH around S25 (from Y20 to V30), namely YWHAH-11. The umbrella sampling technique [37, 38] was used to compute the potential of mean force (PMF), which corresponds to the free energy change associated with YWHAH-11 experiencing its molecular environment, when the hydroxyl group at S25 of YWHAH-11 (S25-OH) approached the γ-phosphoryl group of ATP (ATP-γPO_3) on KHK-A. The PMF profile as a function of the distance (*d*) between the oxygen of S25-OH and the phosphorus of ATP-γPO_3 (Figure 37A) indicates that YWHAH-11 can form a ternary complex with KHK-A-bound ATP by reaching a local minimum at $d \cong 3.5$ Å. The structure of the ternary complex YWHAH-11/ATP/KHK-A is shown in Figure 37B. Such a P-O distance at the local minimum, which is the closest distance before the phosphorylation reaction occurs (i.e., reactant state), agrees well with previous quantum mechanical approaches[39, 40] (d = 3.2–3.3 Å), which also identified the transition and product state of the phosphorylation reaction at d = 2.2–2.3 Å and d = 1.7–1.8 Å, respectively. Having obtained the PMF for the YWHAH-11/ATP/KHK-A complex, it is interesting to investigate how PMF can be

altered for YWHAH/ATP/KHK-C and PRPS1/ATP/KHK-A. These systems were modeled by the same method, and their PMFs are compared to YWHAH-11/ATP/KHK complex. For the model of PRPS1/ATP/KHK-A, I employed the 11-residue peptide model, PRPS1-11, for the fragment of PRPS1 around T225 (from D219 to I229), which was similar to YWHAH-11. Notably, the PMF for PRPS1-11/ATP/KHK-A has a profile similar to that of YWHAH-11/ATP/KHK-A, with a nearly identical local minimum at $d \cong 3.6$ Å, whereas the profile for YWHAH-11/ATP/KHK-C has no minima in the entire profile. To further analyze this profile similarity in YWHAH-11/ATP/KHK-A and PRPS1-11/ATP/KHK-A, the residue-residue contact maps were computed for YWHAH-11/ATP/KHK-A and PRPS1-11/ATP/KHK-A at the local minimum state (Figure 38A). In the contact map, the region of inter-chain contact between KHK-A (aa. 3-298) and YWHAH-11 or PRPS1-11 is specifically focused. Both the contact maps for KHK-A/YWHAH-11 and KHK-A/PRPS1-11 show the similar inter-chain structure, revealing a feature that YWHAH-11 and PRPS1-11 commonly contact with a KHK-A region (aa. 100–114), which lies in the exon 3-derived segment differing from that of KHK-C[17]. These results demonstrate that the KHK-A region plays an important role for the phosphorylation of YWHAH and PRPS1, presumably acting as an auxiliary binder for holding YWHAH and PRPS1 near ATP site. In particular, the average numbers of atoms in contact with the binding region of KHK-A are very high for D21 and D22 in YWHAH (top in Figure 38B) and for D220 and D221 in PRPS1 (bottom in Figure 38B). Interestingly, the amino acids ‘DDMA’ are

commonly placed just before the KHK-A target residues in YWHAH and PRPS1. The MD simulation results also revealed that the double aspartate residues in 'DDMA' play a crucial role in navigation of YWHAH or PRPS1 toward ATP bound to KHK-A. This was verified by the PMF profile computed for YWHAH-11 mutated with D21A (YWHAH-11_D21A), which clearly shows a shifting of distance *d* at the local minimum to a larger value (Figure 37A). With this information on MD simulation, I experimentally tested the possibility that the D21 residue is essential to the KHK-A phosphorylation of YWHAH. The YWHAH_D21A mutant neither interacted with KHK-A nor phosphorylated it (Figure 39A, and B). Taken together, these data further support the notion that KHK-A can phosphorylate the S25 of YWHAH or the T225 of PRPS1.

S25-phosphorylated YWHAH recruits SLUG to the CDH1 promoter

Among representative EMT markers, CDH1 expression was the most strikingly changed by fructose in both MDA-MB-231, MCF-7 and MTV-TM-011 cells. The fructose-dependent suppression of CDH1 was augmented by KHK-A overexpression, which was reversed by YWHAH knockdown (Figure 40A-C). CDH1 expression was regulated at the transcriptional level (Figure 41A-C). A previous study demonstrated that YWHAH regulates CDH1 expression by interacting with the transcription factor SNAIL[41]; therefore, I examined whether YWHAH interacts with SNAIL and other CDH1 repressors.

As reported, YWHAH interacted with SNAIL, but this interaction was independent of fructose or KHK-A. By contrast, SLUG was found to interact with YWHAH in fructose- and KHK-A-dependent manners (Figure 42A, and B). When co-expressed with KHK-A, YWHAH also showed a fructose-dependent interaction with SLUG (Figure 42C). In chromatin immunoprecipitation analyses, the recruitments of YWHAH and SLUG to the CDH1 promoter were shown to depend on fructose and KHK-A (Figure 43A, B, D, and E), but the SNAIL recruitment was not (Figure 43C). Despite its existence in the nucleus (Figure 43A), YWHAH_S25A did not interact with SLUG in response to fructose (Figure 44B, and C). This indicates that the S25 phosphorylation of YWHAH is critical for the SLUG interaction. As expected, the fructose-dependent suppression of CDH1 was diminished by SLUG knockdown in the presence of wild-type YWHAH but not in the presence of YWHAH_S25A (Figure 45A, and C). These results were also verified at the mRNA level of CDH1 (Figure 45B, and D-E). I next examined for the recruitment of YWHAH to the *CDH1* promoter. The binding of YWHAH to the *CDH1* promoter was enhanced by fructose, whereas that of YWHAH_S25A was not affected by fructose (Figure 46A). Likewise, fructose facilitated SLUG binding to the *CDH1* promoter, which was also augmented by wild-type YWHAH (Figure 46B). As expected, the binding of SNAIL to the *CDH1* promoter was not regulated by S25 phosphorylation (Figure 46C). I assessed whether the sequential binding of proteins also affected cell invasiveness. A Matrigel invasion assay was performed on MDA-MB-231 or MTV-TM-011

cells that were stably expressing KHK-A. Fructose-induced invasiveness was determined by SLUG in YWHAH-expressing cells but not in YWHAH_S25A-expressing cells (Figure 47A, and B). To examine the degree to which the CDH1 suppression contributes to fructose-induced invasion, I restored CDH1 expression in KHK-A-overexpressing cells, which almost completely blocked the fructose-induced invasion (Figure 48A, and B). This result suggests that CDH1 suppression is the key event for cell invasion. Finally, I examined the KHK-A signaling pathway in breast cancer tissues, which were obtained from mice presented in Figure 14, and 17. Immunohistochemical analyses showed the suppression of CDH1 and the nuclear expressions of KHK and LRRC59 in the tumors of fructose-fed mice (Figure 49A, and B). I also confirmed the YWHAH phosphorylation in the nucleus by immunostaining breast cancer grafts that were primarily removed from mice in Figure 34 (Figure 50). Taken together, these data suggest that fructose induces cancer invasion through the KHK-A-YWHAH-SLUG-CDH1 pathway.

KHK-A-phosphorylated YWHAH axis correlates with metastasis in breast cancer patients.

Next, I investigated whether the KHK-A phosphorylation of YWHAH is clinically associated with the breast cancer metastasis. To examine the association of KHK-A and S25-phosphorylated YWHAH, I immunologically stained human breast cancer arrays (Figure 51A). The cancer specimens were

histologically graded according to the Nottingham grading system (Figure 51B). The nuclear KHK-A and S25-phosphorylated YWHAH levels both were significantly higher in the grade 3 group than in the grade 2 group (Figure 51C). Even when the breast cancer specimens were divided into non-metastasis and metastasis groups, the nuclear KHK-A and S25-phosphorylated YWHAH levels were much higher in the metastasis group. Spearman correlation analysis showed that nuclear KHK-A expression correlates with the S25-phosphorylated YWHAH expression (Figure 51D). Collectively, the KHK-A-mediated phosphorylation of YWHAH is likely to be clinically associated with breast cancer metastasis.

A

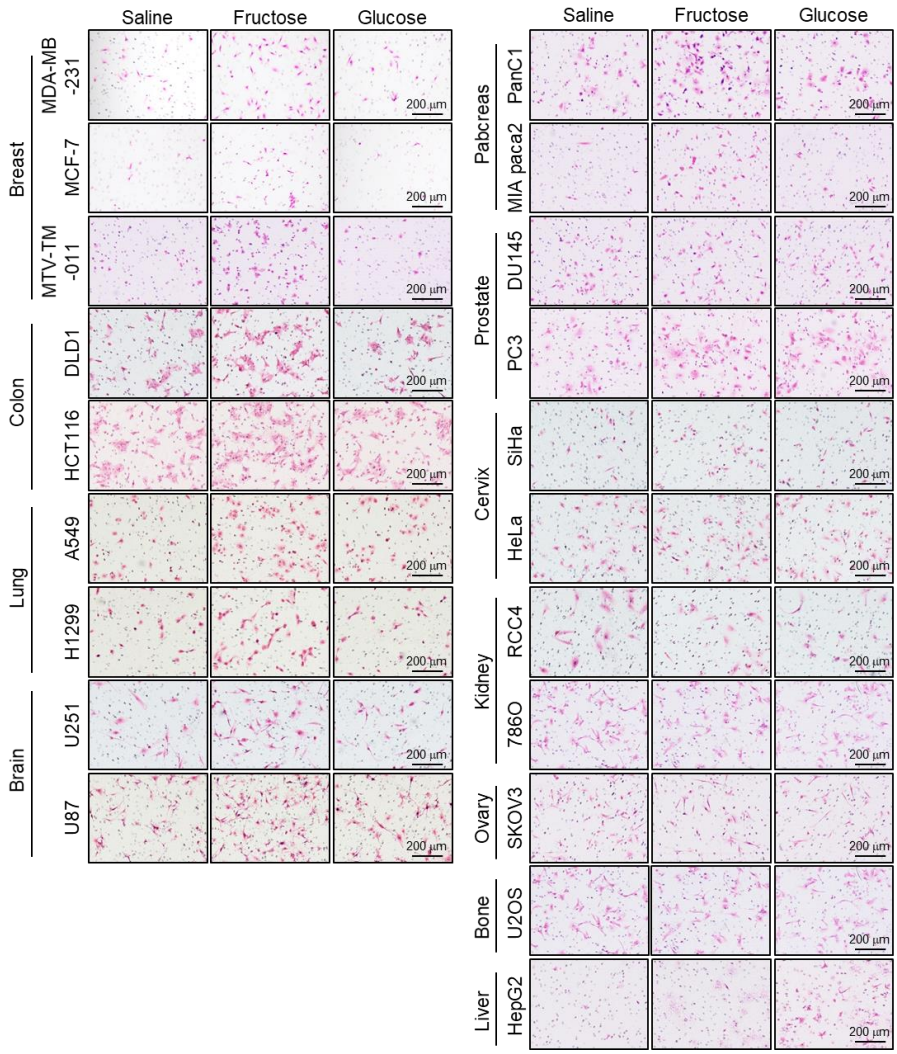
Saline
Fructose
Glucose
Breast
MDA-MB -231
MCF-7
MTV-TM -011
Colon
DLD1
HCT116
Lung
A549
H1299
Brain
U251
U87
Pabcreas
PanC1
MIA paca2
Prostate
DU145
PC3
Cervix
SiHa
HeLa
Kidney
RCC4
786O
Ovary
SKOV3
Bone
U2OS
Liver
HepG2
200 μm

B

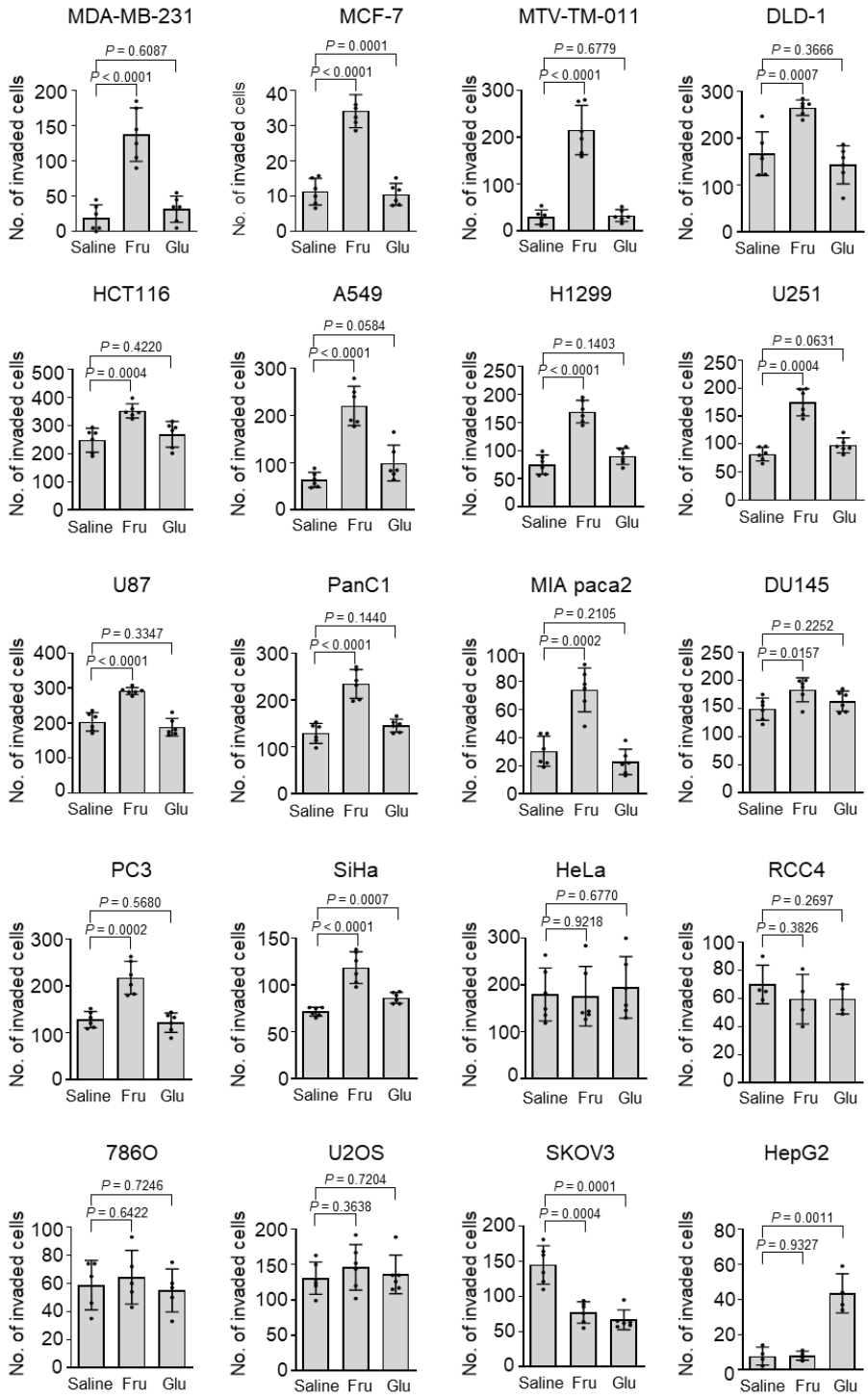
MDA-MB-231
P = 0.6087
P < 0.0001
MCF-7
P = 0.0001
P < 0.0001
MTV-TM-011
P = 0.6779
P < 0.0001
DLD-1
P = 0.3666
P = 0.0007
HCT116
P = 0.4220
P = 0.0004
A549
P = 0.0584
P < 0.0001
H1299
P = 0.1403
P < 0.0001
U251
P = 0.0631
P = 0.0004
U87
P = 0.3347
P < 0.0001
PanC1
P = 0.1440
P < 0.0001
MIA paca2
P = 0.2105
P = 0.0002
DU145
P = 0.2252
P = 0.0157
PC3
P = 0.5680
P = 0.0002
SiHa
P = 0.0007
P < 0.0001
HeLa
P = 0.6770
P = 0.9218
RCC4
P = 0.2697
P = 0.3826
786O
P = 0.7246
P = 0.6422
U2OS
P = 0.7204
P = 0.3638
SKOV3
P = 0.0001
P = 0.0004
HepG2
P = 0.0011
P = 0.9327
No. of invaded cells
Saline
Fru
Glu

Figure 3. Fructose enhances the invasion potential of various cancer cells

The invasion potential of cancer cells was analyzed using Boyden-camber with a Matrigel-coated membrane. Indicated cell lines were incubated with 5 mM fructose or additional 5 mM glucose for 48 hours, and placed in the upper chamber. After 24 hours, cells passing through the interface membrane were stained and counted (means ± S.D. from 4 independent experiment for RCC4 and HepG2; means ± S.D. from 5 independent experiment for 786O; and means ± S.D. from 6 independent experiment for rest of the cell lines). **A**. The pictures are representative of three independent experiments. **B**. The numbers of invaded cells are presented as bar graph. Bar graphs are Significance was calculated by an unpaired, two-sided, Student's *t*-test, and *P*-values are represented in each panel. Representative photographs of invasion assays from one out of three experiments. Significance was calculated by unpaired, two-sided Student's *t*-test. The results for significance tests are included in each panel.

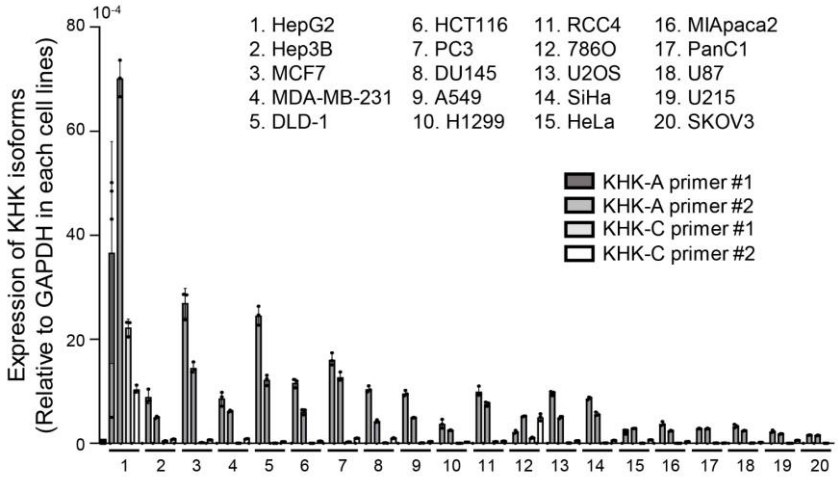

Figure 4. KHK-A and KHK-C expression level analysis from various cancer cell lines

The mRNA levels of KHK-A and KHK-C were measured by quantitative RT-PCR. The mRNA levels (means ± S.D. from 3 independent experiments) were normalized to the GAPDH mRNA level.

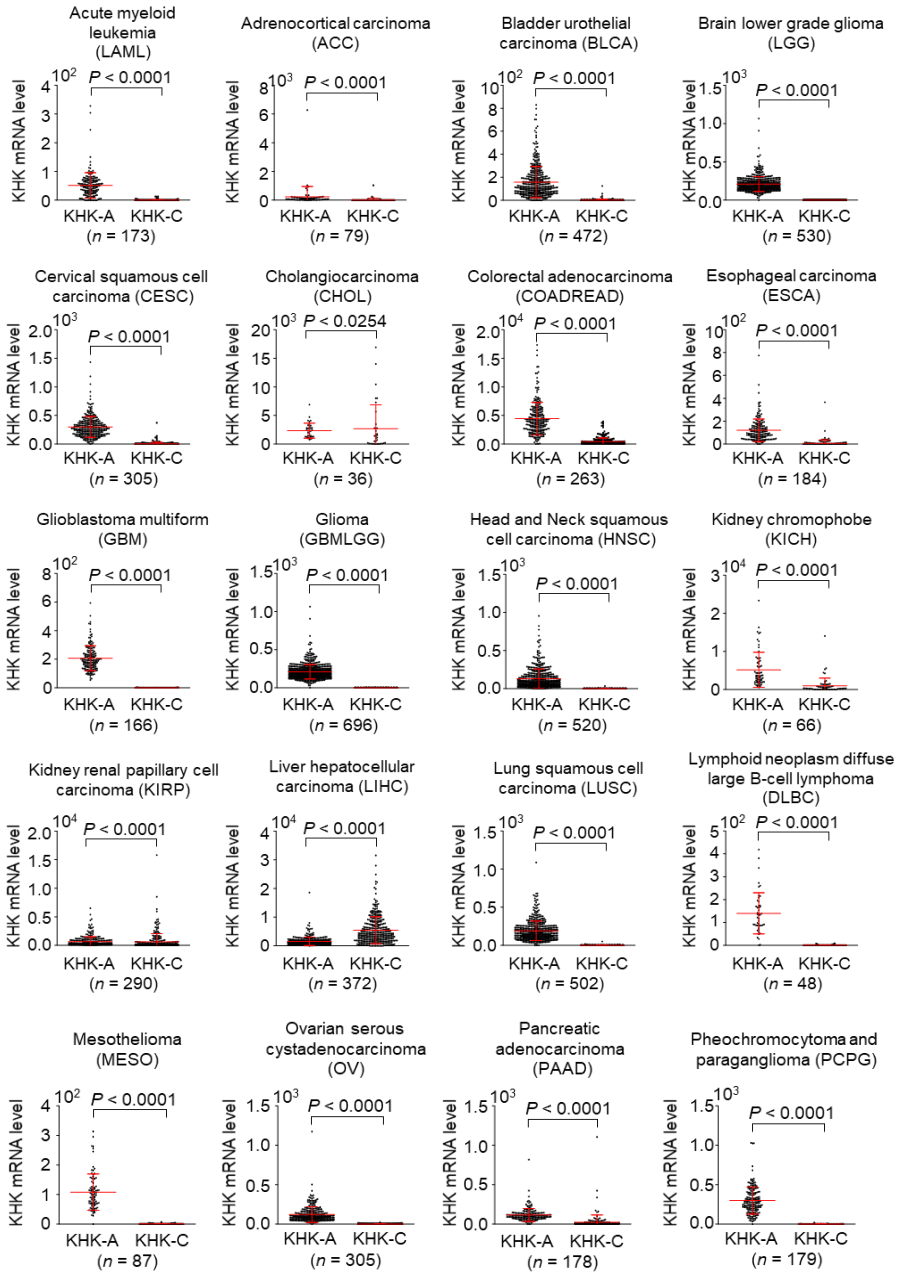
Acute myeloid leukemia (LAML)
Adrenocortical carcinoma (ACC)
Bladder urothelial carcinoma (BLCA)
Brain lower grade glioma (LGG)
Cervical squamous cell carcinoma (CESC)
Cholangiocarcinoma (CHOL)
Colorectal adenocarcinoma (COADREAD)
Esophageal carcinoma (ESCA)
Glioblastoma multiform (GBM)
Glioma (GBMLGG)
Head and Neck squamous cell carcinoma (HNSC)
Kidney chromophobe (KICH)
Kidney renal papillary cell carcinoma (KIRP)
Liver hepatocellular carcinoma (LIHC)
Lung squamous cell carcinoma (LUSC)
Lymphoid neoplasm diffuse large B-cell lymphoma (DLBC)
Mesothelioma (MESO)
Ovarian serous cystadenocarcinoma (OV)
Pancreatic adenocarcinoma (PAAD)
Pheochromocytoma and paraganglioma (PCPG)
KHK mRNA level
P < 0.0001
P < 0.0254
KHK-A
KHK-C
(n = 173)
(n = 79)
(n = 472)
(n = 530)
(n = 305)
(n = 36)
(n = 263)
(n = 184)
(n = 166)
(n = 696)
(n = 520)
(n = 66)
(n = 290)
(n = 372)
(n = 502)
(n = 48)
(n = 87)
(n = 305)
(n = 178)
(n = 179)

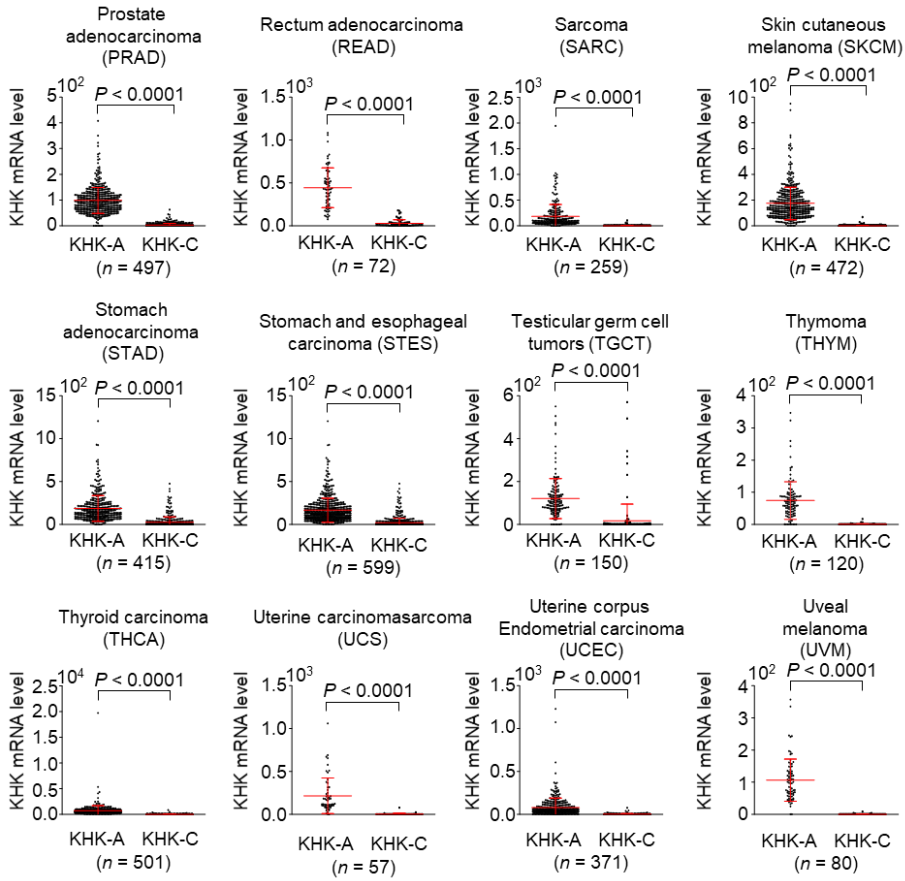

Figure 5. KHK-A and KHK-C expression level analysis from TCGA dataset

The mRNA levels of KHK-A and KHK-C in various cancers on TCGA dataset. Data are presented as means ± S.D. from the number of samples derived from independent cancer patients were provided by TCGA database are shown in each panel. To evaluate significance, two-sided Mann-Whitney *U* test was used.

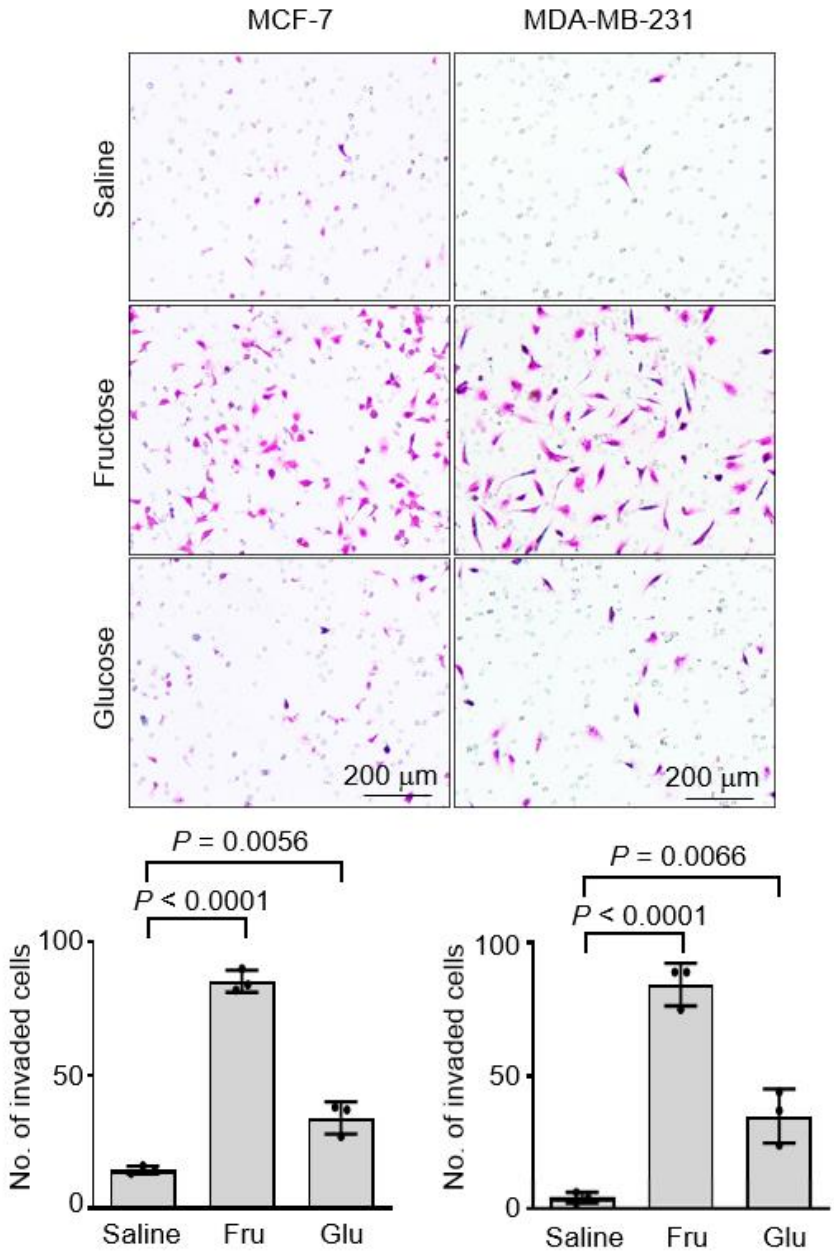
MCF-7
MDA-MB-231
Saline
Fructose
Glucose
200 µm
200 µm
P = 0.0056
P < 0.0001
No. of invaded cells
100
50
0
Saline
Fru
Glu
P = 0.0066
P < 0.0001
No. of invaded cells
100
50
0
Saline
Fru
Glu

Figure 6. Fructose robustly stimulated cell invasion

MDA-MB-231 and MCF-7 cells incubated with 5 mM fructose or 5 mM glucose in glucose-free medium for 24 hours, and subjected to invasion assay (means ± S.D. from 3 independent experiments). Significance was calculated by an unpaired, two-sided Student's *t*-test. Representative photographs of Matrigel-coated transwell invasion assays are presented at the top panel.

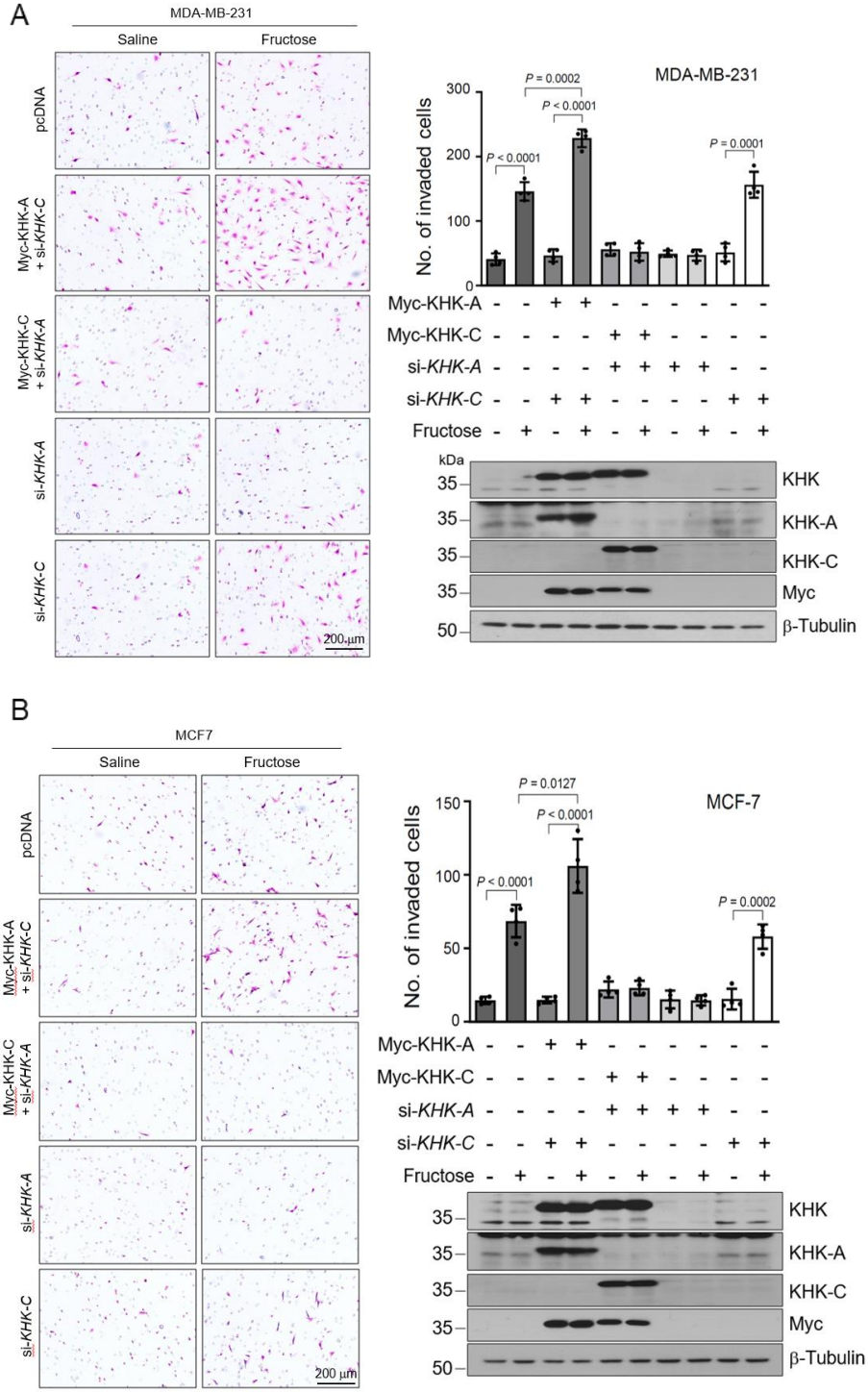
A
MDA-MB-231
Saline
Fructose
pcDNA
Myc-KHK-A + si-KHK-C
Myc-KHK-C + si-KHK-A
si-KHK-A
si-KHK-C
200 μm
MDA-MB-231
No. of invaded cells
P = 0.0002
P < 0.0001
P < 0.0001
P = 0.0001
Myc-KHK-A
Myc-KHK-C
si-KHK-A
si-KHK-C
Fructose
kDa
KHK
KHK-A
KHK-C
Myc
β-Tubulin
B
MCF7
Saline
Fructose
pcDNA
Myc-KHK-A + si-KHK-C
Myc-KHK-C + si-KHK-A
si-KHK-A
si-KHK-C
200 μm
MCF-7
No. of invaded cells
P = 0.0127
P < 0.0001
P < 0.0001
P = 0.0002
Myc-KHK-A
Myc-KHK-C
si-KHK-A
si-KHK-C
Fructose
KHK
KHK-A
KHK-C
Myc
β-Tubulin

Figure 7. Fructose-induced invasion was attenuated by silencing KHK-A, rather than KHK-C

A. MDA-MB-231 which had been transfected with 1 μg of Myc-tagged plasmid or 60 nM si-RNA, were subjected to the invasion assay (means ± S.D. from 4 independent experiments). Significance was calculated by unpaired, two-sided Student's *t*-test. The results for significance tests are included in each panel. **B**. MCF-7 which had been transfected with 1μg of Myc-tagged plasmid or 60 nM si-RNA, were subjected to the invasion assay (means ± S.D. from 4 independent experiments). Significance was calculated by unpaired, two-sided Student's *t*-test. The results for significance tests are included in each panel.

A

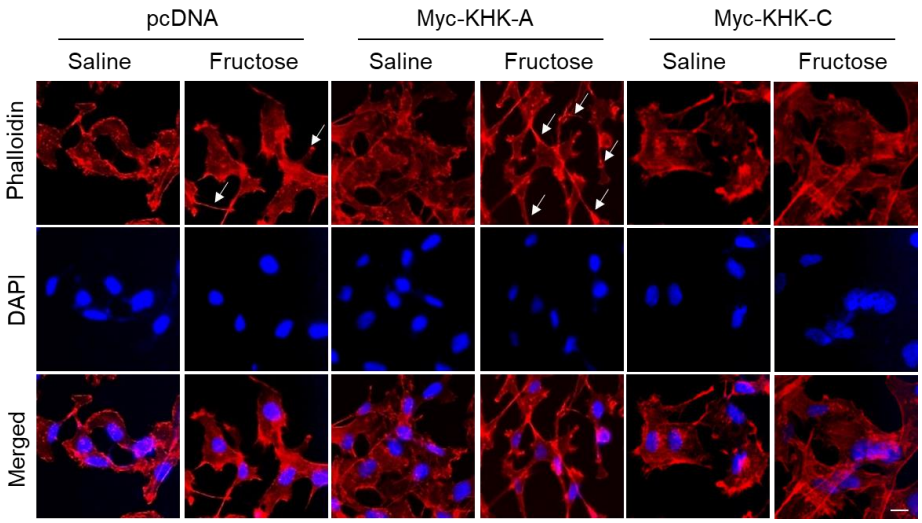
pcDNA
Myc-KHK-A
Myc-KHK-C
Saline
Fructose
Saline
Fructose
Saline
Fructose
Phalloidin
DAPI
Merged

B

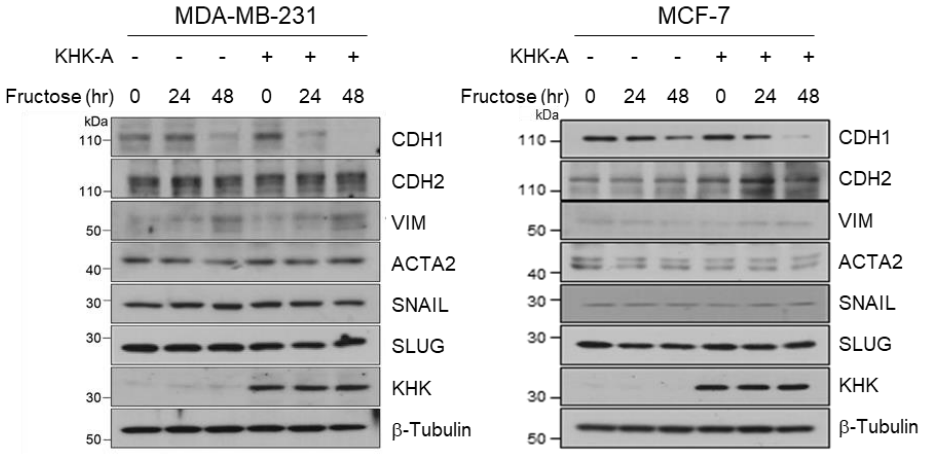
MDA-MB-231
MCF-7
KHK-A - - - + + +
Fructose (hr) 0 24 48 0 24 48
kDa
110
110
50
40
30
30
30
50
CDH1
CDH2
VIM
ACTA2
SNAIL
SLUG
KHK
β-Tubulin

Figure 8. Analyses of EMT markers and cytoskeleton rearrangement in KHK-A overexpressing cells

A. MDA-MB-231 cells, which had been transfected with Myc-KHK-A or –C, were treated with 5 mM fructose (or saline) for 48 hr. F-actin and nucleus were stained with Alexa Fluor 633 Phalloidine (red) and DAPI (blue), and visualized under a fluorescence microscope (scale bar = 10 μm). **B**. MDA-MB-231, and MCF-7 stable cells expressing KHK-A were incubated with 5 mM fructose with indicated incubation times. The cell lysates were subjected to Western blotting for EMT markers. The blots are representative of three independent experiments.

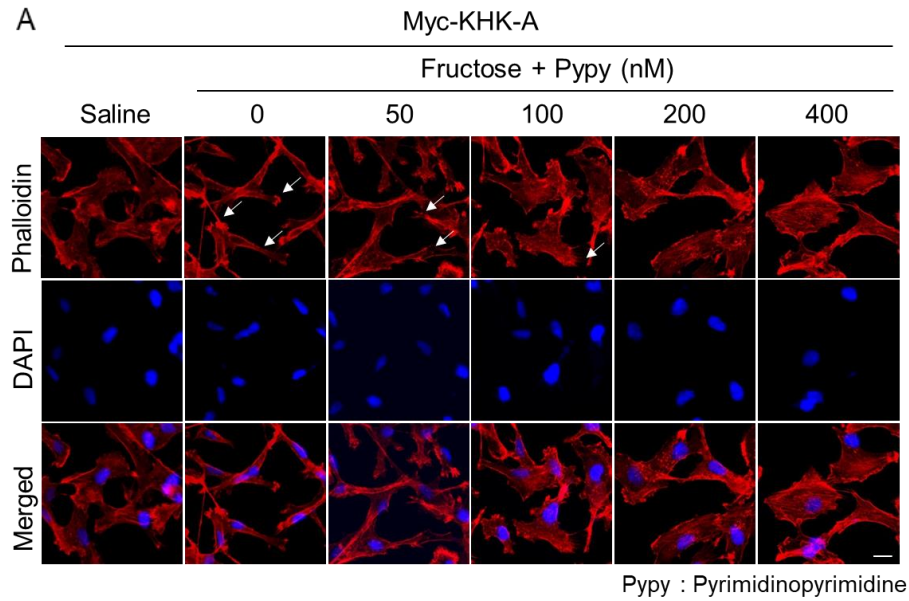

Pypy : Pyrimidinopyrimidine

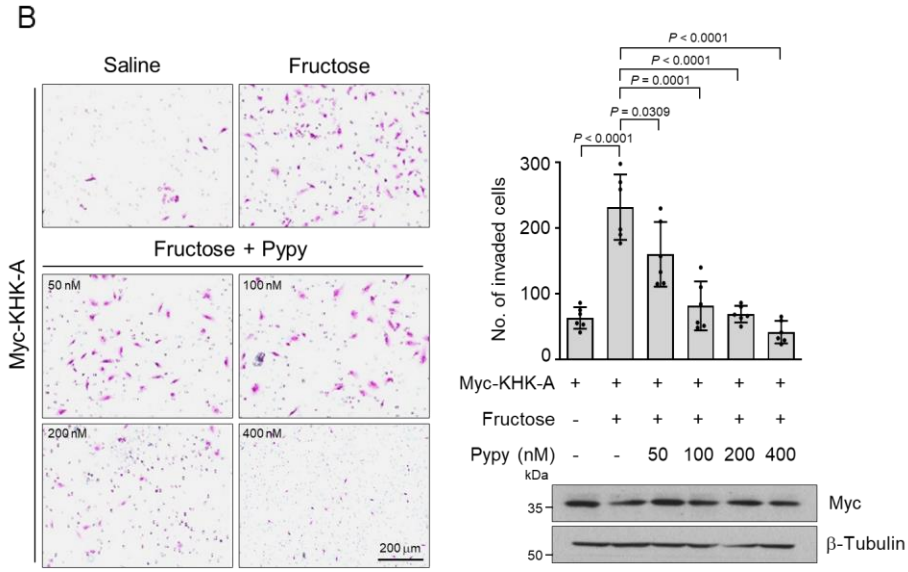

Figure 9. KHK-A promotes cell invasion due to its kinase function

A. MDA-MB-231 cells, which had neem transfected with Myc-KHK-A, were treated with 5 mM fructose and pyrimidinopyrimidine for 48 hr. F-actin and nucleus were stained with Alexa Fluor 633 Phalloidine (red) and DAPI (blue), and visualized under fluorescence microscope (scale bar = 10 μm). **B**. Transfected MDA-MB-231 cells were treated with 5 mM fructose and various concentration of pyrimidinopyrimidine, and subjected to Matrigel invasion assay (means ± S.D. from 4 independent experiments). Significance was calculated by unpaired, two-sided Student's *t*-test. The results for significance tests are included in each panel.

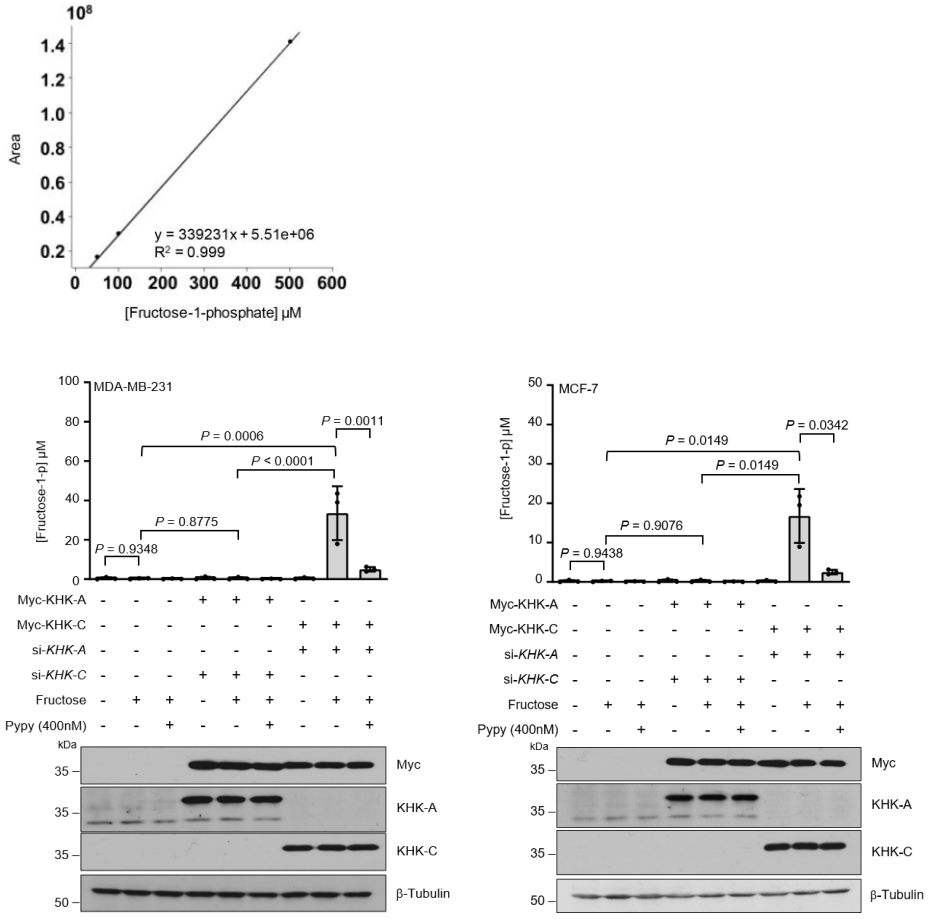

Figure 10. KHK-A does not phosphorylate fructose

MDA-MB-231 and MCF-7 cells, which had been transfected with 1 μg of Myc-tagged plasmid or 60 nM si-RNA, were treated with 5 mM fructose and/or Pyrimidinopyrimidine, and were subjected to the GC-MS analysis to measure fructose-1-phosphate. Data represented as means ± S.D. from 3 independent experiments. Significance was calculated by unpaired, two-sided Student's *t*-test. The results for significance tests are included in each panel.

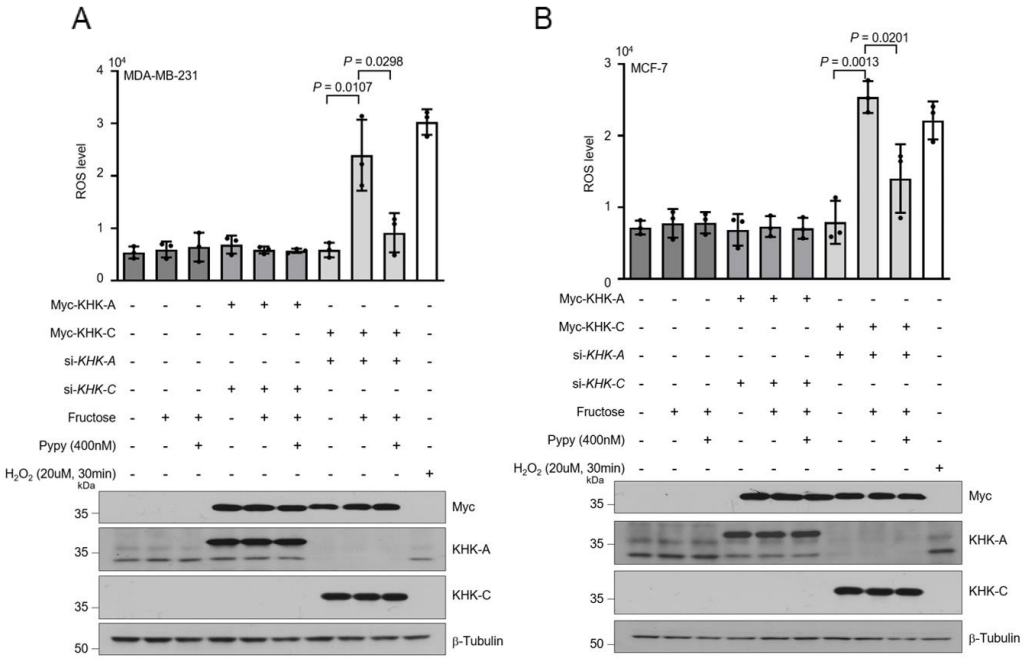

Figure 11. KHK-A does not involve in fructose metabolism

A. MDA-MB-231 and **B**. MCF-7 cells, which had been transfected with 1μg of Myc-tagged plasmid or 60 nM si-RNA, were treated with 5 mM fructose and/or Pyrimidinopyrimidine, and were subjected to the DCF-DA assay. 20 μM H_2O_2 was used as positive control. Data are presented as means ± S.D. from 3 independent experiments. Significance was calculated by an unpaired, two-sided Student's *t*-test, *P*-values are represented in the panel.

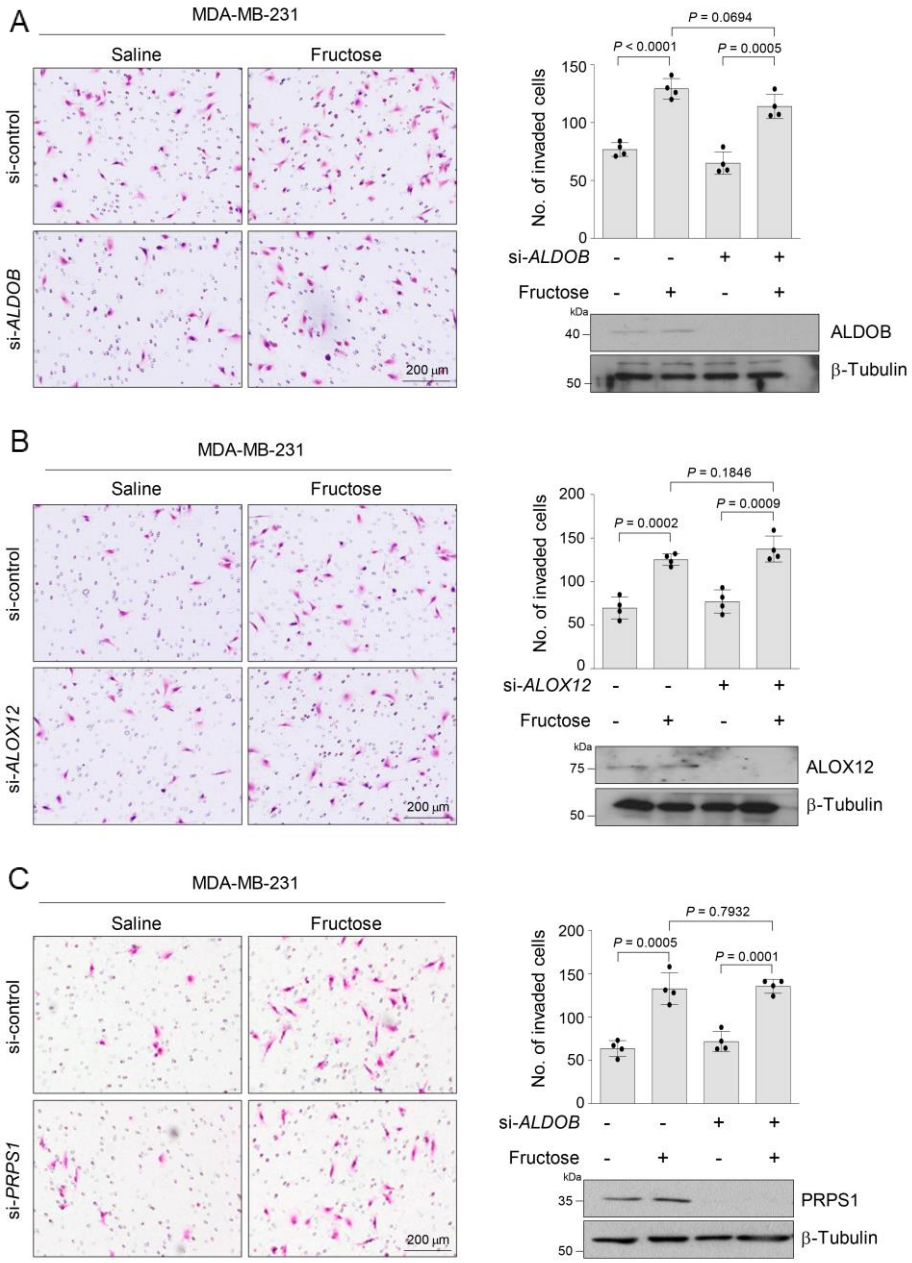
A
MDA-MB-231
Saline
Fructose
si-control
si-ALDOB
200 μm
P = 0.0694
P < 0.0001
P = 0.0005
No. of invaded cells
150
100
50
0
si-ALDOB - - + +
Fructose - + - +
kDa
40
50
ALDOB
β-Tubulin
B
MDA-MB-231
Saline
Fructose
si-control
si-ALOX12
200 μm
P = 0.1846
P = 0.0009
P = 0.0002
No. of invaded cells
200
150
100
50
0
si-ALOX12 - - + +
Fructose - + - +
kDa
75
50
ALOX12
β-Tubulin
C
MDA-MB-231
Saline
Fructose
si-control
si-PRPS1
200 μm
P = 0.7932
P = 0.0005
P = 0.0001
No. of invaded cells
200
150
100
50
0
si-ALDOB - - + +
Fructose - + - +
kDa
35
50
PRPS1
β-Tubulin

Figure 12. Knockdown of ALDOB, ALOX12 or PRPS1 failed to fructose stimulated call invasion

A. MDA-MB-231 cells, which had been transfected with 80 nM *ALDOB* si-RNA, were incubated with 5 mM fructose for 48 hours. Cells were subjected to Matrigel-coated invasion assay (means ± S.D. from 4 independent experiments). **B**. MDA-MB-231 cells, which had been transfected with 60 nM *ALOX12* si-RNA, were incubated with 5 mM fructose for 48 hours. Cells were subjected to Matrigel-coated invasion assay (means ± S.D. from 4 independent experiments). **C**. MDA-MB-231 cells, which had been transfected with 60 nM *PRPS1* si-RNA, were incubated with 5 mM fructose for 48 hours. Cells were subjected to Matrigel-coated invasion assay (means ± S.D. from 4 independent experiments). In **a**-**c**, statistical significance was calculated by an unpaired, two-sided Student's *t*-test.

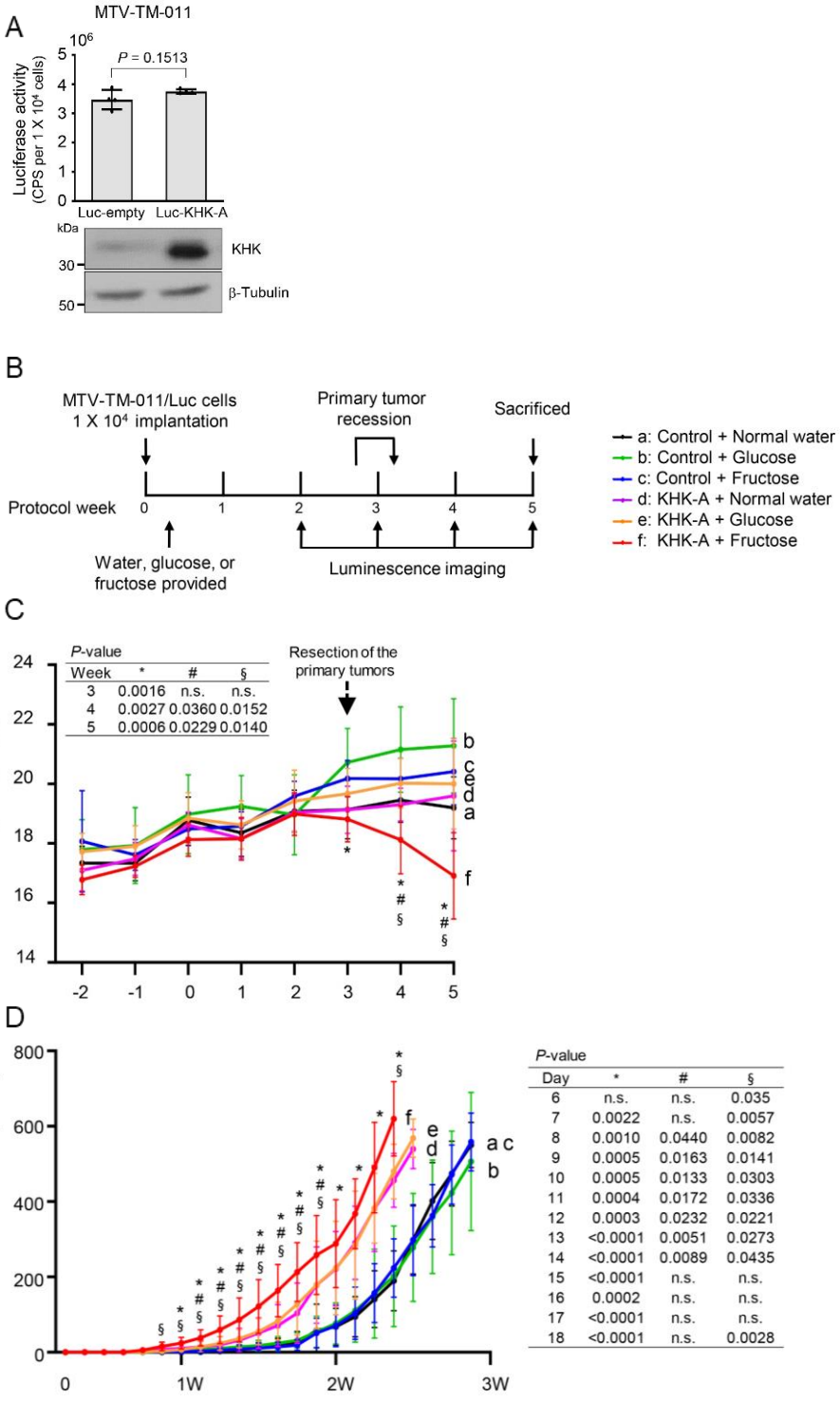
A
MTV-TM-011
Luciferase activity (CPS per 1 X 10⁴ cells)
P = 0.1513
Luc-empty
Luc-KHK-A
kDa
KHK
β-Tubulin
B
MTV-TM-011/Luc cells 1 X 10⁴ implantation
Primary tumor recession
Sacrificed
Protocol week
Water, glucose, or fructose provided
Luminescence imaging
a: Control + Normal water
b: Control + Glucose
c: Control + Fructose
d: KHK-A + Normal water
e: KHK-A + Glucose
f: KHK-A + Fructose
C
P-value
Week * # §
3 0.0016 n.s. n.s.
4 0.0027 0.0360 0.0152
5 0.0006 0.0229 0.0140
Resection of the primary tumors
Body weight (g)
D
Tumor volume (mm³)
1W
2W
3W
P-value
Day * # §
6 n.s. n.s. 0.035
7 0.0022 n.s. 0.0057
8 0.0010 0.0440 0.0082
9 0.0005 0.0163 0.0141
10 0.0005 0.0133 0.0303
11 0.0004 0.0172 0.0336
12 0.0003 0.0232 0.0221
13 <0.0001 0.0051 0.0273
14 <0.0001 0.0089 0.0435
15 <0.0001 n.s. n.s.
16 0.0002 n.s. n.s.
17 <0.0001 n.s. n.s.
18 <0.0001 n.s. 0.0028

Figure 13. Implantation of KHK-A expressing MTV-TM-011 cells in the mammary fat pad

A. Establishment of stable cell lines. MTV-TM-011 cells were transfected with the Luciferase-IRES-GFP or Luciferase-IRES-KHK-A plasmid, and transfected cells were selected using G418. The expressions of luciferase and KHK-A were checked by luminometry and Western blotting respectively. (means ± S.D. from 4 independent experiments, and statistical significance was calculated by an unpaired, two-sided Student's *t*-test). **B**. Schematic diagram for the breast cancer xenograft study. MTV-TM-011 stable cells expressing luciferase and KHK-A (or GFP) were implanted into mammary pads of mice. Tumor-bearing mice were fed with water, 15% glucose or 15% fructose. Primary tumors were removed when the tumor volumes reached 500 - 600 mm^3, and metastatic tumors were observed weekly by luminascence imaging. The condition of each experiemntal group (7 per each group) is described in the right panel. **C**. Body weights of mice were checked once a week and expressed as the means ± S.D. from 7 mice per group. **D**. The volumes of breast tumors were monitored daily using calipers and expressed as the means ± S.D. from 7 mice per group. * denotes $P < 0.05$ between group 'f' versus 'c'; # denotes $P < 0.05$ between group 'f' versus 'd'; § denotes $P < 0.05$ between group 'f' versus 'e'. In **C**, **D**, significance was calculated by a two-sided Mann Whitney *U* test. The results for significance tests are included in each panel.

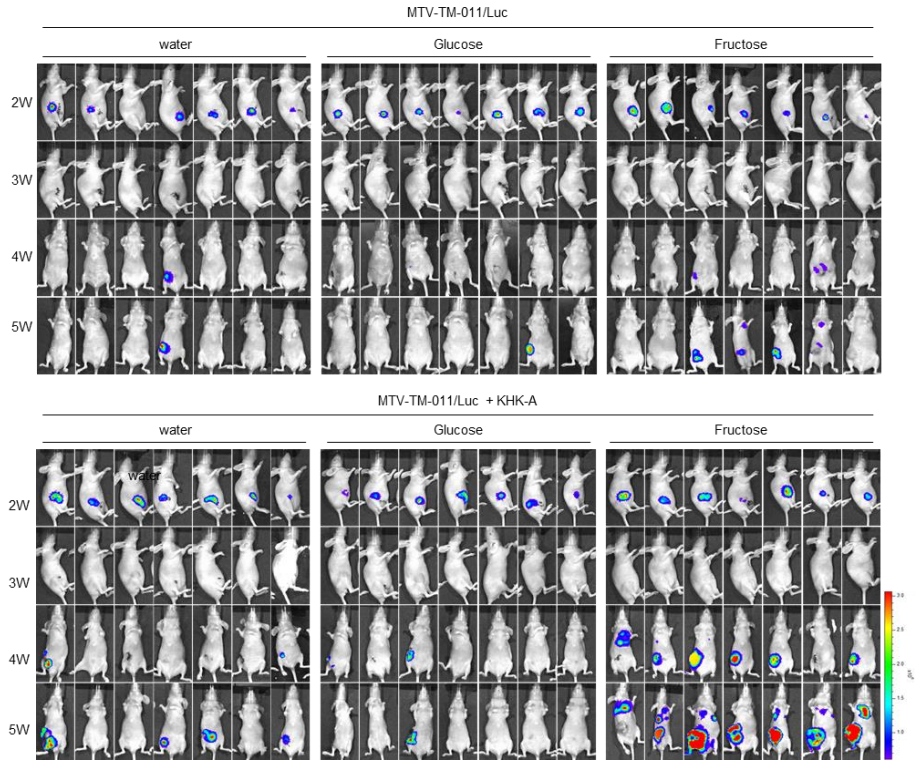

Figure 14. KHK-A potentiates the fructose-induced metastasis in xenografted breast cancer

Bioluminescence images of tumor-bearing mice were taken weekly using Xenogen IVIS 100. The color bar represents bioluminescence intensity counts.

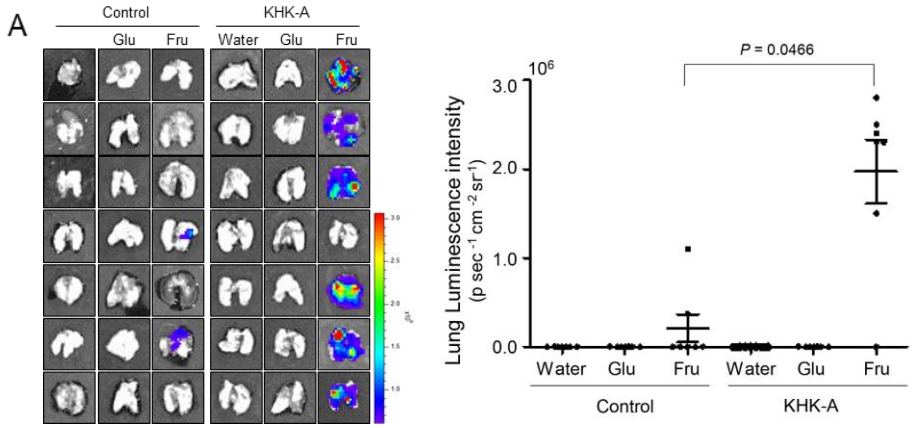
A
Control
KHK-A
Glu
Fru
Water
Glu
Fru
P = 0.0466
10^6
3.0
2.0
1.0
0.0
Lung Luminescence intensity
(p sec^-1 cm^-2 sr^-1)
Water
Glu
Fru
Water
Glu
Fru
Control
KHK-A

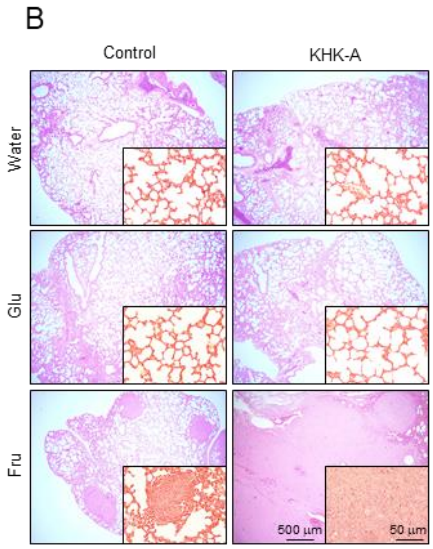
B
Control
KHK-A
Water
Glu
Fru
500 μm
50 μm

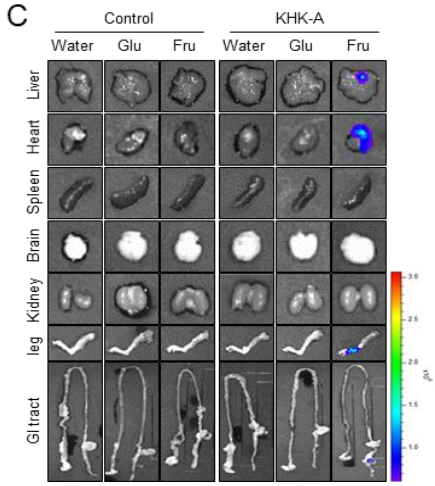
C
Control
KHK-A
Water
Glu
Fru
Water
Glu
Fru
Liver
Heart
Spleen
Brain
Kidney
leg
GI tract

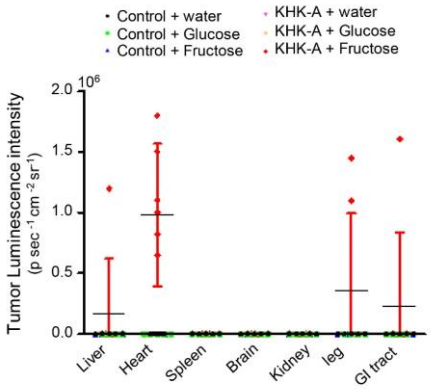
Control + water
Control + Glucose
Control + Fructose
KHK-A + water
KHK-A + Glucose
KHK-A + Fructose
2.0
10^6
1.5
1.0
0.5
0.0
Tumor Luminescence intensity
(p sec^-1 cm^-2 sr^-1)
Liver
Heart
Spleen
Brain
Kidney
leg
GI tract

Figure 15. KHK-A-fructose axis promotes breast to lung metastasis

A. On the 5th week after cancer graft, the organs were excised from mice. Bioluminescence images were captured in the lungs (left). Bioluminescence intensity (photons/sec/ cm^2/sr) in the lungs was quantitatively analyzed (right). Data are represented as means ± S.D. from the lungs harvested from 7 mice per group. Significance was calculated by two-sided Mann Whitney *U* test. The results for significance tests are included in the panel. **B**. Representative pictures of H&E-stained lungs. **C**. In other organs, representative bioluminescence images (left) and quantitative analyses of bioluminescence emission (right). Dots represent the bioluminescence intensities from individual samples, and horizontal bars show the means ± S.D. from all vital orgnas obtained from 7 mice per group.

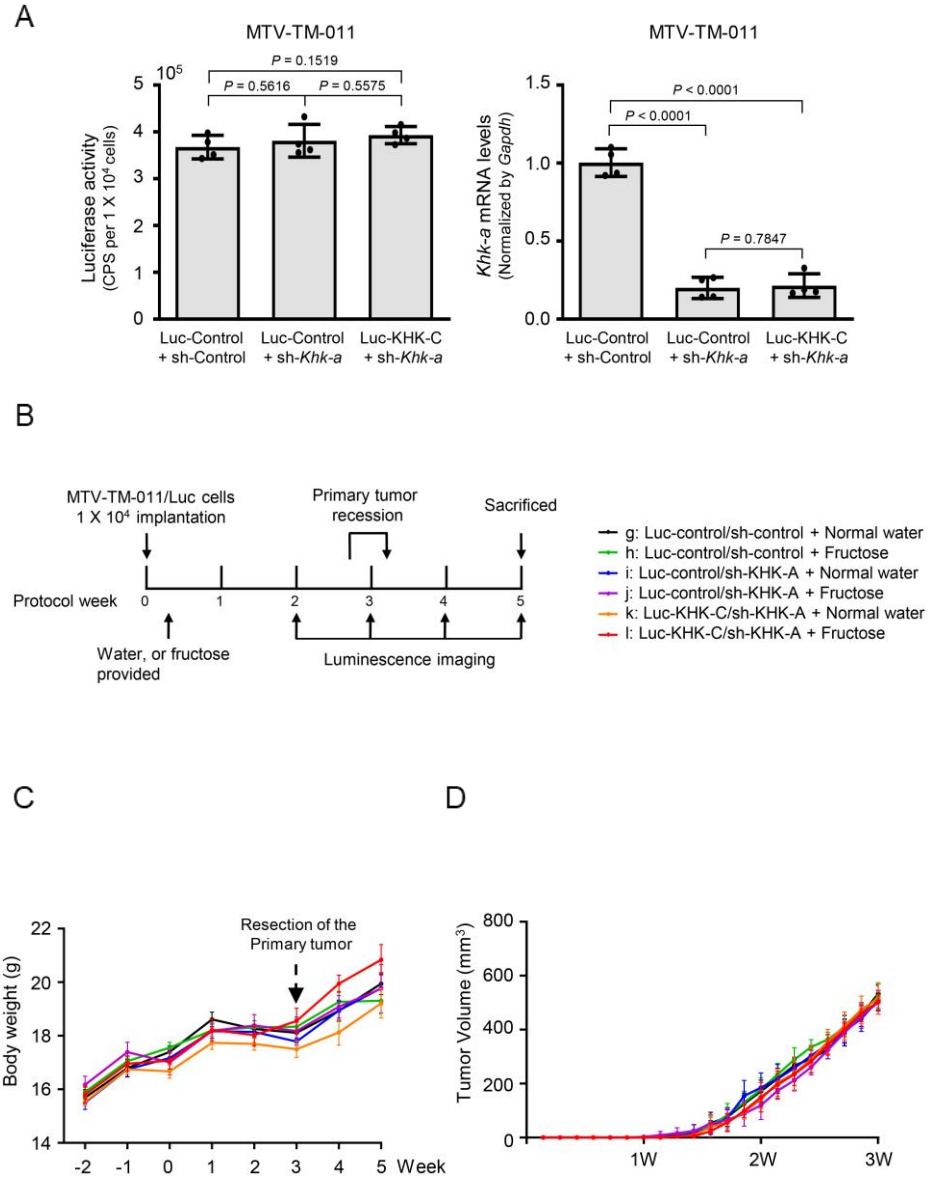
A
MTV-TM-011
P = 0.1519
P = 0.5616
P = 0.5575
10^5
Luciferase activity
(CPS per 1 X 10^4 cells)
Luc-Control + sh-Control
Luc-Control + sh-Khk-a
Luc-KHK-C + sh-Khk-a
MTV-TM-011
P < 0.0001
P < 0.0001
P = 0.7847
Khk-a mRNA levels
(Normalized by Gapdh)
B
MTV-TM-011/Luc cells
1 X 10^4 implantation
Primary tumor recession
Sacrificed
Protocol week
Water, or fructose provided
Luminescence imaging
g: Luc-control/sh-control + Normal water
h: Luc-control/sh-control + Fructose
i: Luc-control/sh-KHK-A + Normal water
j: Luc-control/sh-KHK-A + Fructose
k: Luc-KHK-C/sh-KHK-A + Normal water
l: Luc-KHK-C/sh-KHK-A + Fructose
C
Resection of the Primary tumor
Body weight (g)
Week
D
Tumor Volume (mm^3)
1W
2W
3W

Figure 16. Implantation of KHK-C expressing MTV-TM-011 cells in the mammary fat pad

A. Establishment of stable cell lines. MTV-TM-011 cells were transfected with the Luciferase-IRES-GFP or Luciferase-IRES-KHK-C plasmid, and the cells were also infected with lentiviral shRNA targeting *Khk-a* or a scrambled sequence. Successfully transfected cells were selected using G418, and puromycin. The expression of luciferase and KHK-C were confirmed by luminometry, and silencing of endogenous *Khk-a* were checked by qRT-PCR. Data are presented as means ± S.D. from 4 independent experiments. Significance was calculated by an unpaired, two-sided Student's *t*-test. **B**. Schematic diagram for the breast cancer xenograft study. MTV-TM-011 stable cells expressing luciferase and/or sh-*Khk-a* and/or KHK-C were implanted into mammary pads of mice. Tumor-bearing mice were fed with water, or 15% fructose. Primary tumors were removed when the tumor volumes reached 500 - 600 mm^3, and metastatic tumors were observed weekly by luminascence imaging. **C**. Body weights of mice were checked once a week and expressed as the means ± S.D. from 7 biologically independent mice per group. **D**. The volumes of breast tumors were monitored daily using calipers and expressed as the means ± S.D. The condition of each experimental group is described in the right panel (7 biologically independent mice per group).

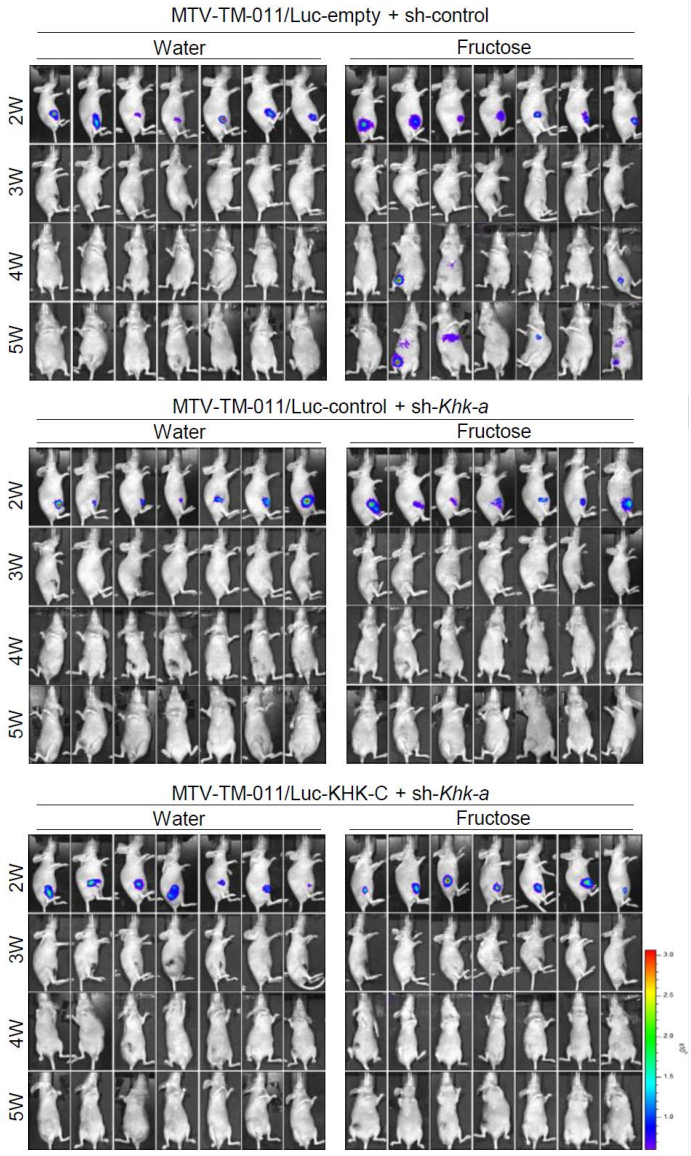

Figure 17. KHK-C does not participate breast cancer metastasis in fructose-fed mice

Bioluminescence images of tumor-bearing mice were taken weekly using Xenogen IVIS 100. The color bar represents bioluminescence intensity counts.

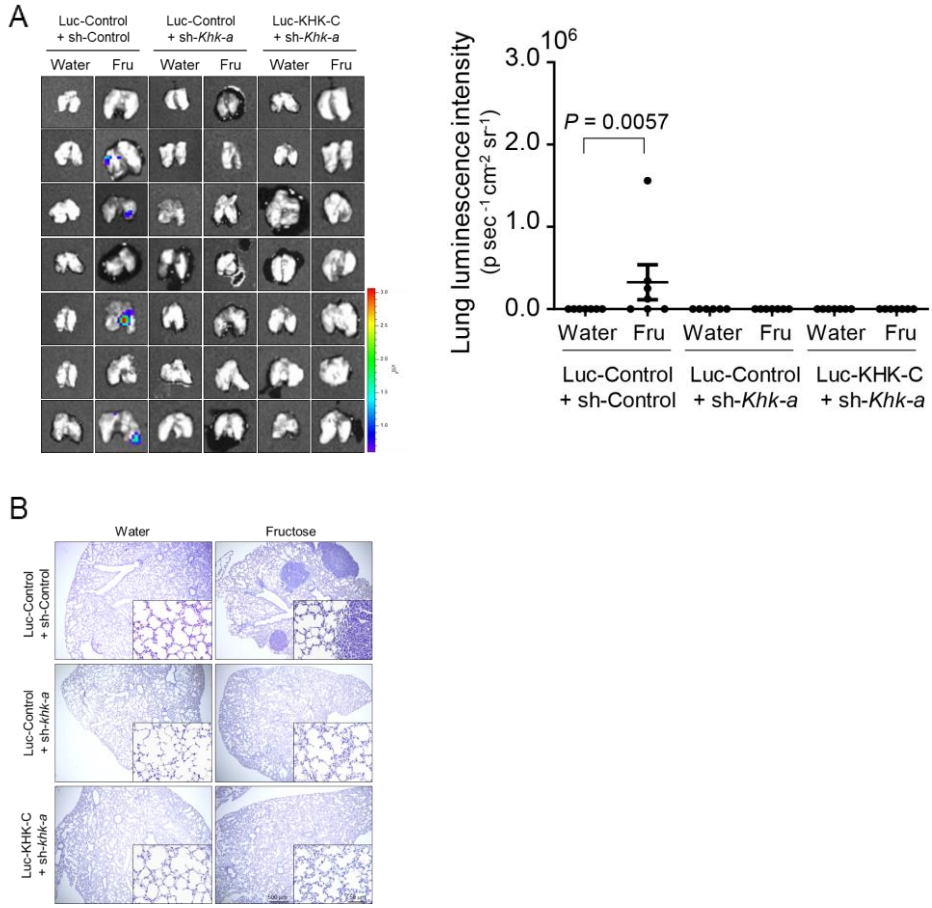

Figure 18. KHK-C shows no effect on breast to lung cancer metastasis in fructose-fed mice

A. On the 5th week after cancer graft, the organs were excised from mice. Bioluminescence images were captured in the lungs (left). Bioluminescence intensity (photones/sec/cm^2/sr) in the lungs was quantitatively analyzed (right). Data are presented as means ± S.D. from 7 lungs from biologically independent mice per group, and statistical significance was calculated by a two-sided Mann Whitney *U* test. **B**. Representative pictures of H&E-stained lungs from the mice represented in figure 14.

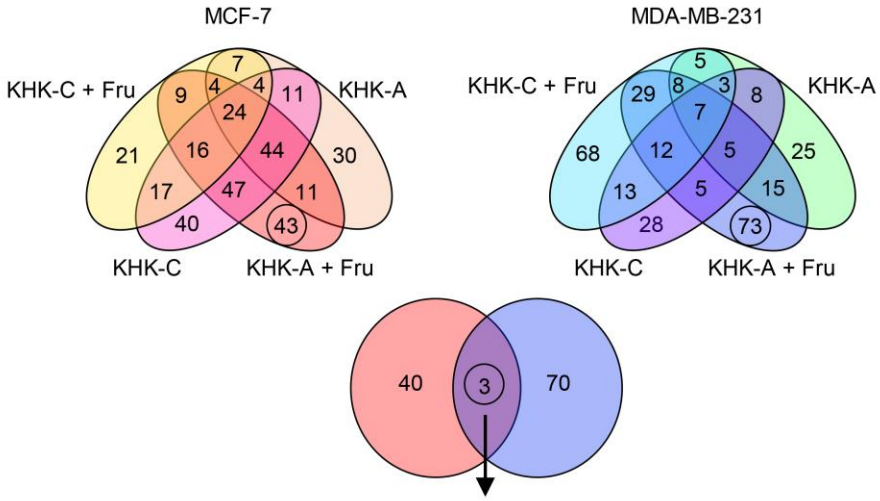

Gene	Protein
YWHAH	14-3-3 protein eta
LRRC59	Leucine-rich repeat-containing protein 59
GLOD4	Glyoxalase domain-containing protein 4

Figure 19. Identification of proteins interacting KHK-A fructose-dependently

Proteomics analyses to identify KHK-A-specific interactome. MCF-7 and MDA-MB-231 cells, which had been transfected with His-KHK-A or -C, were incubated with or without 5 mM fructose for 8 hr. His-tagged proteins were pulled down using Ni-affinity beads, eluted by imidazole, and analyzed by LC-MS/MS. This experiment was performed 3 times independently. Venn diagrams show the numbers of identified proteins in each group (the top panels). Three KHK-A-interacting proteins were identified commonly in two cell lines and are listed in the bottom panel.

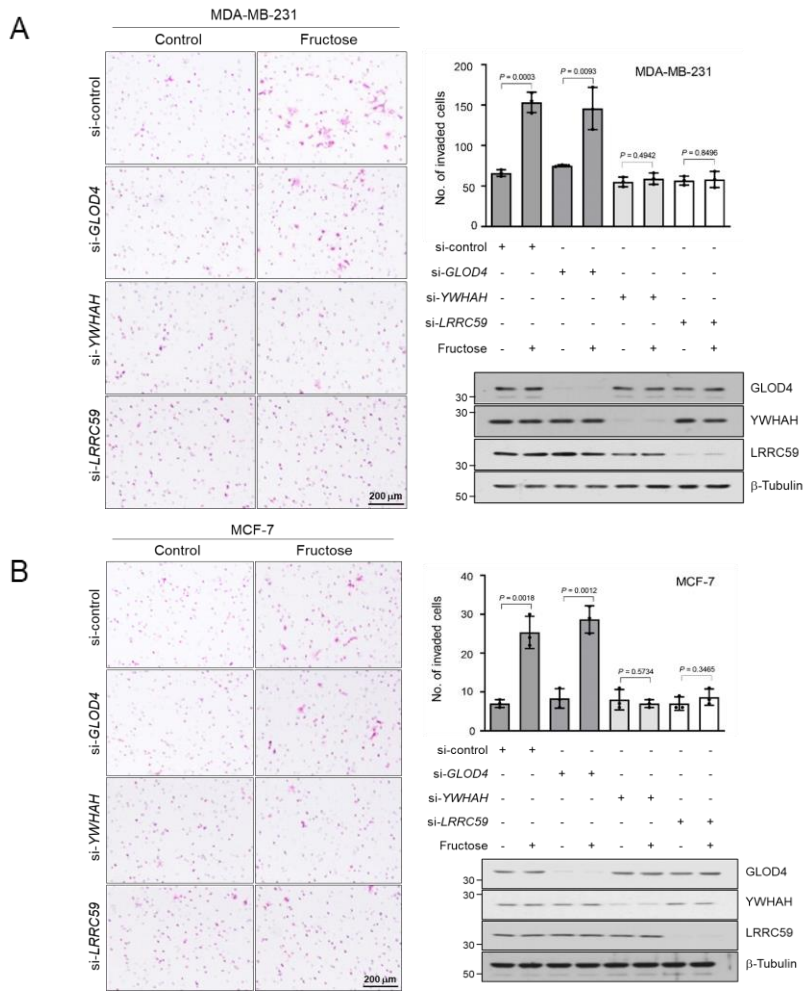

Figure 20. Fructose induced invasions were attenuated by silencing YWHAH or LRRC59

A. MDA-MB-231 and **B**. MCF-7 cells were transfected with the indicated siRNAs, incubated with 5 mM fructose for 48 hours, and subjected to Matrigel invasion analysis. The numbers (means ± S.D. from 3 independent experiments) of invaded cells are presented as bar graphs. Significance was calculated by unpaired, two-sided Student's *t*-test.

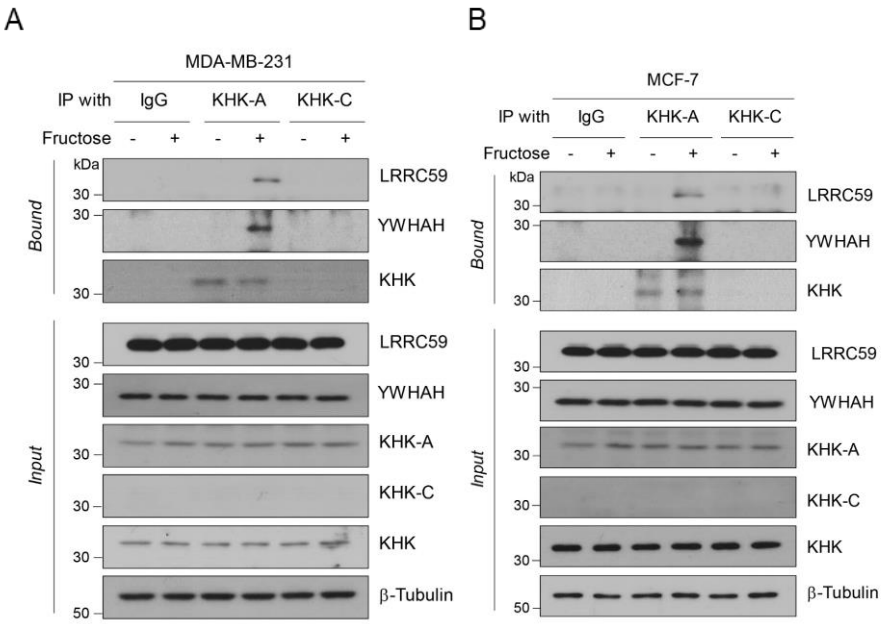

Figure 21. Validation of fructose-dependent interactions in breast cancer cell

A. MDA-MB-23 and **B**. MCF-7 cells were incubated with 5 mM fructose for 8 hr, and cell lysates were immunoprecipitated with IgG, anti-KHK-A or anti-KHK-C, and immunoblotted with anti-LRRC59 or anti-YWHAH antibody.

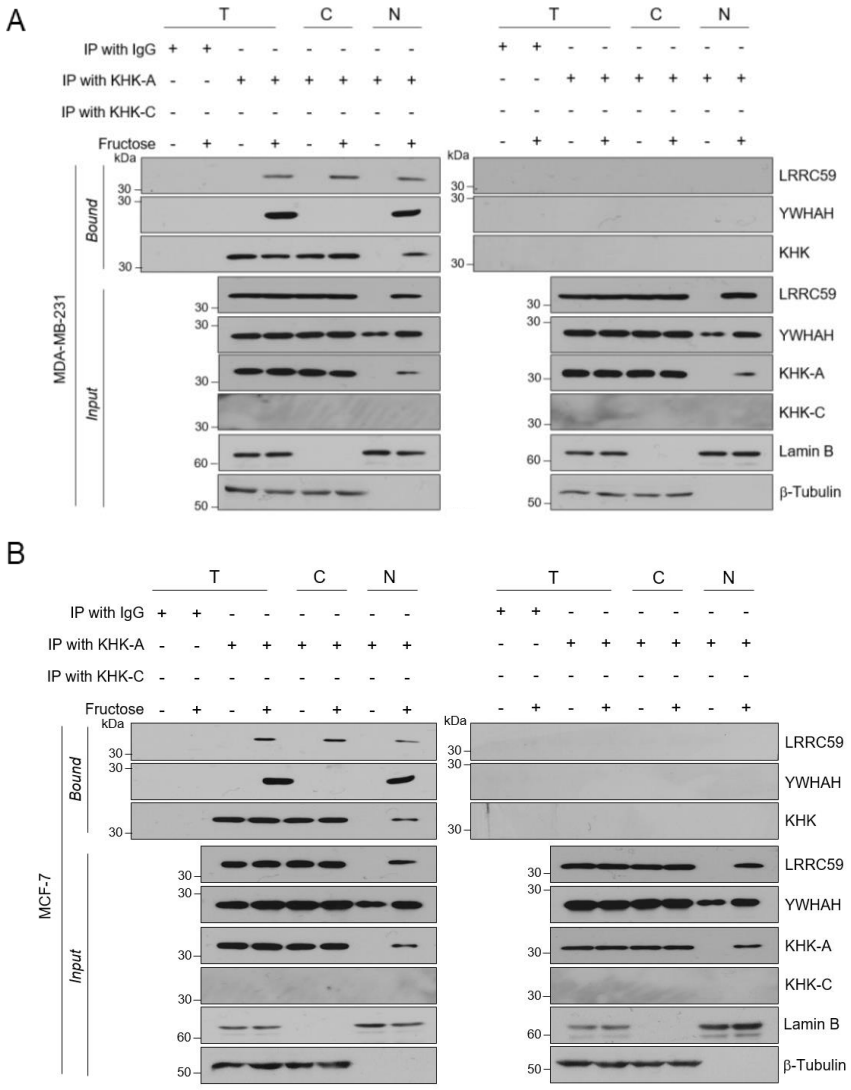

Figure 22. Subcellular localization of KHK-interacting proteins.

A. MDA-MB-231 and **B**. MCF-7 cells were incubated with 5 mM fructose for 8 hr, total lysates (T) were fractionated to cytosolic (C) and nuclear (N) components, which were immunoprecipitated with IgG, anti-KHK-A or anti-KHK-C, and immunoblotted with the indicated antibodies.

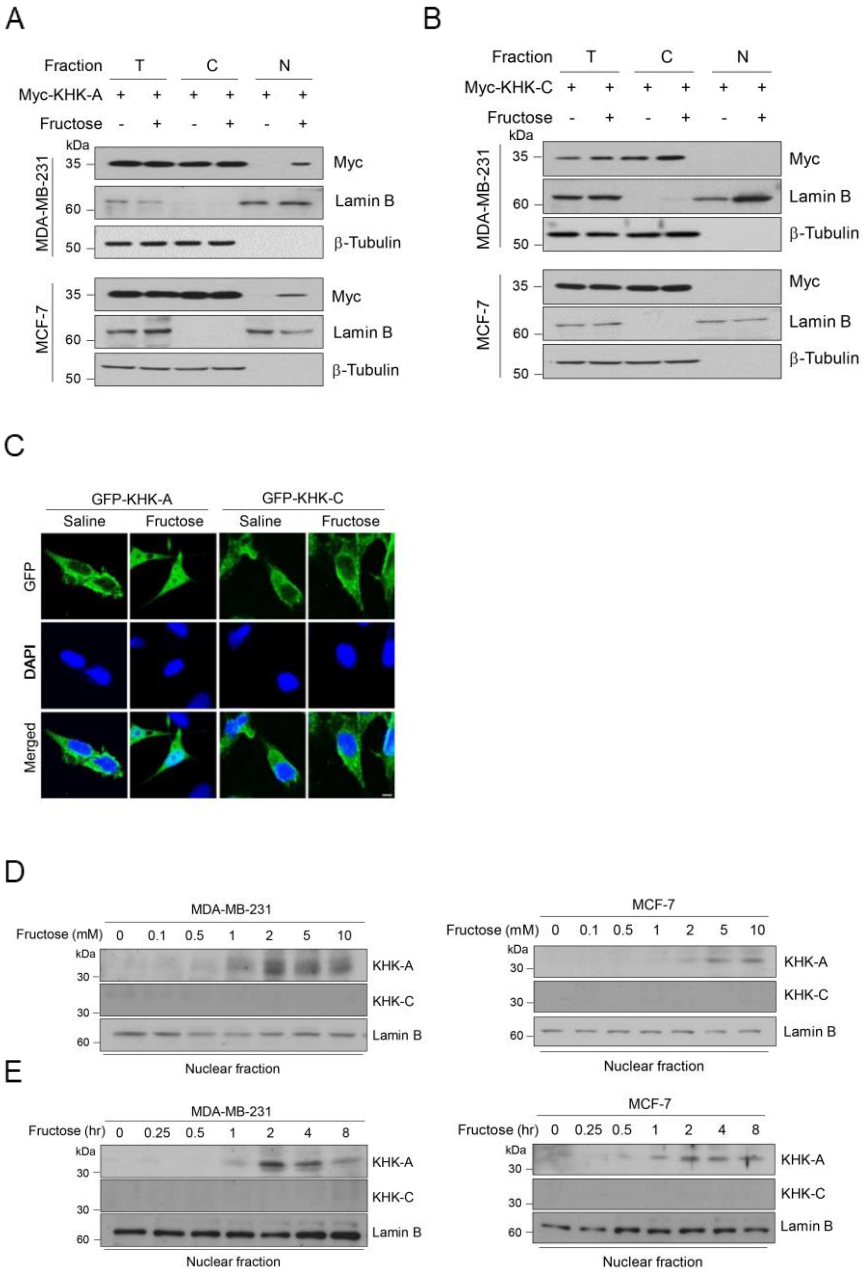
A
Fraction T C N
Myc-KHK-A + + + + + +
Fructose - + - + - +
kDa
MDA-MB-231
35
60
50
Myc
Lamin B
β-Tubulin
MCF-7
35
60
50
Myc
Lamin B
β-Tubulin
B
Fraction T C N
Myc-KHK-C + + + + + +
Fructose - + - + - +
kDa
MDA-MB-231
35
60
50
Myc
Lamin B
β-Tubulin
MCF-7
35
60
50
Myc
Lamin B
β-Tubulin
C
GFP-KHK-A
GFP-KHK-C
Saline
Fructose
Saline
Fructose
GFP
DAPI
Merged
D
MDA-MB-231
Fructose (mM) 0 0.1 0.5 1 2 5 10
kDa
30
30
60
KHK-A
KHK-C
Lamin B
Nuclear fraction
MCF-7
Fructose (mM) 0 0.1 0.5 1 2 5 10
kDa
30
30
60
KHK-A
KHK-C
Lamin B
Nuclear fraction
E
MDA-MB-231
Fructose (hr) 0 0.25 0.5 1 2 4 8
kDa
30
30
60
KHK-A
KHK-C
Lamin B
Nuclear fraction
MCF-7
Fructose (hr) 0 0.25 0.5 1 2 4 8
kDa
30
30
60
KHK-A
KHK-C
Lamin B
Nuclear fraction

Figure 23. Fructose induces translocation of KHK-A from the cytoplasm to the nucleus

A. Subcellular localization of KHK-A. MDA-MB-231 and MCF7 cells were transfected with Myc-KHK-A, and incubated with fructose. Total lysates (T) were fractionated to cytosolic (C) and nuclear (N) components. **B**. MDA-MB-231 and MCF-7 cells were transfected with Myc-KHK-C. The cell fractions were immunoblotted with indicated antibodies. **C**. Immunofluorescence imaging of MDA-MB-231 cells expressing GFP-tagged KHK-A/C (green), and nuclei were counterstained with DAPI (blue). Scale bar = 10 μm. **D**. MDA-MB-231 and MCF-7 cells were treated with fructose at the indicated concentrations for 2 hr. KHK-A and KHK-C were immunoblotted in the nuclear fraction. **E**. MDA-MB-231 and MCF-7 cells were treated with 5 mM fructose for the indicated times. Nuclear KHK-A and KHK-C were immunoblotted.

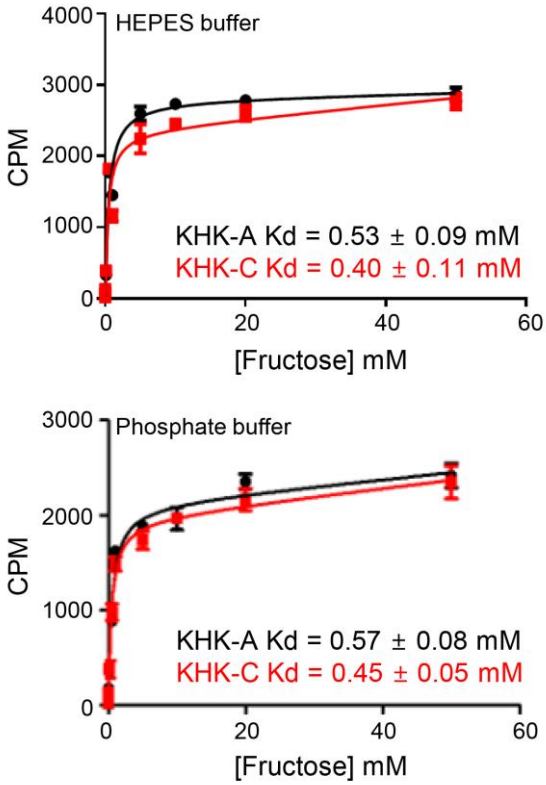

Figure 24. Measurement of the dissociation constant (Kd) for fructose

Recombinant His-KHK-A and His-KHK-C were incubated with various concentrations of fructose in HEPES or phosphate buffer. The K_d values of KHK-A and KHK-C for fructose were calculated based on the binding-saturation model. Data are presented as means ± S.D. from 3 independent experiments.

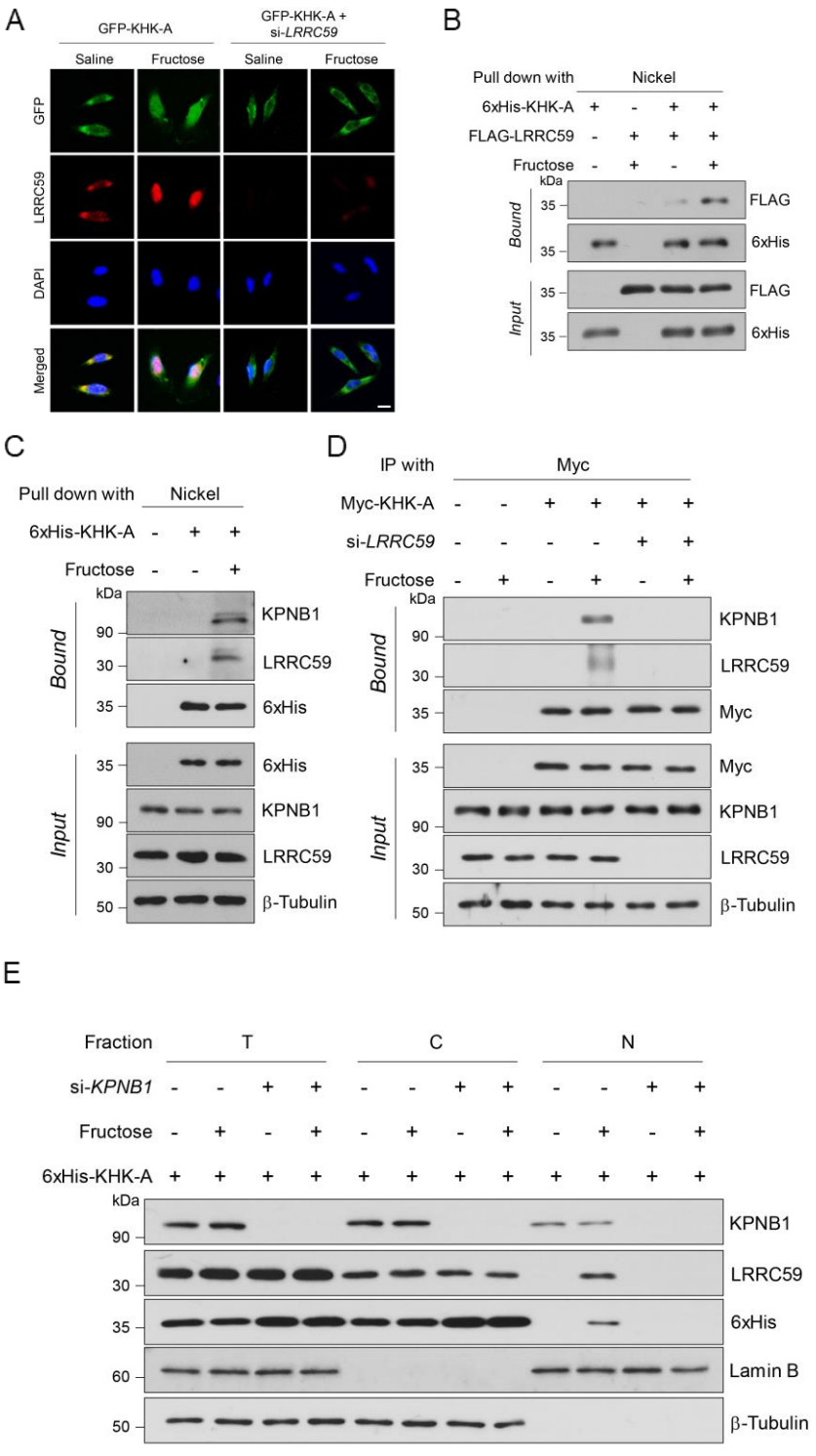
A
GFP-KHK-A
GFP-KHK-A + si-LRRC59
Saline
Fructose
Saline
Fructose
GFP
LRRC59
DAPI
Merged
B
Pull down with
Nickel
6xHis-KHK-A + - + +
FLAG-LRRC59 - + + +
Fructose - + - +
kDa
Bound
35
FLAG
35
6xHis
Input
35
FLAG
35
6xHis
C
Pull down with
Nickel
6xHis-KHK-A - + +
Fructose - - +
kDa
Bound
90
KPNB1
30
LRRC59
35
6xHis
Input
35
6xHis
90
KPNB1
30
LRRC59
50
β-Tubulin
D
IP with
Myc
Myc-KHK-A - - + + + +
si-LRRC59 - - - - + +
Fructose - + - + - +
kDa
Bound
90
KPNB1
30
LRRC59
35
Myc
Input
35
Myc
90
KPNB1
30
LRRC59
50
β-Tubulin
E
Fraction
T
C
N
si-KPNB1 - - + + - - + + - - + +
Fructose - + - + - + - + - + - +
6xHis-KHK-A + + + + + + + + + + + +
kDa
90
KPNB1
30
LRRC59
35
6xHis
60
Lamin B
50
β-Tubulin

Figure 25. LRRC59 in concert with KPNB1 mediates the nuclear translocation of KHK-A

A. Transfected MDA-MB-231 cells were incubated with 5 mM fructose for 8 hr. Immunofluorescence images of GFP-tagged KHK-A (Green), endogenous LRRC59 (Red), and DAPI (blue). Scale bar = 10 μm. **B**. *In vitro* binding of KHK-A and LRRC59. His-KHK-A or Flag-LRRC59 proteins were purified from HEK293T cells using Nickel-NTA or anti-Flag antibody, and incubated together for 1 hr with or without 1 mM fructose. His-KHK-A was pulled down using Nickel-NTA and immunoblotted with anti-Flag antibody. **C**. KHK-A binding to LRRC59 and KPNB1. MDA-MB-231 cells expressng His-KHK-A were treated with 5 mM fructose for 8 hours. His-KHK was pulled down using Nickel-NTA, and the co-precipitated LRRC59 and KPNB1were immunoblotted. **D**. LRRC59 is required for the KHK-A binding to KPNB1. MDA-MB-231 cells, which had been co-transfected with Myc-KHK-A and LRRC59 si-RNA, were incubated with 5 mM fructose for 8 hours. Myc-KHK-A was immunoprecipitated and co-precipitaed proteins were immunoblotted. **E**. KPNB1-dependent nuclaer translocation of KHK-A. MDA-MB-231 cells, which had been co-transfected with His-KHK-A and KPNB1 si-RNA (or control si-RNA), were treated with 5 mM fructose for 8 hours. The cell fractions were immunoblotted.

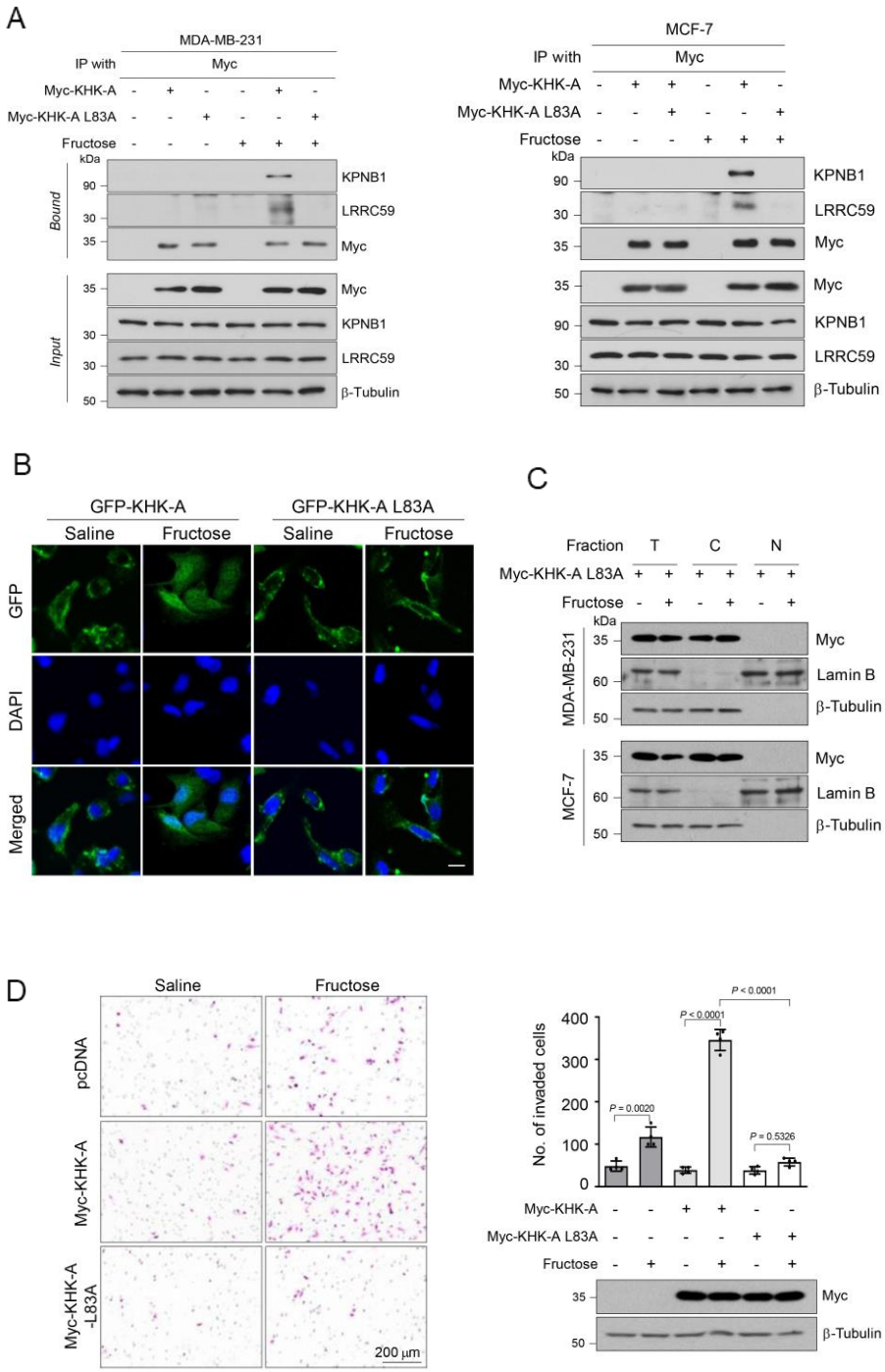
A
MDA-MB-231
IP with
Myc
Myc-KHK-A
Myc-KHK-A L83A
Fructose
kDa
Bound
Input
KPNB1
LRRC59
Myc
β-Tubulin
MCF-7
B
GFP-KHK-A
GFP-KHK-A L83A
Saline
Fructose
GFP
DAPI
Merged
C
Fraction
T
C
N
Myc-KHK-A L83A
Fructose
MDA-MB-231
MCF-7
Lamin B
D
pcDNA
Myc-KHK-A
Myc-KHK-A -L83A
200 μm
No. of invaded cells
P = 0.0020
P < 0.0001
P < 0.0001
P = 0.5326

Figure 26. The L83 residue participates in the KHK-A interaction with LRRC59 and KPNB1

A. MDA-MB-231 and MCF-7 cells were transfected with Myc-KHK-A or Myc-KHK-A_L83A, and incubated with 5 mM fructose. The cell lysates were immunoprecipitated with anti-Myc and immunoblotted with anti-LRRC59 or anti-KPNB1. **B**. Immunofluorescence imaging of GFP-tagged KHK-A wild type or L83A (green) in MDA-MB-231 cells which were treated with fructose. All samples were counter-stained with DAPI (blue). Scale bar = 10 μm. **C**. Subcellular localization of KHK-A L83A. MDA-MB-231 and MCF7 cells were transfected with Myc-KHK-A L83A. **D**. MDA-MB-231 cells were transfected with Myc-KHK-A wild type or L83A mutant plasmid, and treated with 5 mM fructose for 48 hr, then subjected to invasion assay. The numbers (means ± S.D. from 4 independent experiments, *P*-value was calculated by unpaired, two-sided Student's *t*-test) of invaded cells shown in the bar graphs.

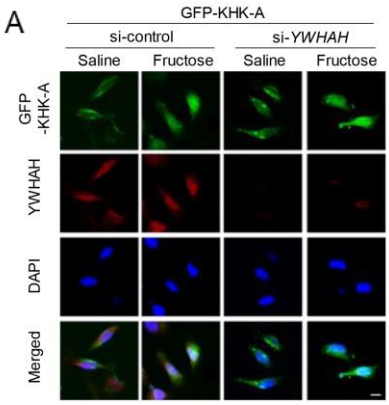
A
GFP-KHK-A
si-control
si-YWHAH
Saline
Fructose
Saline
Fructose
GFP -KHK-A
YWHAH
DAPI
Merged

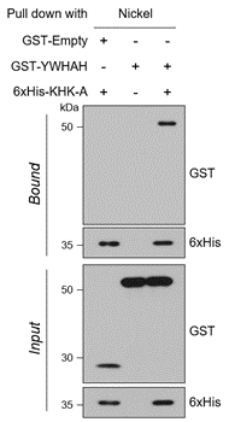
B
Pull down with
Nickel
GST-Empty
GST-YWHAH
6xHis-KHK-A
kDa
Bound
GST
6xHis
Input
GST
6xHis

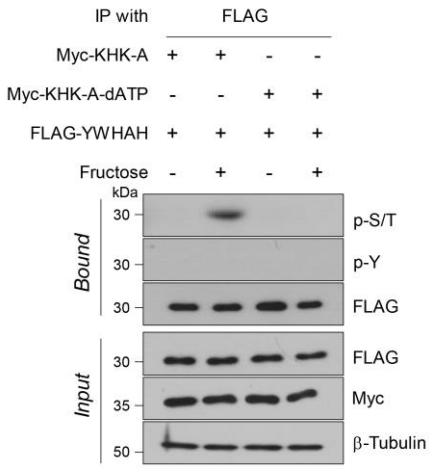
C
IP with
FLAG
Myc-KHK-A
Myc-KHK-A-dATP
FLAG-YWHAH
Fructose
kDa
Bound
p-S/T
p-Y
FLAG
Input
FLAG
Myc
β-Tubulin

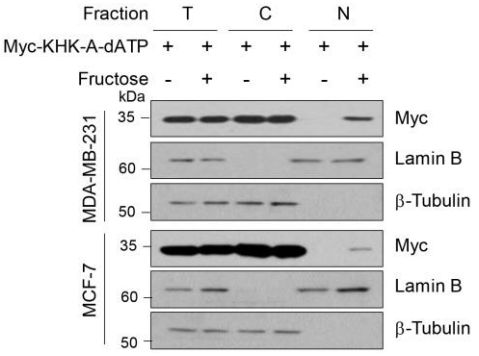
D
Fraction
T
C
N
Myc-KHK-A-dATP
Fructose
kDa
MDA-MB-231
Myc
Lamin B
β-Tubulin
MCF-7
Myc
Lamin B
β-Tubulin

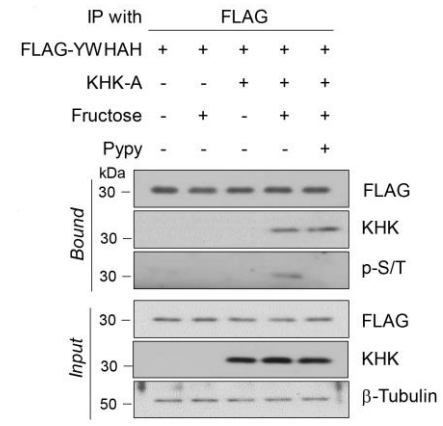
E
IP with
FLAG
FLAG-YWHAH
KHK-A
Fructose
Pypy
kDa
Bound
FLAG
KHK
p-S/T
Input
FLAG
KHK
β-Tubulin

Figure 27. KHK-A functions as a nuclear protein kinase

A. Immunofluorescence imaging of KHK-A (green) and YWHAH (red). MDA-MB-231 cells were incubated with 5 mM fructose for 8 hours. Scale bar represent 10 μm. **B**. *In vitro* binding assay. Purified recombinant GST-YWHAH (or GST) were incubated with purified KHK-A in a test tube for 1 hr and pulled down using nickel-affinity beads. Interaction between KHK-A and YWHAH was evaluated by immunoblotting. **C**. KHK-A-dependent phosphorylation of YWHAH. FLAG-YWHAH was co-transfected with Myc-KHK-A or Myc-KHK-A-dATP. After 8 h-incubation with 5 mM fructose, MDA-MB-231 cells were subjected to immunoprecipitation and immunoblotting. **D**. MDA-MB-231 and MCF7 cells were transfected with Myc-KHK-A_dATP, and incubated with 5 mM fructose for 8 hours, and total lysates (T) were fractionated to cytosolic (C) and nuclear (N) components. **E**. MDA-MB-231 stable cells expressing KHK-A were transfected with FLAG-YWHAH, were incubated with 5 mM fructose and/or 400 nM Pypy for 8 hours.

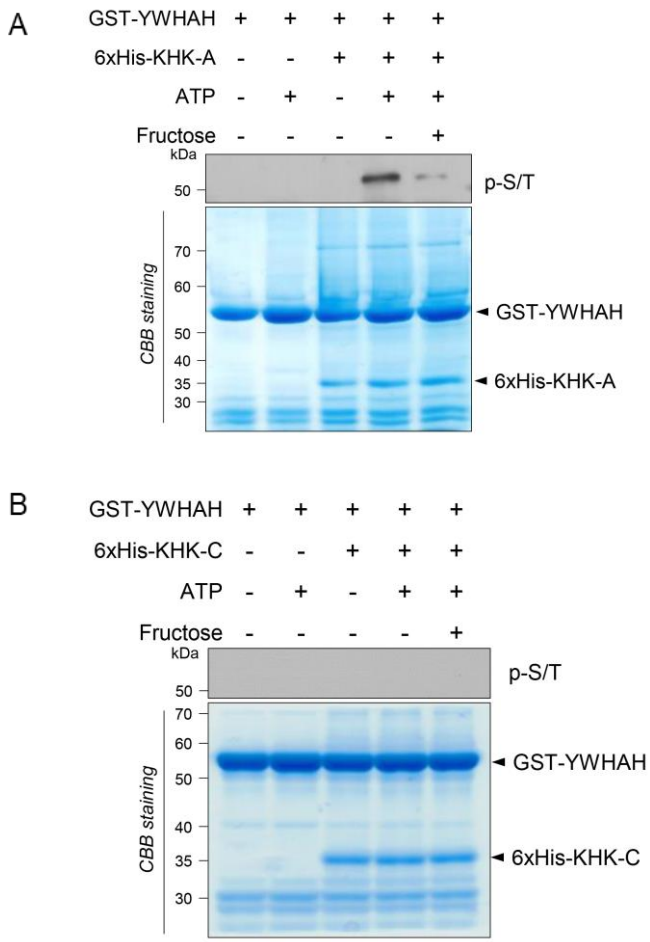

Figure 28. KHK-A, rather than KHK-C phosphorylates YWHAH *in vitro*. **A**. *In vitro* kinase assay. Recombinant GST-YWHAH and His-KHK-A were co-incubated without or with 1 mM fructose in a kinase buffer. The Ser/Thr-phosphorylation of YWHAH was evaluated by immunoblotting, and the protein loading was verified by Coomassie staining. **B**. Recombinant GST-YWHAH and His-KHK-C were co-incubated without or with 1 mM fructose in a kinase buffer. The Ser/Thr-phosphorylation of YWHAH was confirmed by immunoblotting

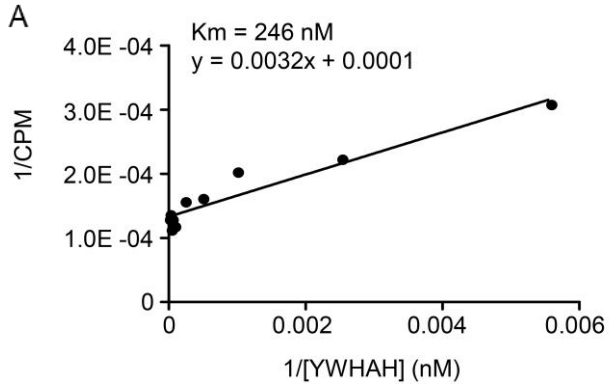
A
Km = 246 nM
y = 0.0032x + 0.0001
4.0E -04
3.0E -04
2.0E -04
1.0E -04
0
1/CPM
0
0.002
0.004
0.006
1/[YWHAH] (nM)

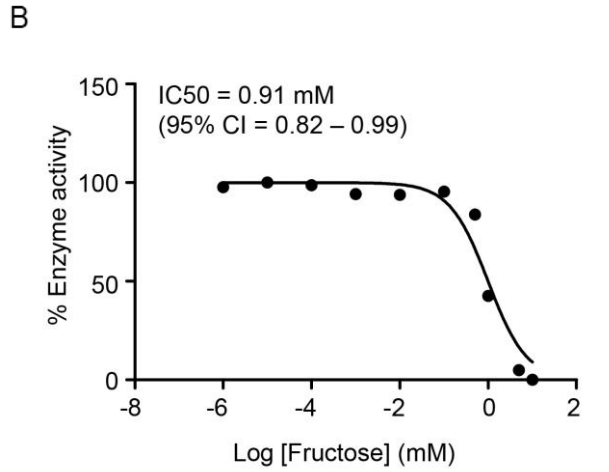
B
IC50 = 0.91 mM
(95% CI = 0.82 – 0.99)
150
100
50
0
% Enzyme activity
-8
-6
-4
-2
0
2
Log [Fructose] (mM)

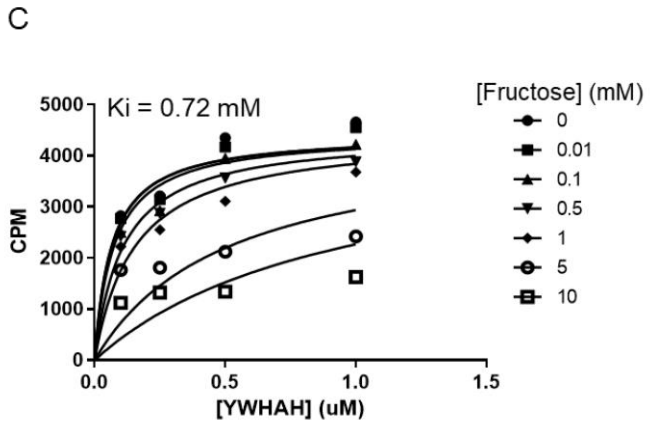
C
Ki = 0.72 mM
5000
4000
3000
2000
1000
0
CPM
0.0
0.5
1.0
1.5
[YWHAH] (uM)
[Fructose] (mM)
0
0.01
0.1
0.5
1
5
10

Figure 29. Effects of fructose on the YWHAH phosphorylation by KHK-A

A. The Km value of GST-KHK-A for GST-YWHAH with representative plotting of 1/CPM versus 1/[YWHAH] was analyzed. **B**. The IC50 of KHK-A for YWHAH was calculated by plotting of percentage of KHK-A enzyme activity versus log[fructose]. **C**. The K_i of fructose for the KHK-A-mediated YWHAH phosphorylation was fitted with the competitive inhibition model.

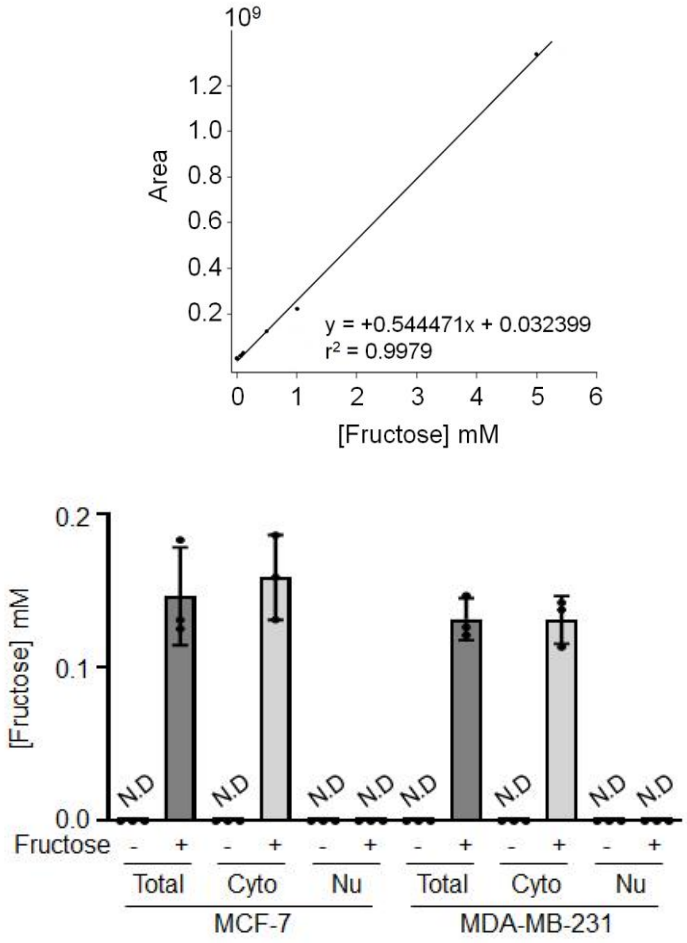

Figure 30. Subcellular fructose concentration

MCF-7 and MDA-MB-231 cells were treated with 5 mM fructose for 4 hours. Fructose concentration in each total, cytoplasmic, and nuclear fraction were calculated based on a standard curve which is generated by known fructose concentration. Measured fructose levels were normalized by packed cell volume. Data are presented as means ± S.D. from 3 independent experiments

A

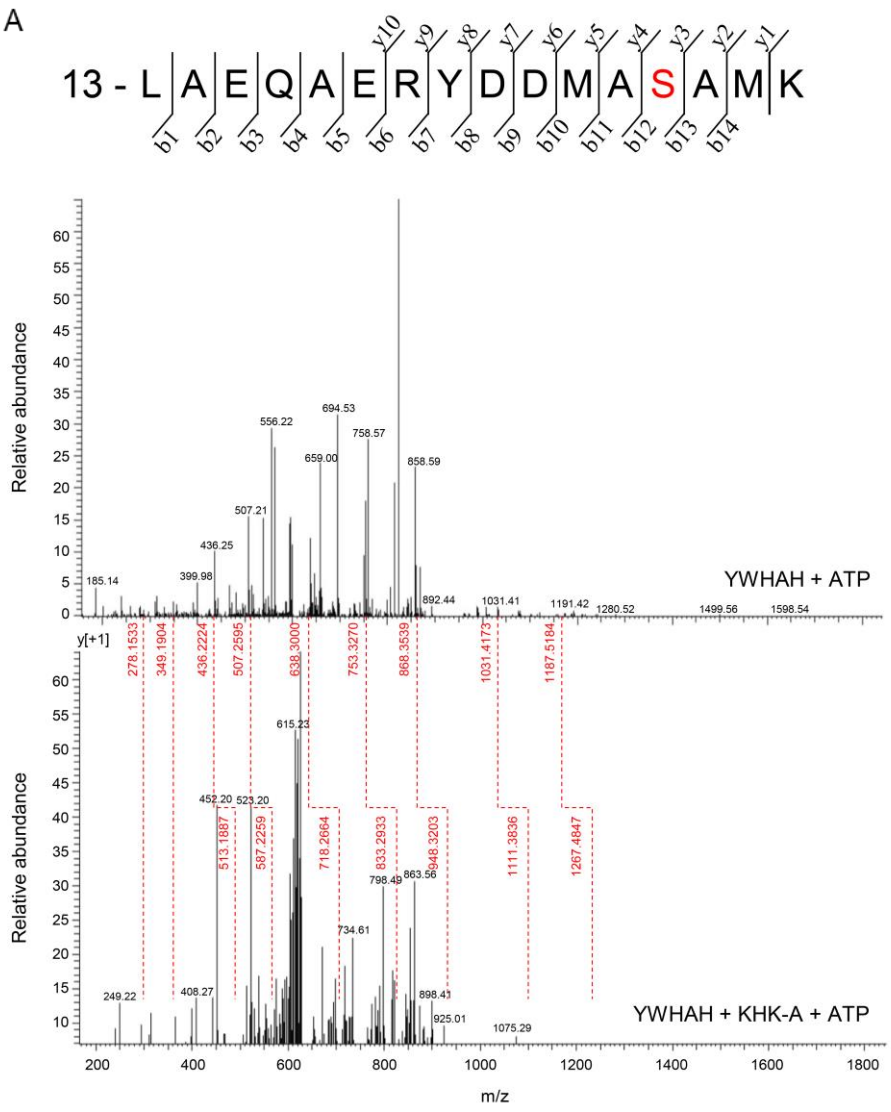
13 - L A E Q A E R Y D D M A S A M K
b1 b2 b3 b4 b5 b6 b7 b8 b9 b10 b11 b12 b13 b14
y10 y9 y8 y7 y6 y5 y4 y3 y2 y1
Relative abundance
YWHAH + ATP
y[+1]
YWHAH + KHK-A + ATP
m/z

B

#1	b^{+}	b^{2+}	b^{3+}	Seq.	y^{+}	y^{2+}	y^{3+}	#2
1	114.09135	57.54931	38.70197	L				16
2	185.12847	93.06787	62.38101	A	1715.73644	858.37186	572.58366	15
3	314.17107	157.58917	105.39521	E	1644.69932	822.85330	548.90462	14
4	442.22965	221.61846	148.08140	Q	1515.65672	758.33200	505.89042	13
5	513.26677	257.13702	171.76044	A	1387.59814	694.30271	463.20423	12
6	642.30937	321.65832	214.77464	E	1316.56102	658.78415	439.52519	11
7	798.41049	399.70888	266.80835	R	1187.51842	594.26285	396.51099	10
8	961.47381	481.24054	321.16279	Y	1031.41730	516.21229	344.47728	9
9	1076.50076	538.75402	359.50510	D	868.35398	434.68063	290.12284	8
10	1191.52771	596.26749	397.84742	D	753.32703	377.16715	251.78053	7
11	1322.56821	661.78774	441.52759	M	638.30008	319.65368	213.43821	6
12	1393.60533	697.30630	465.20663	A	507.25958	254.13343	169.75804	5
13	1480.63736	740.82232	494.21730	S	436.22246	218.61487	146.07900	4
14	1551.67448	776.34088	517.89634	A	349.19043	175.09885	117.06833	3
15	1682.71498	841.86113	561.57651	M	278.15331	139.58029	93.38929	2
16				K	147.11281	74.06004	49.70912	1

#1	b^{+}	b^{2+}	b^{3+}	Seq.	y^{+}	y^{2+}	y^{3+}	#2
1	114.09135	57.54931	38.70197	L				16
2	185.12847	93.06787	62.38101	A	1795.70277	898.35502	599.23911	15
3	314.17107	157.58917	105.39521	E	1724.66565	862.83646	575.56007	14
4	442.22965	221.61846	148.08140	Q	1595.62305	798.31516	532.54587	13
5	513.26677	257.13702	171.76044	A	1467.56447	734.28587	489.85968	12
6	642.30937	321.65832	214.77464	E	1396.52735	698.76731	466.18064	11
7	798.41049	399.70888	266.80835	R	1267.48475	634.24601	423.16644	10
8	961.47381	481.24054	321.16279	Y	1111.38363	556.19545	371.13273	9
9	1076.50076	538.75402	359.50510	D	948.32031	474.66379	316.77829	8
10	1191.52771	596.26749	397.84742	D	833.29336	417.15032	278.43597	7
11	1322.56821	661.78774	441.52759	M	718.26641	359.63684	240.09366	6
12	1393.60533	697.30630	465.20663	A	587.22591	294.11659	196.41349	5
13	1560.60389	780.80548	520.87275	S-Phospho	516.18879	258.59803	172.73445	4
14	1631.64081	816.32404	544.55179	A	349.19043	175.09885	117.06833	3
15	1762.68131	881.84429	588.23195	M	278.15331	139.58029	93.38929	2
16				K	147.11281	74.06004	49.70912	1

C

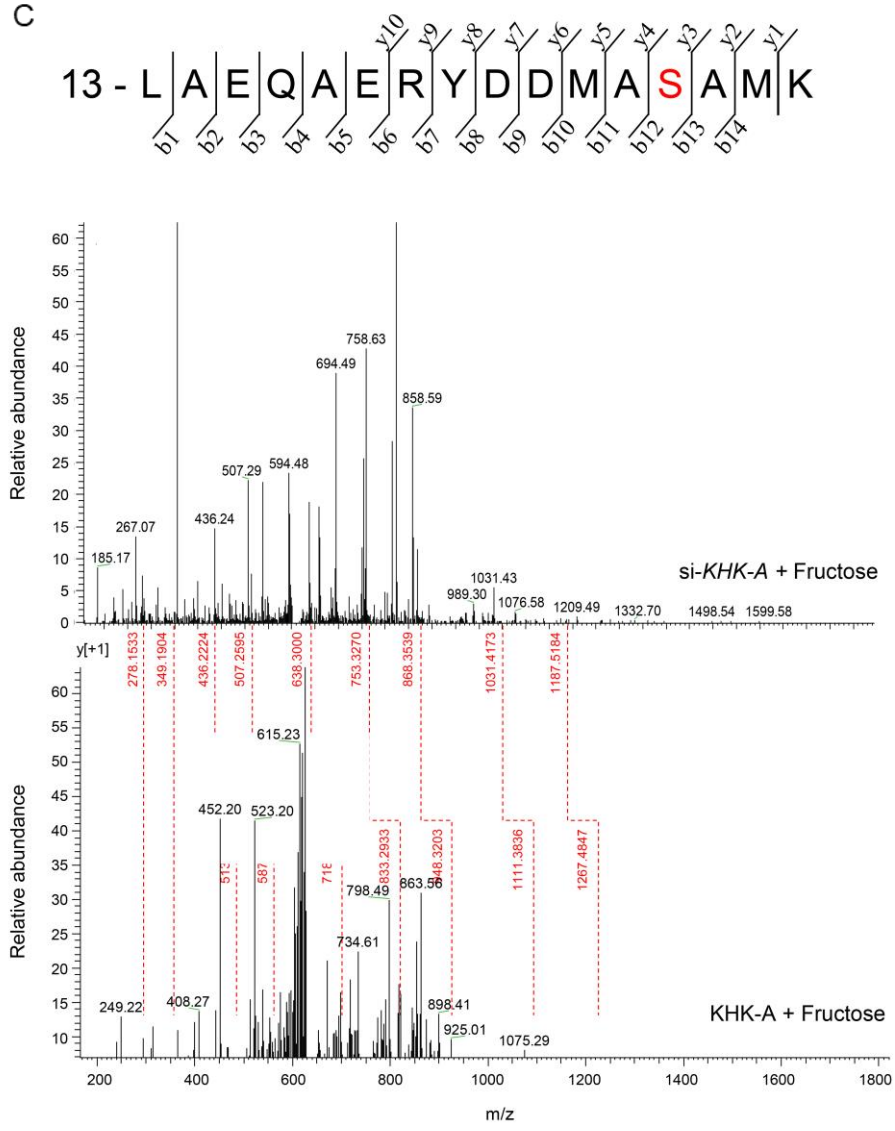
13 - L A E Q A E R Y D D M A S A M K
b1 b2 b3 b4 b5 b6 b7 b8 b9 b10 b11 b12 b13 b14
y10 y9 y8 y7 y6 y5 y4 y3 y2 y1
Relative abundance
si-KHK-A + Fructose
KHK-A + Fructose
y[+1]
m/z

D

#1	b^{+}	b^{2+}	b^{3+}	Seq.	y^{+}	y^{2+}	y^{3+}	#2
1	114.09135	57.54931	38.70197	L				16
2	185.12847	93.06787	62.38101	A	1715.73644	858.37186	572.58366	15
3	314.17107	157.58917	105.39521	E	1644.69932	822.85330	548.90462	14
4	442.22965	221.61846	148.08140	Q	1515.65672	758.33200	505.89042	13
5	513.26677	257.13702	171.76044	A	1387.59814	694.30271	463.20423	12
6	642.30937	321.65832	214.77464	E	1316.56102	658.78415	439.52519	11
7	798.41049	399.70888	266.80835	R	1187.51842	594.26285	396.51099	10
8	961.47381	481.24054	321.16279	Y	1031.41730	516.21229	344.47728	9
9	1076.50076	538.75402	359.50510	D	868.35398	434.68063	290.12284	8
10	1191.52771	596.26749	397.84742	D	753.32703	377.16715	251.78053	7
11	1322.56821	661.78774	441.52759	M	638.30008	319.65368	213.43821	6
12	1393.60533	697.30630	465.20663	A	507.25958	254.13343	169.75804	5
13	1480.63736	740.82232	494.21730	S	436.22246	218.61487	146.07900	4
14	1551.67448	776.34088	517.89634	A	349.19043	175.09885	117.06833	3
15	1682.71498	841.86113	561.57651	M	278.15331	139.58029	93.38929	2
16				K	147.11281	74.06004	49.70912	1

#1	b^{+}	b^{2+}	b^{3+}	Seq.	y^{+}	y^{2+}	y^{3+}	#2
1	114.09135	57.54931	38.70197	L				16
2	185.12847	93.06787	62.38101	A	1795.70277	898.35502	599.23911	15
3	314.17107	157.58917	105.39521	E	1724.66565	862.83646	575.56007	14
4	442.22965	221.61846	148.08140	Q	1595.62305	798.31516	532.54587	13
5	513.26677	257.13702	171.76044	A	1467.56447	734.28587	489.85968	12
6	642.30937	321.65832	214.77464	E	1396.52735	698.76731	466.18064	11
7	798.41049	399.70888	266.80835	R	1267.48475	634.24601	423.16644	10
8	961.47381	481.24054	321.16279	Y	1111.38363	556.19545	371.13273	9
9	1076.50076	538.75402	359.50510	D	948.32031	474.66379	316.77829	8
10	1191.52771	596.26749	397.84742	D	833.29336	417.15032	278.43597	7
11	1322.56821	661.78774	441.52759	M	718.26641	359.63684	240.09366	6
12	1393.60533	697.30630	465.20663	A	587.22591	294.11659	196.41349	5
13	1560.60369	780.80548	520.87275	S-Phospho	516.18879	258.59803	172.73445	4
14	1631.64081	816.32404	544.55179	A	349.19043	175.09885	117.06833	3
15	1762.68131	881.84429	588.23195	M	278.15331	139.58029	93.38929	2
16				K	147.11281	74.06004	49.70912	1

E

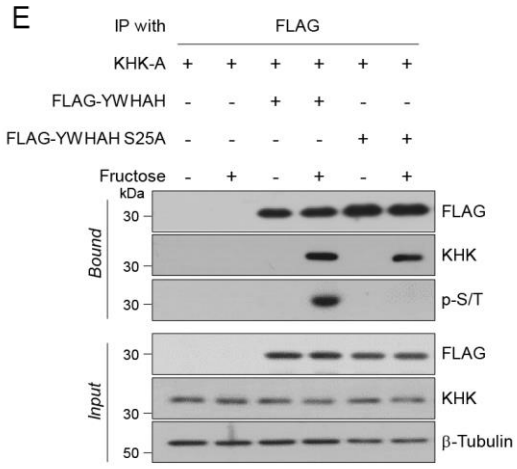

Figure 31. KHK-A phosphorylates YWHAH at Ser25

A. Recombinant GST-YWHAH was reacted with or without GST-KHK-A in a kinase buffer, electrophoresed on SDS-PAGE, and digested in gel. The phosphorylation of Ser25 residue in YWHAH was identified based on LC-MS/MS spectra. **B**. MS/MS spectra of the trypsin-digested YWHAH-derived peptides LAEQAERYDDMASAMK in control (MH+:1828.82279, upper left panel) and phosphorylated (MH+: 1908.79209, lower left panel). The coverage of YWHAH protein was 63% and 65% in control and phosphorylated group, respectively, where protein sequence coverage was calculated based on peptide sequence comparison by Proteome Discoverer (v1.2.0.208 with SEQUEST algorithm) (NCBI Reference Sequence: NP_003396.1, 14-3-3 protein eta [Homo sapience]). Fragment ions detected in MS/MS spectra of LAEQAERYDDMASAMK in un-phosphorylated (upper right panel). Fragment ions detected in MS/MS spectra of LAEQAERYDDMASAMK in phosphorylated (lower right panel). Matched b ions are colored in red and y ions in blue (right panel). **C**. Mass spectrometric analysis for phosphorylation site of YWHAH in MCF-7 cell lysate. The cell lysates were subjected to LC-MS/MS analysis. **D**. MS/MS spectra of the trypsin-digested YWHAH-derived peptides LAEQAERYDDMASAMK in control (MH+:1828.82151, upper left panel) and phosphorylated (MH+: 1908.79428, lower left panel). The coverage of YWHAH protein was 67% and 67% in control and phosphorylated group, respectively, where protein sequence coverage was calculated based on peptide

sequence comparison by Proteome Discoverer (v1.2.0.208 with SEQUEST algorithm) (NCBI Reference Sequence: NP_003396.1, 14-3-3 protein eta [Homo sapience]). Fragment ions detected in MS/MS spectra of LAEQAERYDDMASAMK in un-phosphorylated (upper right panel). Fragment ions detected in MS/MS spectra of LAEQAERYDDMASAMK in phosphorylated (lower right panel). Matched b ions are colored in red and y ions in blue. **E**. MDA-MB-231 stable cells expressing KHK-A, which had been co-transfected with Flag-YWHAH or S25A plasmid, were incubated with 5 mM fructose for 8 hr. The cell lysates were immunoprecipitated with anti-FLAG, and the phosphorylation of YWHAH was evaluated by immunoblotting.

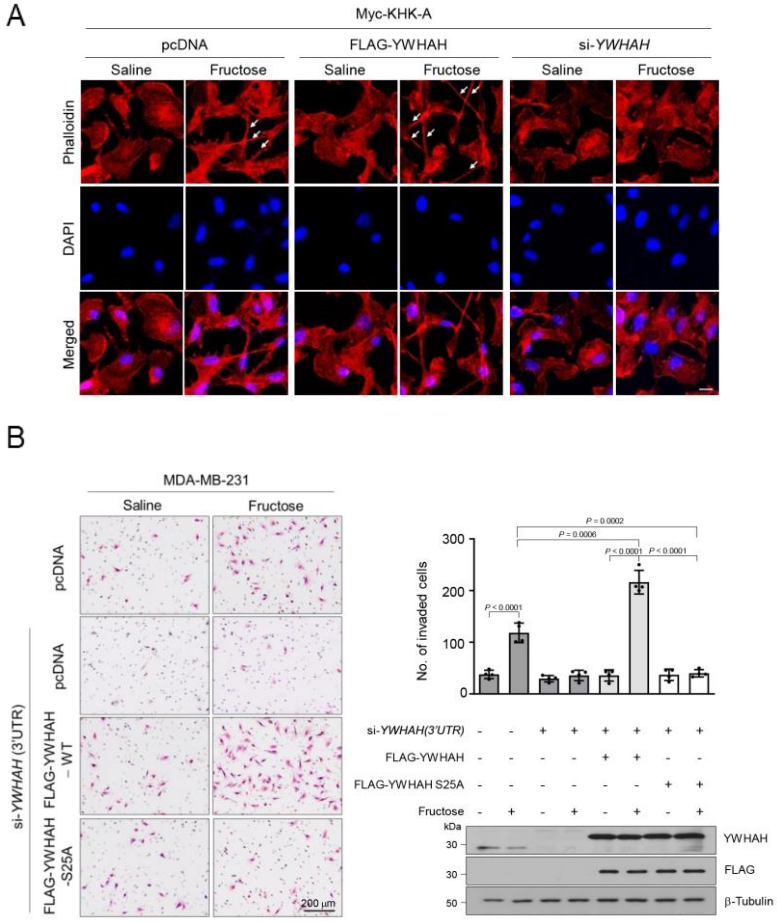
A
Myc-KHK-A
pcDNA
FLAG-YWHAH
si-YWHAH
Saline
Fructose
Saline
Fructose
Saline
Fructose
Phalloidin
DAPI
Merged
B
MDA-MB-231
Saline
Fructose
pcDNA
pcDNA
FLAG-YWHAH – WT
FLAG-YWHAH -S25A
si-YWHAH (3'UTR)
200 μm
No. of invaded cells
300
200
100
0
P = 0.0002
P = 0.0006
P < 0.0001
P < 0.0001
P < 0.0001
si-YWHAH(3'UTR)
FLAG-YWHAH
FLAG-YWHAH S25A
Fructose
kDa
30
30
50
YWHAH
FLAG
β-Tubulin

Figure 32. YWHAH promotes fructose-dependent cytoskeleton rearrangement and cancer cell invasion

A. MDA-MB-231 cells, which had been co-transfected with Myc-KHK-A and si-YWHAH, were incubated with 5 mM fructose for 48 hr. F-actin and nucleus were stained with Alexa Flouor 633 Phalloidine (red) and DAPI (blue), and visualized under a fluorescence microscope (scale bar = 10 μm). White arrows indicate filopodia. **B**. Endogenous YWHAH was knocked down in MDA-MB-231 cells using an siRNA targeting the 3′-UTR region of YWHAH mRNA, and YWHAH or S25A mutant proteins were restored in the cells. After incubated with 5 mM fructose for 48 hr, cells were subjected to Matrigel invasion assay. The numbers (means ± S.D. from 4 independent experiments) of invaded cells are shown as bar graphs. Significance was calculated by unpaired, two-sided Student's *t*-test.

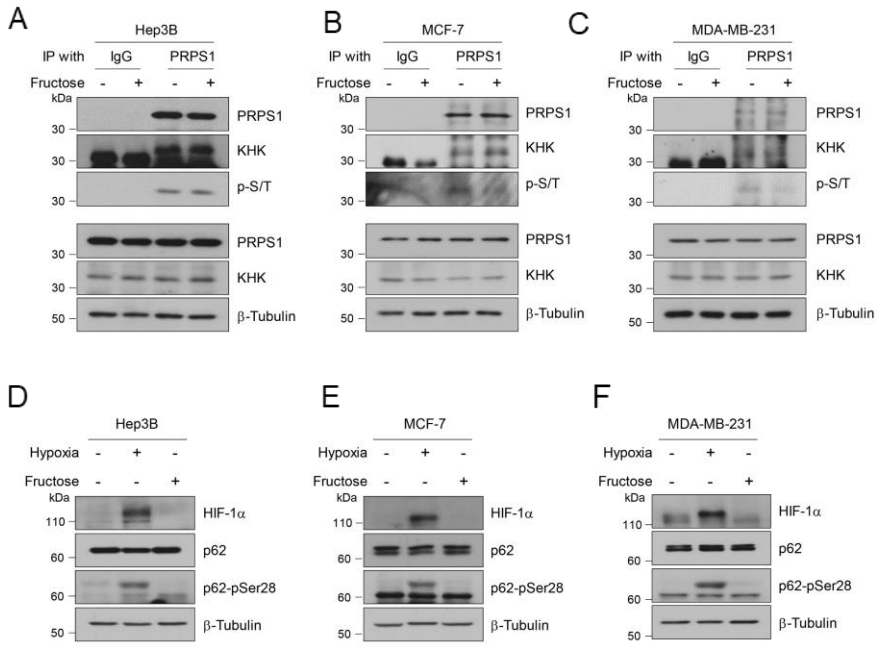

Figure 33. Effects of fructose on kinase activity of KHK-A

A. Hep3B, **B**. MCF-7 and **C**. MDA-MB-231 cells were incubated with 5 mM fructose, and cell lysates were subjected to immunoprecipitation with PRPS1 antibody (or IgG), and immunoblotted with anti-KHK or anti-phospho-S/T antibody. **D**. Hep3B, **E**. MCF-7 and **F**. MDA-MB-231 cells were incubated under hypoxia (1% O_2) or 5 mM fructose for 6 hours. Total lysates were subjected to Western blotting with the indicated antibodies. In a-f, data represent one out of three experiments.

A

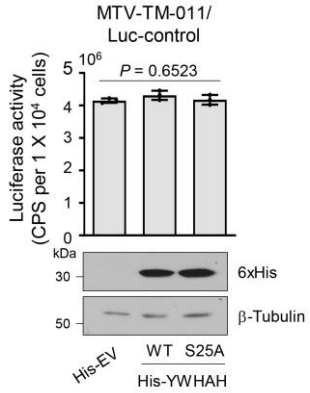

B

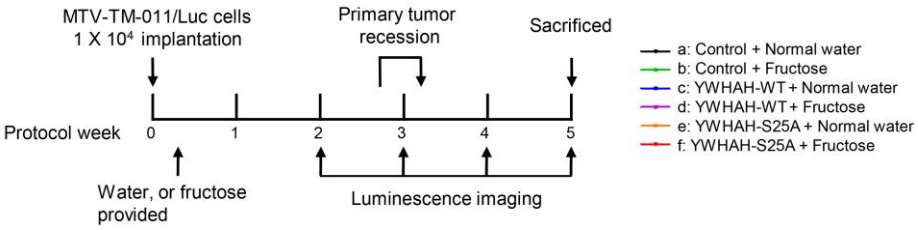

C

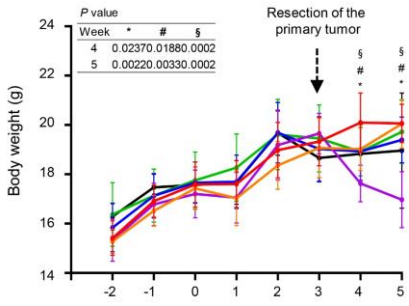

D

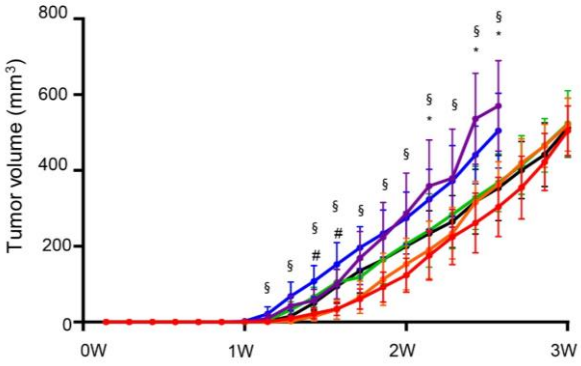

P value			
Day	*	#	§
8	n.s.	n.s.	0.04070
9	n.s.	n.s.	<0.0001
10	n.s.	0.01150	0.00580
11	n.s.	0.02880	<0.0001
12	n.s.	n.s.	<0.0001
13	n.s.	n.s.	0.00010
14	n.s.	n.s.	0.00030
15	0.02320	n.s.	0.00110
16	n.s.	n.s.	0.04330
17	0.01150	n.s.	0.00100
18	0.00010	n.s.	<0.0001

Figure 34. Implantation of YWHAH WT or S25A expressing MTV-TM-011 cells in the mammary fat pad

A. Establishment of stable cell lines. MTV-TM-011 cells were transfected with the Luciferase-IRES-GFP, and His-empty vector, His-YWHAH-WT or His-YWHAH-S25A plasmid, and transfected cells were double selected using G418 and zeocin. The expressions of luciferase and His-YWHAH-WT and His-YWHAH-S25A were checked by luminometry and Western blotting respectively. (means ± S.D. from 3 independent experiments, statistical significance was calculated by one way ANOVA test). **B**. Schematic diagram for the breast cancer xenograft study. The MTV-TM-011 stable cell line coexpressing luciferase and YWHAH or YWHAH-S25A were implanted into the mammary pads of mice. Tumor-bearing mice were fed with water or 15% fructose. After primary tumors were removed, metastatic tumors were checked weekly by luminascence imaging. The condition of each experiemntal group (7 per each group) is described in the right panel. **C**. Body weights of mice (the means ± S.D. from 7 mice per group). **D**. The volumes of breast tumors (the means ± S.D. from 7 mice per group). * denotes $P < 0.05$ between group 'd' versus 'b'; # denotes $P < 0.05$ between group 'd' versus 'c'; § denotes $P < 0.05$ between group 'd' versus 'f'. In (C, and D), a two-sided Mann Whitney *U* test was used to calculate significance. *P*-values are represented in each panel.

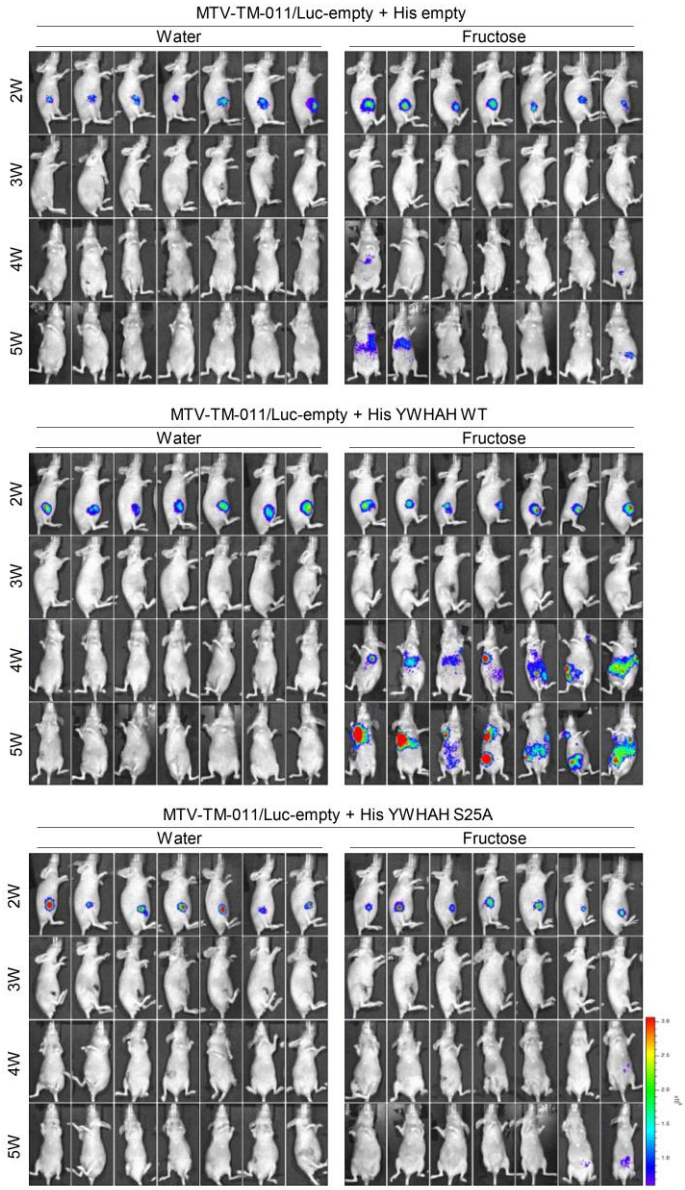

Figure 35. Phosphorylation of YWHAH promotes breast cancer metastasis in fructose fed mice

Bioluminescence images of tumor-bearing mice were taken weekly using Xenogen IVIS 100. The color bar represents bioluminescence intensity counts.

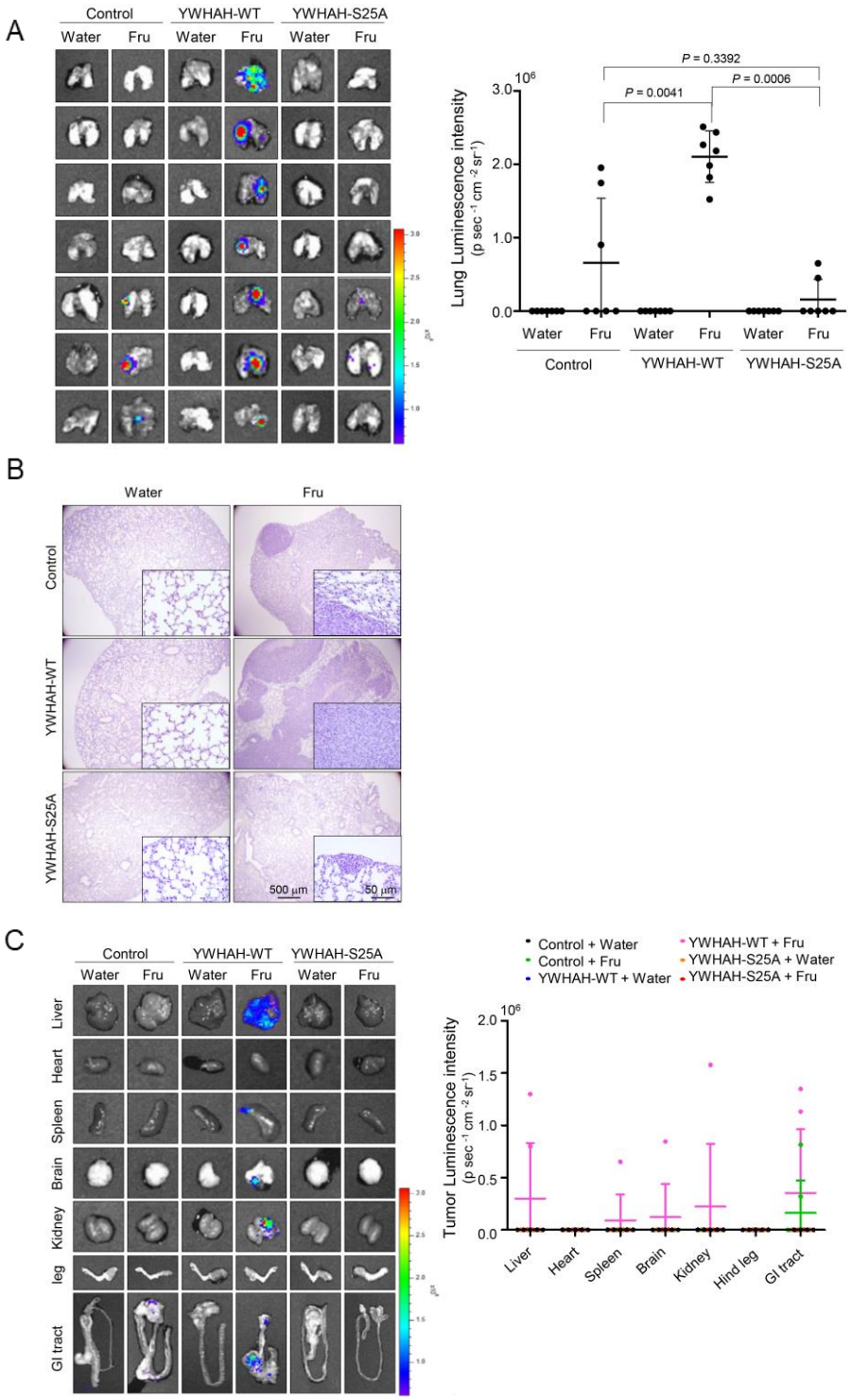
A
Control
YWHAH-WT
YWHAH-S25A
Water
Fru
P = 0.3392
P = 0.0041
P = 0.0006
Lung Luminescence intensity
(p sec-1 cm-2 sr-1)
B
Water
Fru
Control
YWHAH-WT
YWHAH-S25A
500 μm
50 μm
C
Liver
Heart
Spleen
Brain
Kidney
leg
GI tract
Control + Water
Control + Fru
YWHAH-WT + Water
YWHAH-WT + Fru
YWHAH-S25A + Water
YWHAH-S25A + Fru
Tumor Luminescence intensity
(p sec-1 cm-2 sr-1)
Hind leg

Figure 36. Phosphorylation of YWHAH enhances metastatic potential in fructose fed mice

A. On the 5th week after cancer graft, bioluminescence images were captured in the excised lungs (left). Bioluminescence intensity (photons/sec/cm^2/sr) was quantitatively analyzed (right). Data are represented as means ± S.D. from the lungs from 7 mice per group. **B**. Representative pictures of H&E-stained lungs. **C**. In other organs, representative bioluminescence images (left) and quantitative analyses of bioluminescence emission (right). Dots represent the bioluminescence intensities from individual samples, and horizontal bars show the means ± S.D. from all vital orgnas obtained from 7 mice per group. In A, C, a two-sided Mann Whitney *U* test was used to calculate significance. *P*-values are represented in each panel.

A

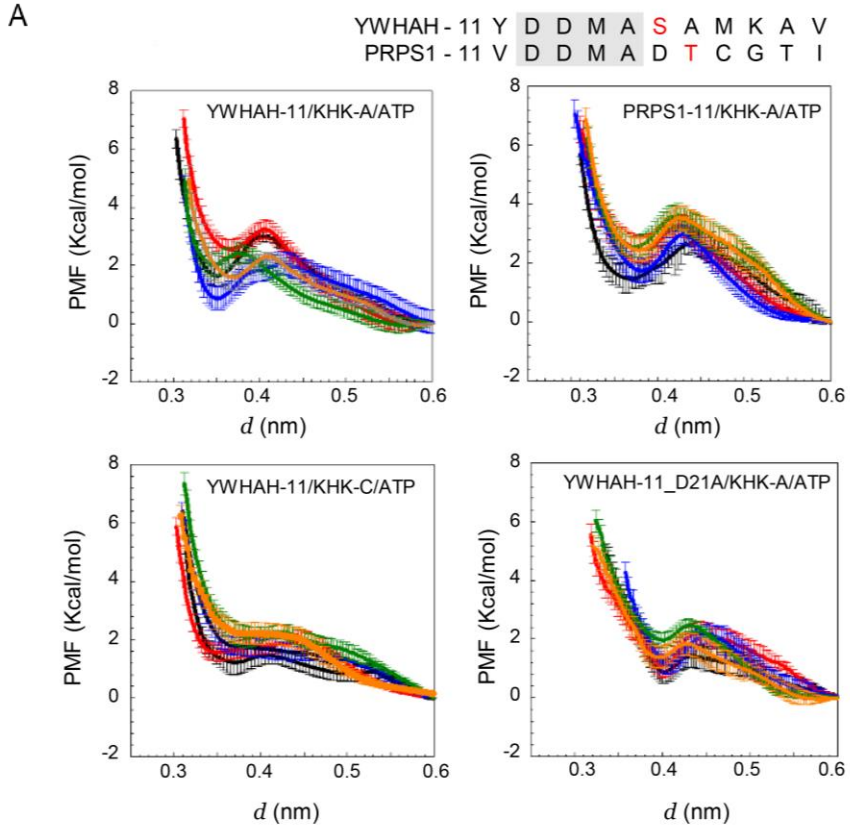
YWHAH - 11 Y D D M A S A M K A V
PRPS1 - 11 V D D M A D T C G T I
YWHAH-11/KHK-A/ATP
PRPS1-11/KHK-A/ATP
YWHAH-11/KHK-C/ATP
YWHAH-11_D21A/KHK-A/ATP
PMF (Kcal/mol)
d (nm)

B

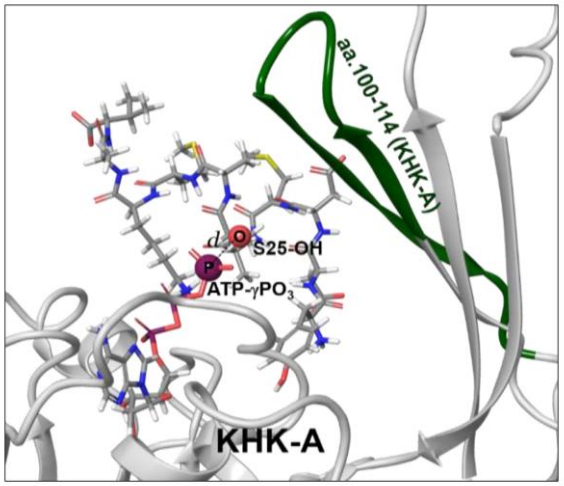
aa.100-114 (KHK-A)
d
S25-OH
ATP-γPO3
KHK-A

Figure 37. Molecular dynamics analysis to support the KHK-A phosphorylation of YWHAH

A. Potential of mean force (PMF) profiles as a function of the distance (*d*) between the oxygen of S25-OH and the phosphorus of ATP-γPO_3 for YWHAH/KHK-A/ATP, PRPS1-11/KHK-A/ATP, YWHAH/KHK-C/ATP, and YWHAH-11_D21A/KHK-A/ATP. Amino acid sequences of YWHAH-11 and PRPS1-11 are shown above panel. The conserved amino acids are highlighted and the phosphorylated residues are red. For data reproducibility, 5 different PMF profiles for each case were obtained from fully independent umbrella simulations, which are marked with 5 different colors. The error bars were obtained from bootstrap analysis with 200 bootstraps. **B**. 3D structure of YWHAH-11 bound to KHK-A. YWHAH-11 and ATP are shown by sticks with exceptions for the hydroxyl oxygen group of S25 and the γ-phosphorous of ATP represented by enlarged spheres between which distance is denoted as *d* and KHK-A are represented by cartoons where aa.100-114 are green. Data in figure 35, was provided by Prof. June Huh.

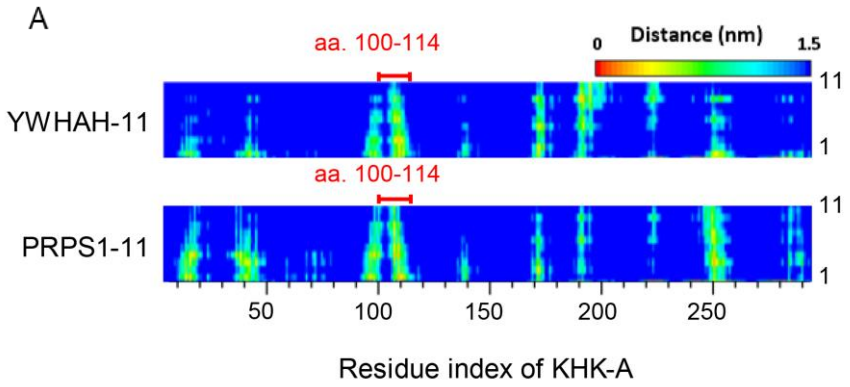
A
aa. 100-114
Distance (nm)
0
1.5
YWHAH-11
11
1
aa. 100-114
PRPS1-11
11
1
50
100
150
200
250
Residue index of KHK-A

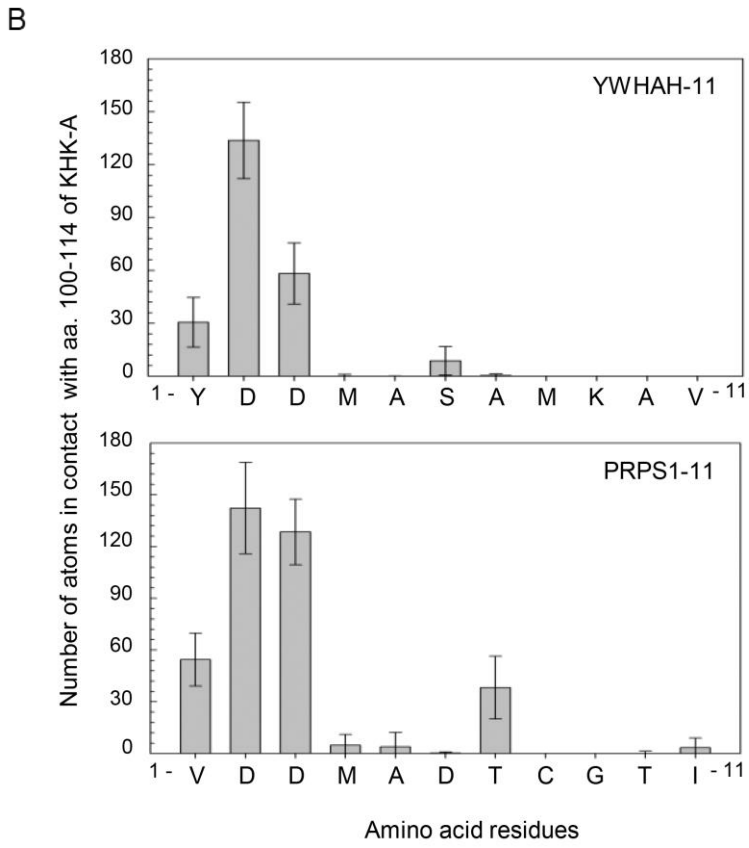
B
Number of atoms in contact with aa. 100-114 of KHK-A
YWHAH-11
180
150
120
90
60
30
0
1 - Y D D M A S A M K A V - 11
PRPS1-11
180
150
120
90
60
30
0
1 - V D D M A D T C G T I - 11
Amino acid residues

Figure 38. YWHAH-11 and PRPS1-11 commonly contact with a KHK-A specific region

A. The residue-residue contact map for ternary complex of YWHAH-11/KHK-A/ATP at $d \cong 3.5$ nm (top) and of PRPS1-11/KHK-A/ATP at $d \cong 3.6$ nm (bottom). The horizontal residues indicate aa. 3-298 of KHK-A and the right vertical residues indicate aa. 1-11 of YWHAH-11 or PRPS1-11. **B**. The average number of atoms contacting the KHK-A 100-114 for YWHAH-11 residues at $d \cong 3.5$ nm (top) and PRPS1-11 residues at $d \cong 3.6$ nm (bottom). The contact is counted in case that the interatomic distance < 5 nm. The averages were taken over 1000 configurations obtained from MD trajectories for 10 ns with 10 ps interval under the restraint of $d = 3.5$ nm (YWHAH-11) and $d \cong 3.6$ nm (PRPS1-11). Data are presented as means ± S.D. Data in figure 36, was provided by Prof. June Huh.

A

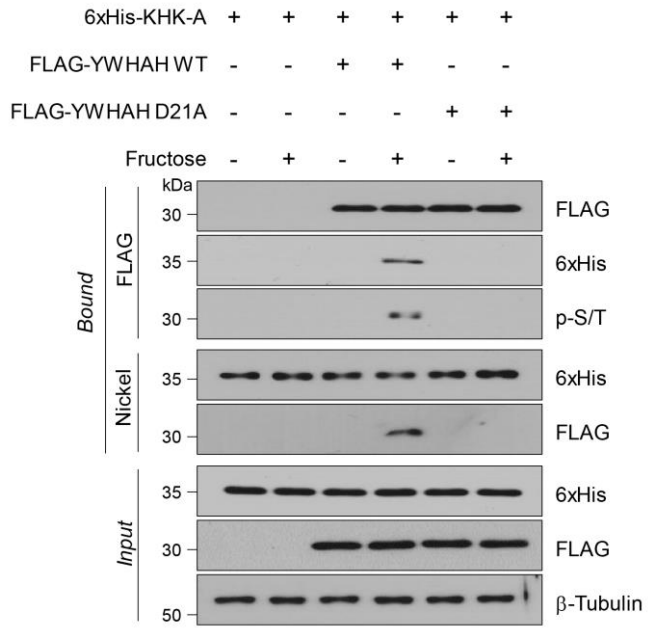
6xHis-KHK-A + + + + + +
FLAG-YWHAH WT - - + + - -
FLAG-YWHAH D21A - - - - + +
Fructose - + - + - +
kDa
Bound
FLAG
30
35
30
FLAG
6xHis
p-S/T
Nickel
35
30
6xHis
FLAG
Input
35
30
50
6xHis
FLAG
β-Tubulin

B

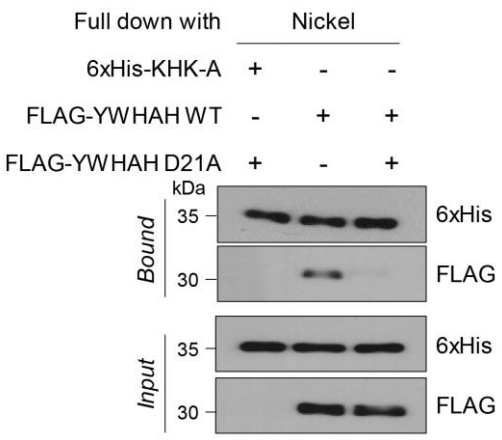
Full down with
Nickel
6xHis-KHK-A + - -
FLAG-YWHAH WT - + +
FLAG-YWHAH D21A + - +
kDa
Bound
35
30
6xHis
FLAG
Input
35
30
6xHis
FLAG

Figure 39. The D21 residue is essential to the KHK-A phosphorylation of YWHAH

A. MDA-MB-231 cells were co-transfected with His-KHK-A and FLAG-YWHAH WT (or D21A) plasmids. The protein interaction was cross-checked by co-precipitation using anti-FLAG and Nickel-NTA affinity gels. The Ser/Thr-phosphorylation of YWHAH were identified by immunoblotting the immunoprecipitated YWHAH with anti-phospho-S/T antibody. **B**. *In vitro* binding assay. Purified FLAG-YWHAH WT (or D21A) and KHK-A were co-incubated for 1 hr. KHK-A was pulled down using Nickel-NTA and the KHK-A-bound YWHAH was immunoblotted.

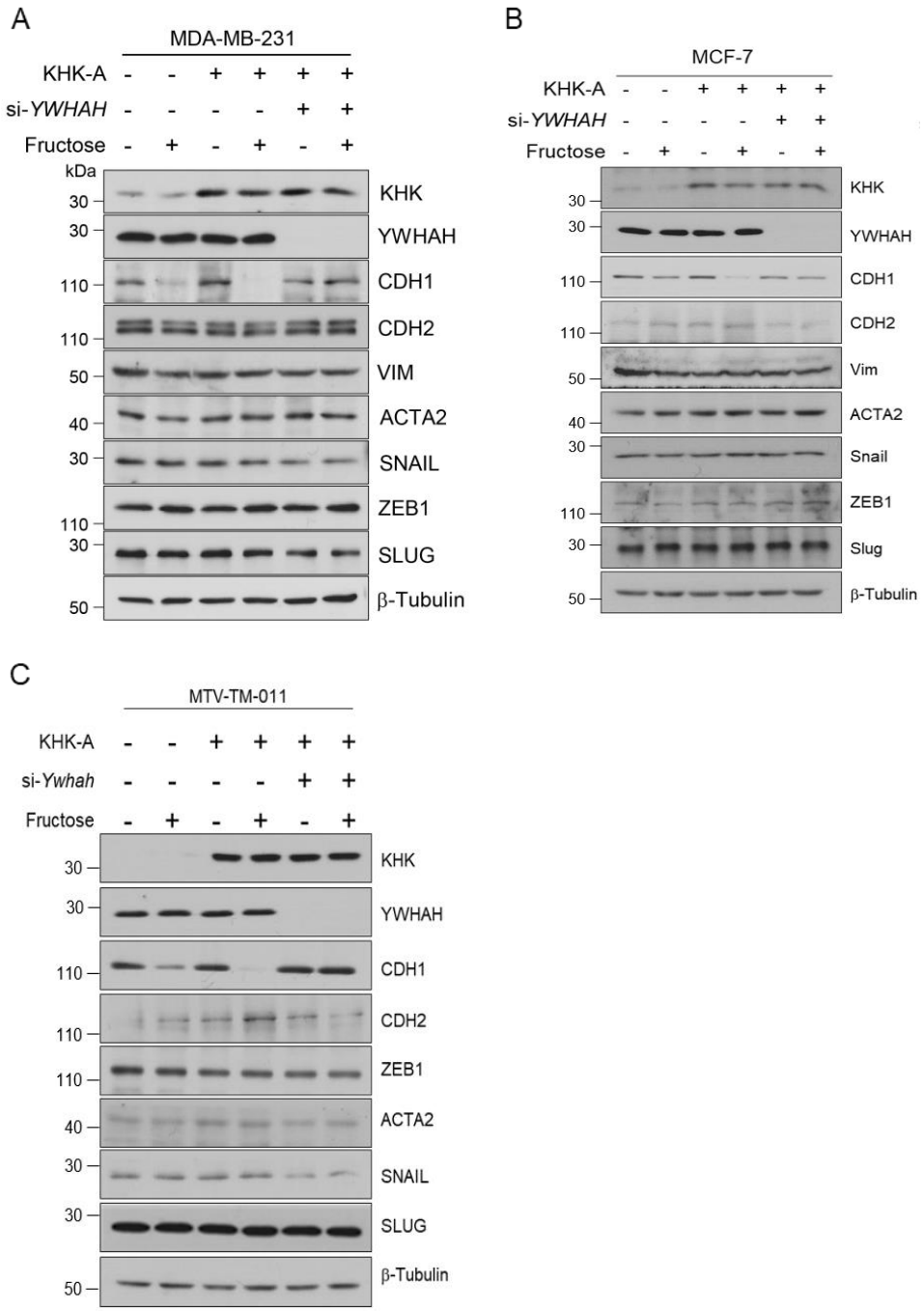
A
MDA-MB-231
KHK-A - - + + + +
si-YWHAH - - - - + +
Fructose - + - + - +
kDa
30
30
110
110
50
40
30
110
30
50
KHK
YWHAH
CDH1
CDH2
VIM
ACTA2
SNAIL
ZEB1
SLUG
β-Tubulin
B
MCF-7
KHK-A - - + + + +
si-YWHAH - - - - + +
Fructose - + - + - +
30
30
110
110
50
40
30
110
30
50
KHK
YWHAH
CDH1
CDH2
Vim
ACTA2
Snail
ZEB1
Slug
β-Tubulin
C
MTV-TM-011
KHK-A - - + + + +
si-Ywhah - - - - + +
Fructose - + - + - +
30
30
110
110
110
40
30
30
50
KHK
YWHAH
CDH1
CDH2
ZEB1
ACTA2
SNAIL
SLUG
β-Tubulin

Figure 40. YWHAH regulates CDH1 expression in fructose- and KHK-A dependently

A. Transfected MDA-MB-231 cells were incubated with 5 mM fructose for 48 hours, and subjected to EMT markers analysis. **B**. Transfected MCF-7 cells were incubated with 5 mM fructose for 48 hours, and subjected to EMT markers analysis. **C**. Transfected MTV-TM-011 cells were incubated with 5 mM fructose for 48 hours, and subjected to EMT markers analysis.

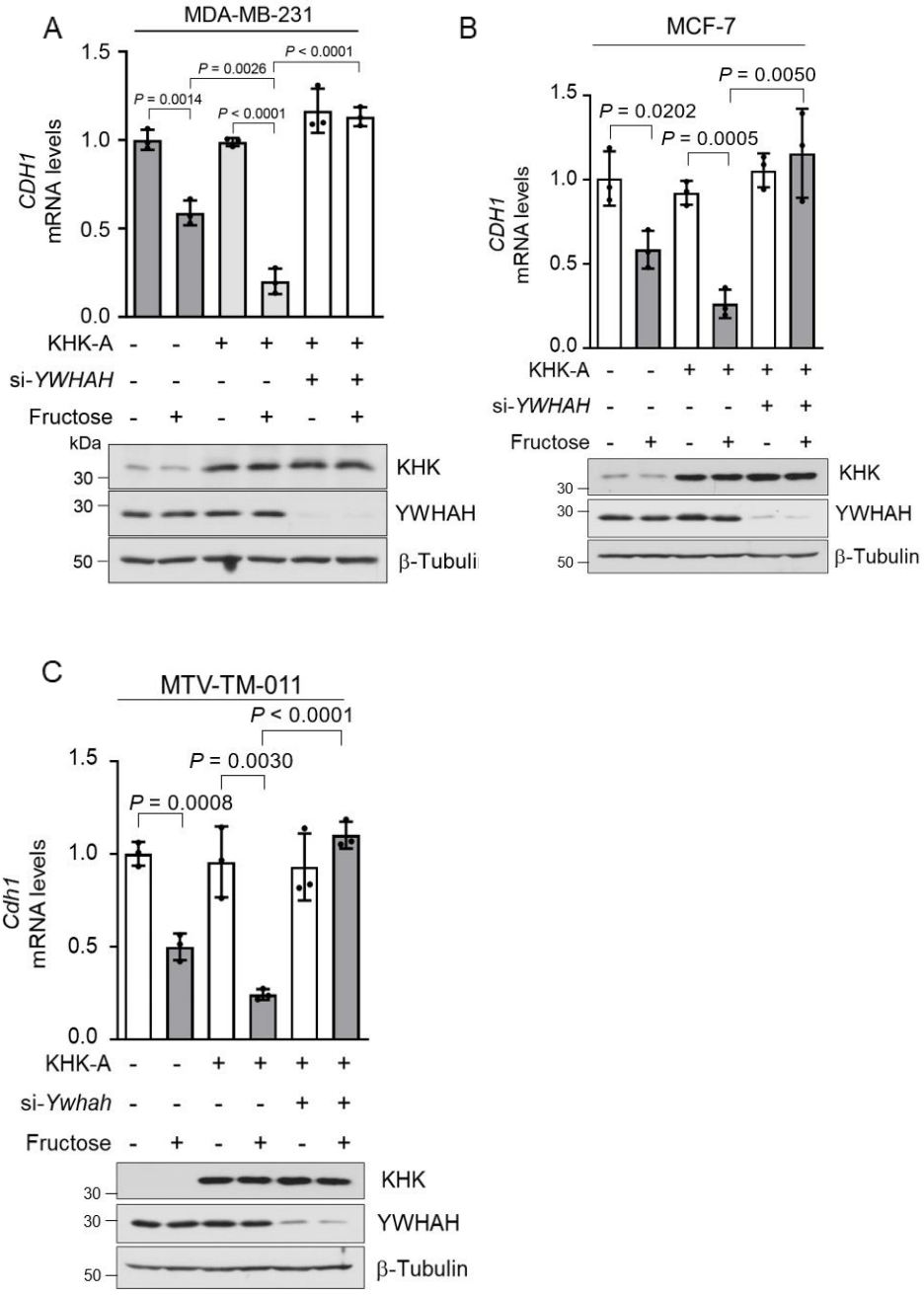
A
MDA-MB-231
CDH1 mRNA levels
1.5
1.0
0.5
0.0
P = 0.0014
P = 0.0026
P < 0.0001
P < 0.0001
KHK-A - - + + + +
si-YWHAH - - - - + +
Fructose - + - + - +
kDa
30
30
50
KHK
YWHAH
β-Tubuli
B
MCF-7
CDH1 mRNA levels
P = 0.0202
P = 0.0005
P = 0.0050
KHK-A - - + + + +
si-YWHAH - - - - + +
Fructose - + - + - +
30
30
50
KHK
YWHAH
β-Tubulin
C
MTV-TM-011
Cdh1 mRNA levels
P < 0.0001
P = 0.0030
P = 0.0008
KHK-A - - + + + +
si-Ywhah - - - - + +
Fructose - + - + - +
30
30
50
KHK
YWHAH
β-Tubulin

Figure 41. YWHAH regulates CDH1 expression at the transcription level

A. The mRNA levels of *CDH1* were analyzed by RT-qPCR in MDA-MB-231 cells incubated with 5 mM fructose for 48 hr. **B**. Transfected MCF-7 cells were incubated with 5 mM fructose for 48 hours. The mRNA levels of *CDH1* were analyzed by RT-qPCR. **C**. The mRNA levels of *CDH1* were analyzed by RT-qPCR in MTV-TM-011 cells incubated with 5 mM fructose for 48 hr. In **A**, **B**, **C**, data represented as the means ± S.D. from 3 independent experiments. Significance was calculated by unpaired, two-sided Student's *t*-test.

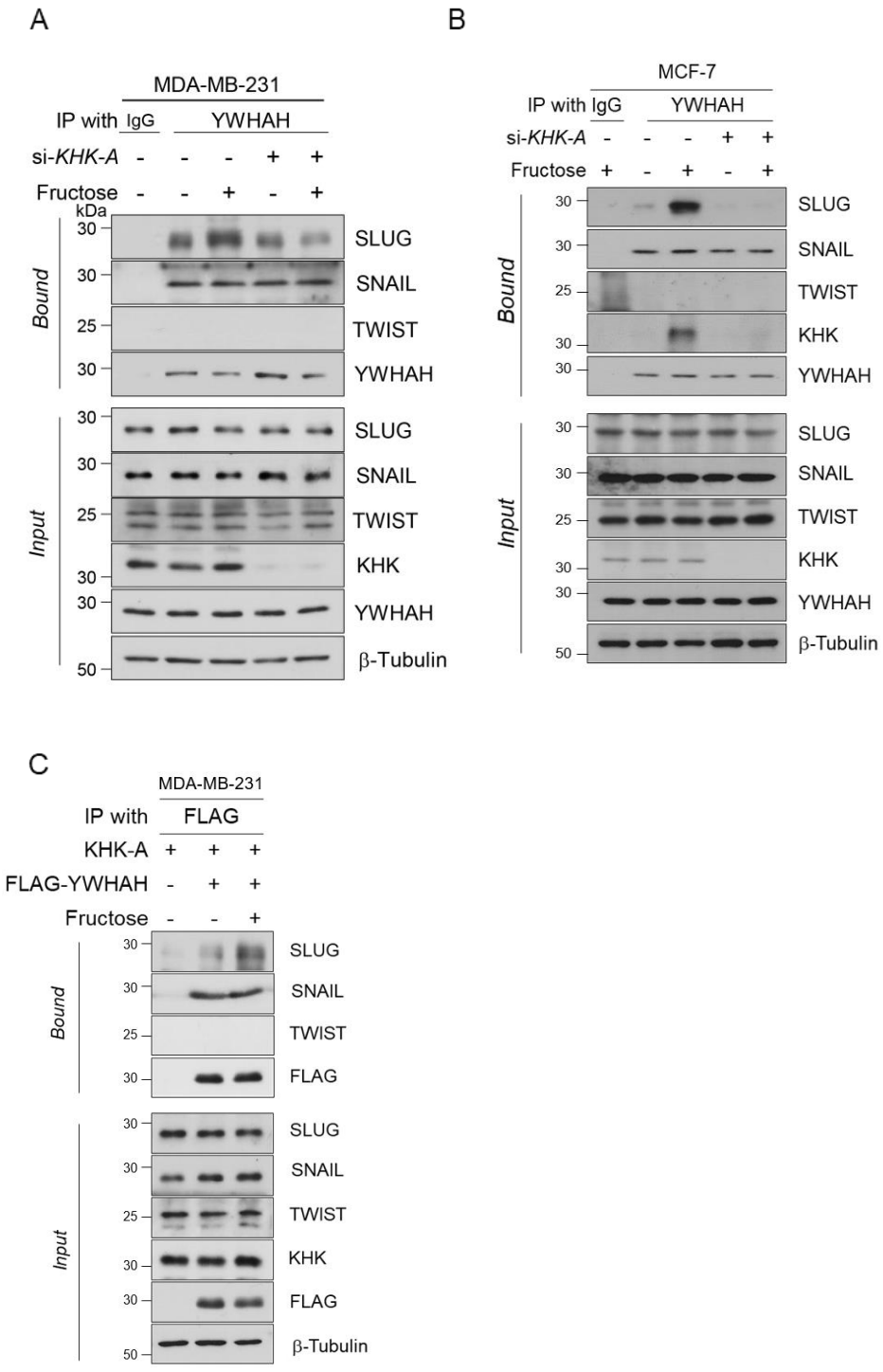
A
MDA-MB-231
IP with IgG YWHAH
si-KHK-A - - - + +
Fructose - - + - +
kDa
Bound
30 SLUG
30 SNAIL
25 TWIST
30 YWHAH
Input
30 SLUG
30 SNAIL
25 TWIST
30 KHK
30 YWHAH
50 β-Tubulin
B
MCF-7
IP with IgG YWHAH
si-KHK-A - - - + +
Fructose + - + - +
Bound
30 SLUG
30 SNAIL
25 TWIST
30 KHK
30 YWHAH
Input
30 SLUG
30 SNAIL
25 TWIST
30 KHK
30 YWHAH
50 β-Tubulin
C
MDA-MB-231
IP with FLAG
KHK-A + + +
FLAG-YWHAH - + +
Fructose - - +
Bound
30 SLUG
30 SNAIL
25 TWIST
30 FLAG
Input
30 SLUG
30 SNAIL
25 TWIST
30 KHK
30 FLAG
50 β-Tubulin

Figure 42. SLUG interacts with YWHAH in fructose- and KHK-A dependent manner

A. YWHAH binding to endogenous SLUG, SNAIL, or TWIST. After treated with 5 mM fructose for 24 hr, MDA-MB-231 cells were subjected to immunoprecipitation and immunoblotting. **B**. YWHAH binding to endogenous SLUG, SNAIL, or TWIST. After treated with 5 mM fructose for 24 hr, MCF-7 cells were subjected to immunoprecipitation and immunoblotting. **C**. MDA-MB-231 cells stably expressing KHK-A were transfected with FLAG-YWHAH. Cell lysates were subjected to immunoprecipitation and immunoblotting.

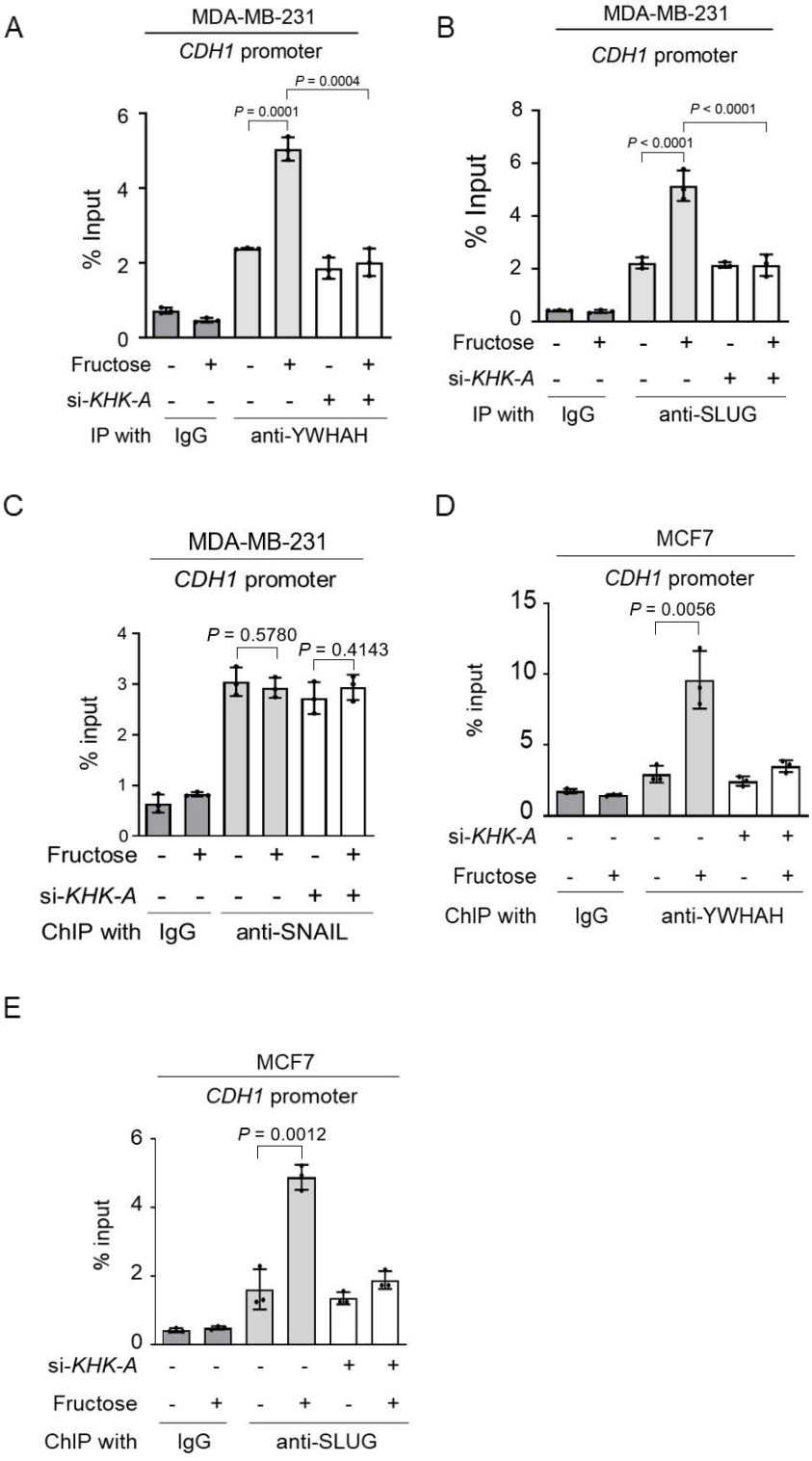
A
MDA-MB-231
CDH1 promoter
P = 0.0004
P = 0.0001
% Input
Fructose
si-KHK-A
IP with
IgG
anti-YWHAH
B
MDA-MB-231
CDH1 promoter
P < 0.0001
P < 0.0001
% Input
Fructose
si-KHK-A
IP with
IgG
anti-SLUG
C
MDA-MB-231
CDH1 promoter
P = 0.5780
P = 0.4143
% input
Fructose
si-KHK-A
ChIP with
IgG
anti-SNAIL
D
MCF7
CDH1 promoter
P = 0.0056
% input
si-KHK-A
Fructose
ChIP with
IgG
anti-YWHAH
E
MCF7
CDH1 promoter
P = 0.0012
% input
si-KHK-A
Fructose
ChIP with
IgG
anti-SLUG

Figure 43. The fructose-induced YWHAH recruitment to the *CDH1* promoter depends on KHK-A

A. MDA-MB-231 cells were transfected with KHK-A si-RNA (or control si-RNA). After incubated with 5 mM fructose for 24 hr, cells were subjected to ChIP-qPCR using anti-YWHAH antibody. **B**. The fructose-induced SLUG recruitment to the *CDH1* promoter depends on KHK-A. MDA-MB-231 cells were transfected with KHK-A si-RNA. After incubated with 5 mM fructose for 24 hr, cells were subjected to ChIP-qPCR using anti-SLUG antibody. **C**. The fructose-induced SNAIL recruitment to the *CDH1* promoter depends on KHK-A. MDA-MB-231 cells were transfected with KHK-A si-RNA. After incubated with 5 mM fructose for 24 hr, cells were subjected to ChIP-qPCR using anti-SNAIL antibody. **D**. The fructose-induced YWHAH recruitment to the CDH1 promoter depends on KHK-A. MCF-7 cells were transfected with KHK-A si-RNA (or control si-RNA). After incubated with 5 mM fructose for 24 hr, cells were subjected to ChIP-qPCR using anti-YWHAH antibody. **E**. The fructose-induced SLUG recruitment to the CDH1 promoter depends on KHK-A. MCF-7 cells were transfected with KHK-A si-RNA. After incubated with 5 mM fructose for 24 hr, cells were subjected to ChIP-qPCR using anti-SLUG antibody. In A, B, C, D, E, data represented as the means ± S.D. from 3 independent experiments. Significance was calculated by unpaired, two-sided Student's *t*-test.

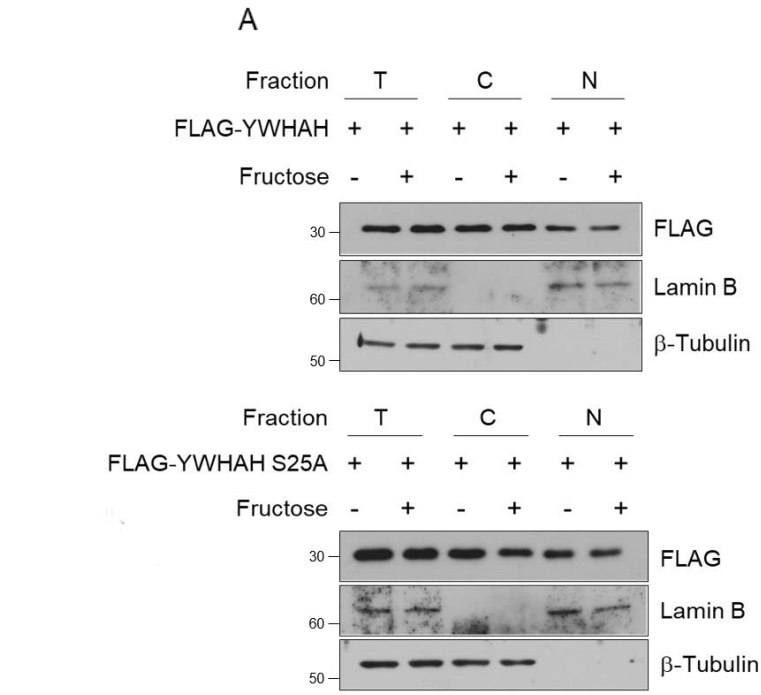
A
Fraction T C N
FLAG-YWHAH + + + + + +
Fructose - + - + - +
30
60
50
FLAG
Lamin B
β-Tubulin
Fraction T C N
FLAG-YWHAH S25A + + + + + +
Fructose - + - + - +
30
60
50
FLAG
Lamin B
β-Tubulin

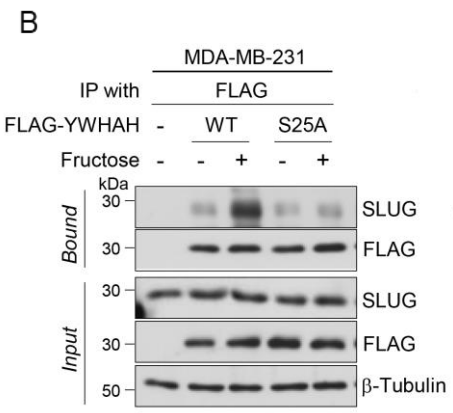
B
MDA-MB-231
IP with FLAG
FLAG-YWHAH - WT S25A
Fructose - - + - +
kDa
Bound
30
30
SLUG
FLAG
Input
30
30
50
SLUG
FLAG
β-Tubulin

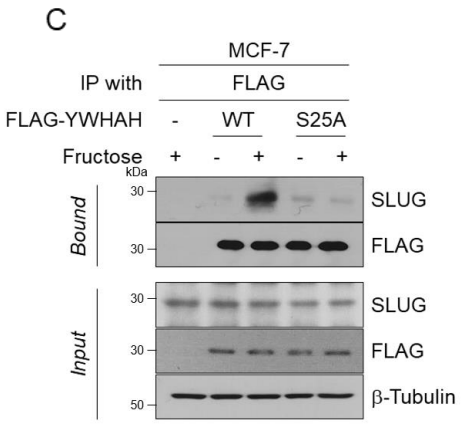
C
MCF-7
IP with FLAG
FLAG-YWHAH - WT S25A
Fructose + - + - +
kDa
Bound
30
30
SLUG
FLAG
Input
30
30
50
SLUG
FLAG
β-Tubulin

Figure 44. The S25 phosphorylation of YWHAH is essential for YWHAH binding to SLUG

A. MDA-MB-231 cells, which had been transfected with Flag-YWHAH (or S25A), were incubated with 5 mM fructose for 24 hr, and subjected to immunoprecipitation and immunoblotting. **B**. MDA-MB-231 cells and **C**. MCF-7 were transfected with FLAG-YWHAH wild type or S25A mutant plasmid, and incubated with 5 mM fructose for 8 hours. Fractionated cell lysates were subjected to western blotting with indicated antibodies. (T), Total lysate; (C), Cytoplasm; (N), Nucleus.

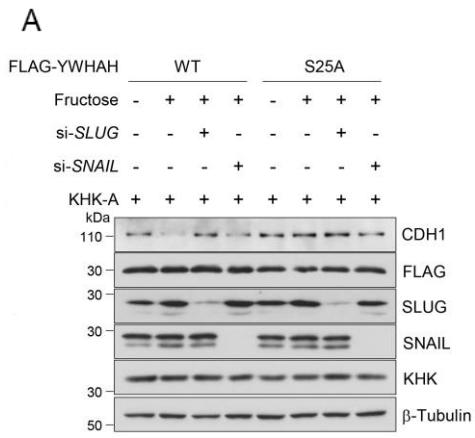
A
FLAG-YWHAH
WT
S25A
Fructose
si-SLUG
si-SNAIL
KHK-A
kDa
110
30
30
30
50
CDH1
FLAG
SLUG
SNAIL
KHK
β-Tubulin

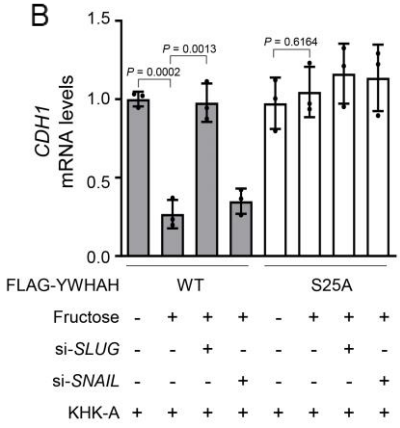
B
CDH1 mRNA levels
1.5
1.0
0.5
0.0
P = 0.0002
P = 0.0013
P = 0.6164
FLAG-YWHAH
WT
S25A
Fructose
si-SLUG
si-SNAIL
KHK-A

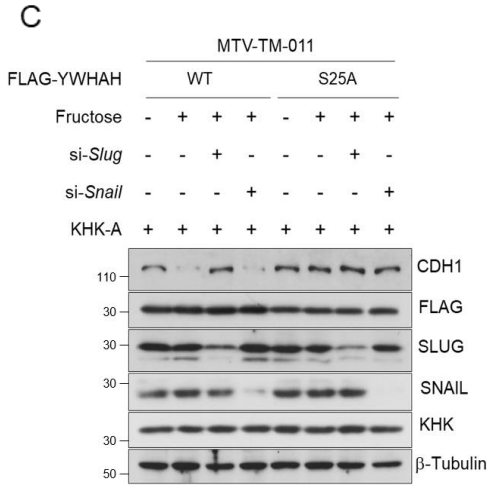
C
MTV-TM-011
FLAG-YWHAH
WT
S25A
Fructose
si-Slug
si-Snail
KHK-A
110
30
30
30
30
50
CDH1
FLAG
SLUG
SNAIL
KHK
β-Tubulin

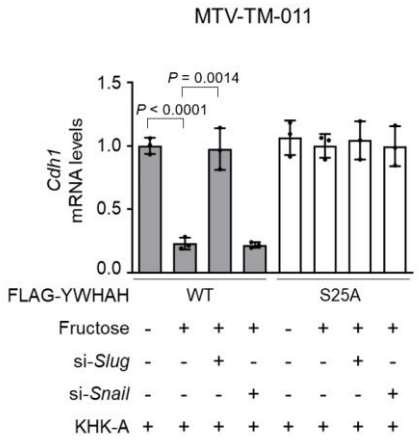
D
MTV-TM-011
Cdh1 mRNA levels
1.5
1.0
0.5
0.0
P = 0.0014
P < 0.0001
FLAG-YWHAH
WT
S25A
Fructose
si-Slug
si-Snail
KHK-A

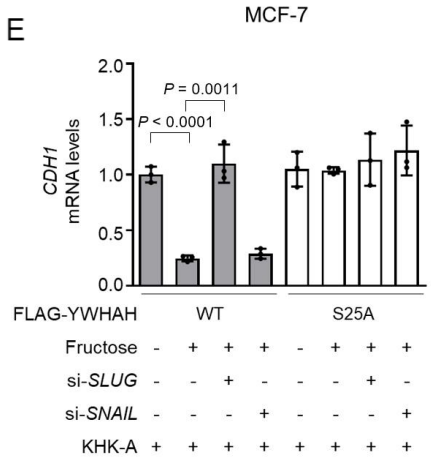
E
MCF-7
CDH1 mRNA levels
2.0
1.5
1.0
0.5
0.0
P = 0.0011
P < 0.0001
FLAG-YWHAH
WT
S25A
Fructose
si-SLUG
si-SNAIL
KHK-A

Figure 45. The S25 phosphorylation of YWHAH is essential for the fructose- and SLUG-dependent suppression of E-cadherin

A. MDA-MB-231 cells, which had been transfected as indicated, were incubated with 5 mM fructose for 48 hr, and subjected to immunoblotting. **B**. The mRNA levels of *CDH1* were analyzed by RT-qPCR in MDA-MB-231 cells which had been transfected as indicated, were incubated with 5 mM fructose for 48 hr. data represented as the means ± S.D. from 3 independent experiments. Significance was calculated by unpaired, two-sided Student's *t*-test. **C**. The S25 phosphorylation of YWHAH is essential for the fructose- and SLUG-dependent suppression of E-cadherine. MTV-TM-011 cells, which had been transfected as indicated, were incubated with 5 mM fructose for 48 hr, and subjected to immunoblotting. **D**. The mRNA levels of *CDH1* were analyzed by RT-qPCR in MTV-TM-011 cells which had been transfected as indicated, were incubated with 5 mM fructose for 48 hr. data represented as the means ± S.D. from 3 independent experiments. Significance was calculated by unpaired, two-sided Student's *t*-test. **E**. The mRNA levels of *CDH1* were analyzed by RT-qPCR in MCF-7 cells which had been transfected as indicated, were incubated with 5 mM fructose for 48 hr. Data represented as the means ± S.D. from 3 independent experiments. Significance was calculated by unpaired, two-sided Student's *t*-test.

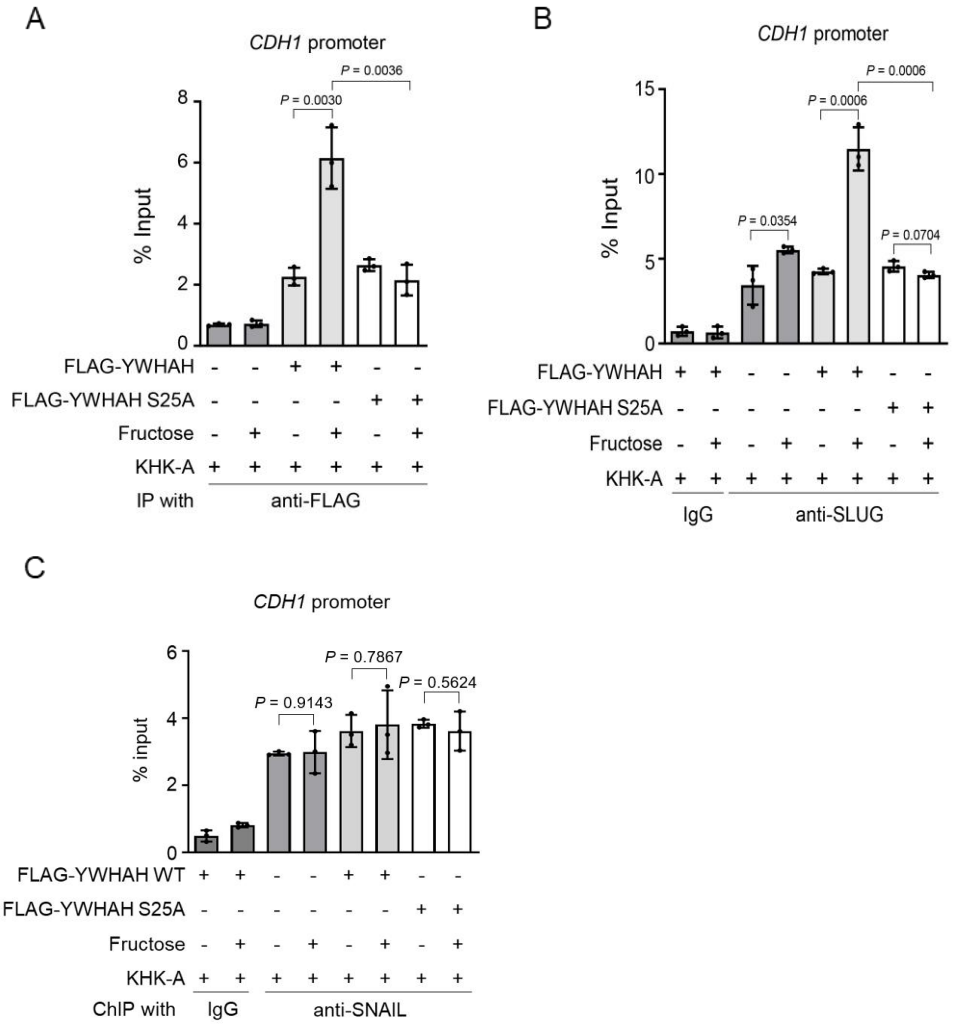
A
CDH1 promoter
P = 0.0036
P = 0.0030
% Input
8
6
4
2
0
FLAG-YWHAH - - + + - -
FLAG-YWHAH S25A - - - - + +
Fructose - + - + - +
KHK-A + + + + + +
IP with anti-FLAG
B
CDH1 promoter
P = 0.0006
P = 0.0006
P = 0.0354
P = 0.0704
% Input
15
10
5
0
FLAG-YWHAH + + - - + + - -
FLAG-YWHAH S25A - - - - - - + +
Fructose - + - + - + - +
KHK-A + + + + + + + +
IgG anti-SLUG
C
CDH1 promoter
P = 0.7867
P = 0.5624
P = 0.9143
% input
6
4
2
0
FLAG-YWHAH WT + + - - + + - -
FLAG-YWHAH S25A - - - - - - + +
Fructose - + - + - + - +
KHK-A + + + + + + + +
ChIP with IgG anti-SNAIL

Figure 46. S25 phosphorylation of YWHAH is critical for the recruitment of YWHAH and SLUG to the *CDH1* promoter

A. FLAG-YWHAH binding to the CDH1 promoter was analyzed by ChIP-qPCR. MDA-MB-231 cells expressing FLAG-YWHAH or S25A mutant were incubated with 5 mM fructose for 24 hr. Data represented as the means ± S.D. from 3 independent experiments. Significance was calculated by unpaired, two-sided Student's *t*-test. **B**. The S25 phosphorylation of YWHAH is essential for the SLUG binding to the *CDH1* promoter. Transfected MDA-MB-231 cells were incubated with 5 mM fructose for 24 hr. The chromatins containing endogenous SLUG were immunoprecipitated with anti-SLUG antibody and the SLUG-bound CDH1 promoter was quantified by real-time PCR. Results were presented as the percentages of input data. Data represented as the means ± S.D. from 3 independent experiments. **C**. The S25 phosphorylation of YWHAH is essential for the SNAIL binding to the *CDH1* promoter. Transfected MDA-MB-231 cells were incubated with 5 mM fructose for 24 hr. The chromatins containing endogenous SLUG were immunoprecipitated with anti-SLUG antibody and the SLUG-bound CDH1 promoter was quantified by real-time PCR. Results were presented as the percentages of input data. Data represented as the means ± S.D. from 3 independent experiments.

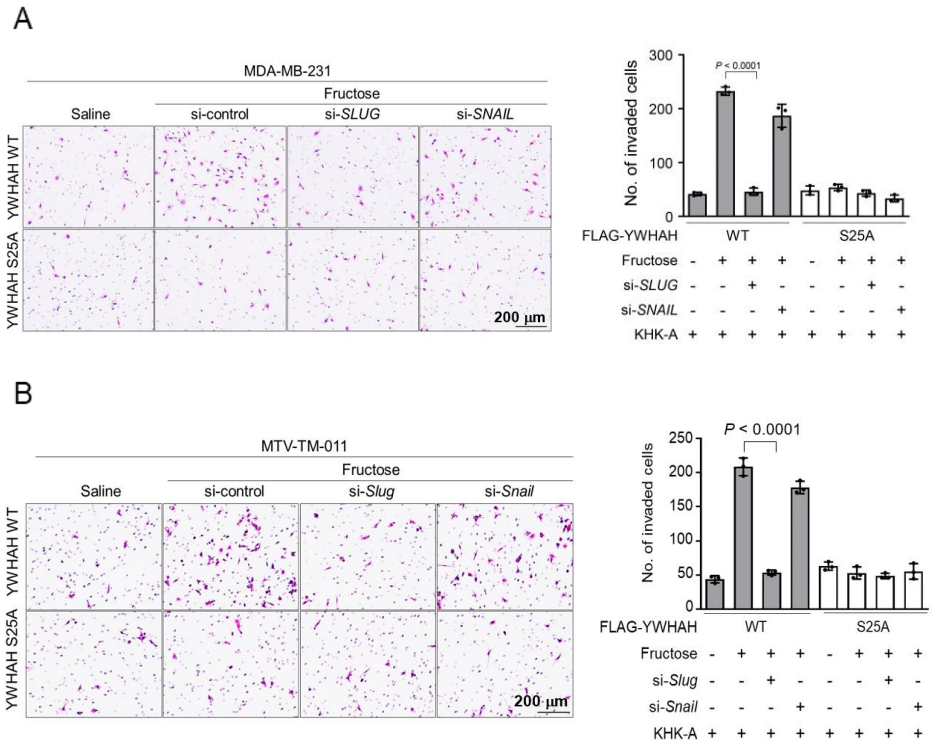

Figure 47. The S25 phosphorylation of YWHAH is essential for the fructose-induced, SLUG-dependent cell invasion

A. Transfected MDA-MB-231 cells were incubated with 5 mM fructose for 48 hr, and subjected to Matrigel invasion assay. Invaded cells were stained and counted. **B**. The S25 phosphorylation of YWHAH is essential for the fructose-induced, SLUG-dependent cell invasion. Transfected MTV-TM-011 cells were incubated with 5 mM fructose for 48 hr, and subjected to Matrigel invasion assay. Invaded cells were stained and counted. In A, B, data represented as the means ± S.D. from 3 independent experiments. Significance was calculated by unpaired, two-sided Student's *t*-test.

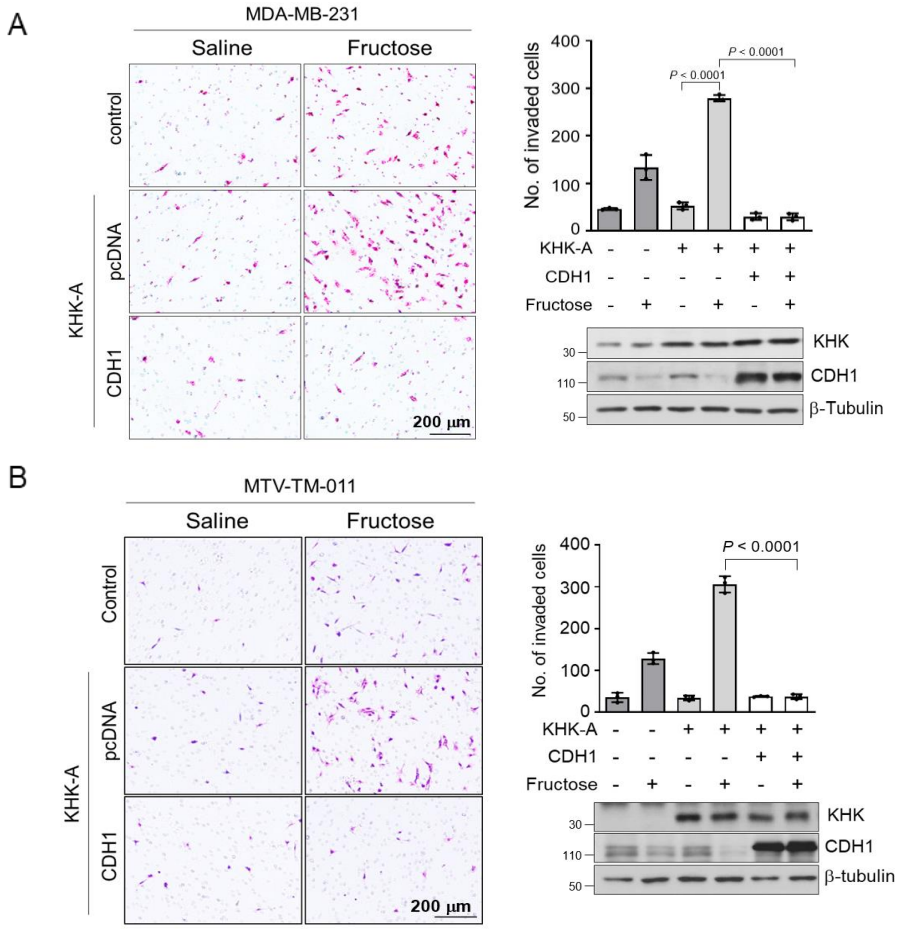

Figure 48. The fructose-induced, KHK-A-dependent cell invasion was attenuated by CDH1 restoration

A. Transfected MDA-MB-231 cells were treated with 5 mM fructose for 48 hr, and subjected to Matrigel invasion assay. **B**. The invasion potential was analysed in MTV-TM-011 cell line. In **A**, **B**, data represented as the means ± S.D. from 3 independent experiments. Significance was calculated by unpaired, two-sided Student's *t*-test.

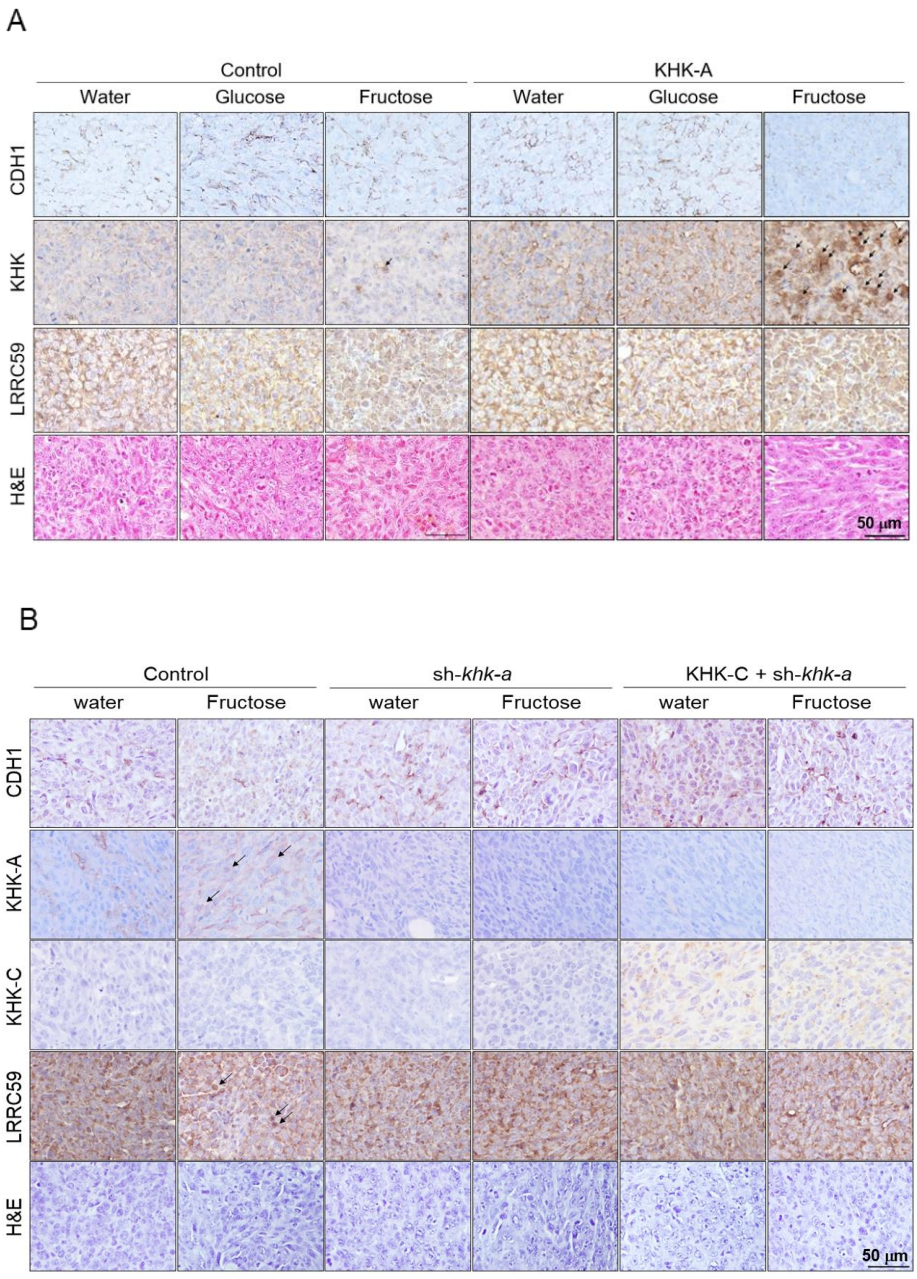
A
Control
KHK-A
Water
Glucose
Fructose
Water
Glucose
Fructose
CDH1
KHK
LRRC59
H&E
50 μm
B
Control
sh-khk-a
KHK-C + sh-khk-a
water
Fructose
water
Fructose
water
Fructose
CDH1
KHK-A
KHK-C
LRRC59
H&E
50 μm

Figure 49. Validation of KHK-A pathway in breast cancer tissue

A. Immunohistochemical analyses of the breast cancer tissues presented in Figure 14. The tumor sections were immunostained with the antibodies against CDH1, KHK, and LRRC59, and stainined with Hematoxylin and Eosin. **B**. The primary breast tumor section from the mice presented in Figure 17, were immunostained with CDH1, KHK-A, KHK-C, and LRRC59 antibodies. The slides were also stained with Hematoxylin and Eosin. In A, B, data represent one out of the three independent experiments.

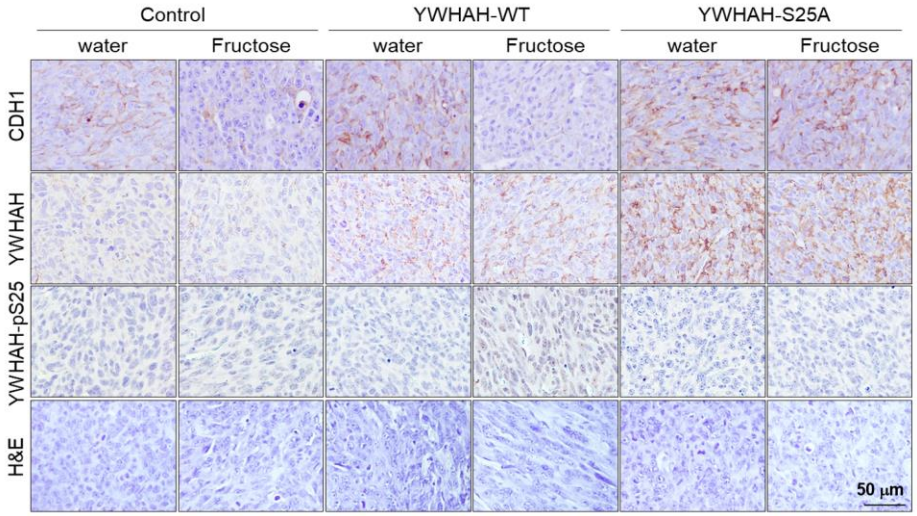

Figure 50. Validation of Fructose-YWHAH-pSer25-CDH1 axis in breast cancer tissue

The primary breast cancer masses sections from the mice presented in Figure 35, were immunostained with YWHAH, YWHAH-pS25, and CDH1. Also, the slides were stained with Hematocylin and Eosin. Data represent one out of three independent experiments.

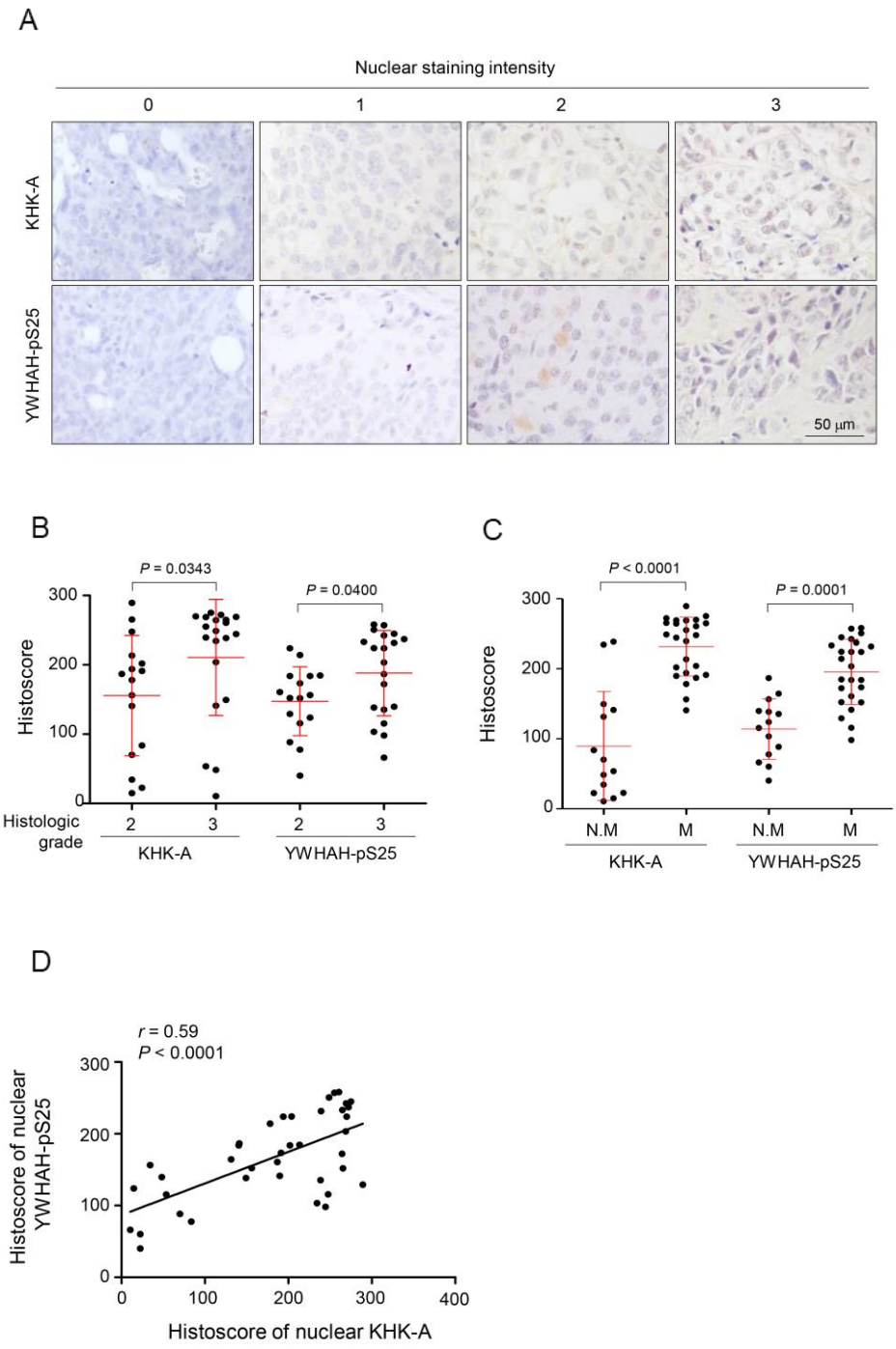
A
Nuclear staining intensity
0
1
2
3
KHK-A
YWHAH-pS25
50 μm
B
P = 0.0343
P = 0.0400
Histoscore
300
200
100
0
Histologic grade
2
3
2
3
KHK-A
YWHAH-pS25
C
P < 0.0001
P = 0.0001
Histoscore
300
200
100
0
N.M
M
N.M
M
KHK-A
YWHAH-pS25
D
r = 0.59
P < 0.0001
Histoscore of nuclear YWHAH-pS25
300
200
100
0
0
100
200
300
400
Histoscore of nuclear KHK-A

Figure 51. The YWHAH phosphorylation at S25 is associated with breast cancer metastasis

A. Representative microscopy photographs of immunohistochemical staining in breast cancer tissue arrays. **B**. The nuclear levels of KHK-A and YWHAH-pS25 were compared between histologic grade 2 and 3 groups (the means ± S.D. from 36 different breast cancer tissues). **C**. Nuclear KHH-A and YWHAH-pS25 levels were compared between the non-metastatic group (N.M) and the metastatic groups (M) including lynphatic and distant metastases(the means ± S.D. from 36 diferrent breast cancer tissues). In b, c, significance was calculated by two-sided Mann Whitney *U* test. **D**. Spearman's correation analysis between nuclear KHK-A and YWHAH-pS25 levels. 'r' is the correlation coefficient.

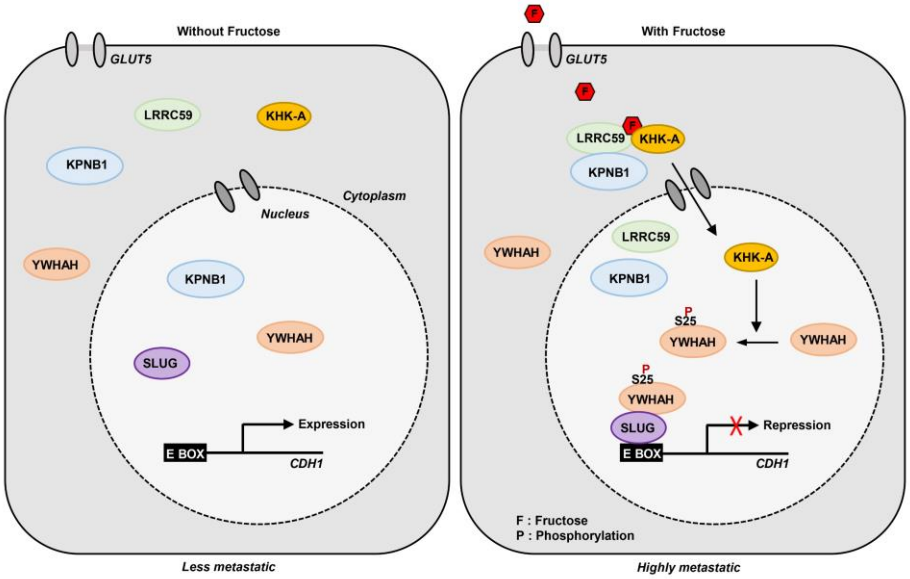

Figure 52. The proposed mechanism underlying fructose-induced cancer metastasis

Nuclear translocalization of Ketohexokinase-A triggered by fructose stimulation, which is accompanied by the interaction to nuclear importer LRRC59 and KPNB1. In the nucleus, KHK-A phosphorylates YWHAH at Ser25 and in turn, YWHAH recruits SLUG to the CDH1 promoter, in turn negatively regulates of expression of E-Cadherin. The KHK-A signaling triggered by fructose promotes cell migration, consequently, cancer cells acquire metastatic power.

DISCUSSION

To explain how fructose promotes cancer development and progression, many investigators have focused on KHK-C-initiated fructose flux in energy metabolism. Fructose metabolism seems to provide cancer cells with the supplementary fuel required for proliferation and metastasis in colon cancer, and glioma [9, 12, 14]. According to the results, however, most cancer cell lines predominantly express KHK-A rather than KHK-C, and KHK-A mediates the fructose-induced cell invasion. As KHK-A does little to phosphorylate fructose at physiological concentrations due to its high Km value[20], it has remained somewhat mysterious that fructose promotes cancer progression through metabolic reprogramming in cancer cells lacking KHK-C [13, 15, 16]. Herein, I demonstrated a protein kinase function of nuclear KHK-A in the fructose-induced metastasis of breast cancer. Upon fructose stimulation, KHK-A is transported to the nucleus by the importers LRRC59 and KPNB1, and there phosphorylates YWHAH at S25. The phospho-YWHAH downregulates CDH1 by recruiting SLUG to the *CDH1* promoter, thereby facilitating cell migration. In conclusion, fructose cues KHK-A to start a cell movement-promoting job. The signaling pathway for fructose-induced metastasis is summarized in Figure 52.

The KHK-C-driven fructose metabolism has been intensively

investigated as a pathologic pathway that aggravates metabolic disorders with excessive intake of fructose[2, 3, 4]. The harmful effect of the fructose metabolism has been also examined in cancer progression[9]. On the contrary, KHK-A is known to make a minor contribution to fructose-mediated metabolic disorders. Interestinly, a recent report suggested a negative function of KHK-A in fructose-medicated metabolic disorders[19]. The KHK-A knock-out aggravated the metabolic profile in AldoB knock-out mice, suggesting that KHK-A plays a protective role in the fructose-mediated metabolic disorders. Yet, the mechanism underlying such a function of KHK-A has not been understood. Given two previous reports[22, 36] and the data in this project, KHK-A might be a protein kinase responsible for cell growth, stress response, and motility. Therefore, it is speculated that KHK-A fine-tunes the fructose-driven metabolic reprograming and this function is related with the protein kinase activity of KHK-A.

Although KHK-C and KHK-A are very similar in terms of molecular structures, they phosphorylate distinct substrates: a small metabolite (fructose) and a polypeptide (YWHAH), respectively. The role of KHK-A as a protein kinase is consistent with a previous report showing that KHK-A phosphorylates PRPS1. KHK-A phosphorylates PRPS1 at Thr225 in the cytoplasm and activates it, which stimulates *de novo* nucleic acid synthesis through the pentose phosphate pathway; by so doing, it promotes hepatoma formation[22]. Taken together, the data indicate that KHK-A seems to be intrinsically a Ser/Thr

protein kinase rather than a fructose kinase. Then, is there any conserved domain targeted by KHK-A? Comparing the amino acid sequences around the phosphorylated Ser/Thr residues, the sequence 'DDMA' commonly precedes the phosphorylated residues in YWHAH and PRPS1. Using molecular dynamics analysis, I suggested that two Ds in the conserved motif play a key role in the substrate binding to KHK-A, which was also experimentally supported. The DDMA motif may be a landmark for identifying new protein substrates targeted by KHK-A and warrants further investigation.

LRRC59 was originally considered a ribosome receptor located at the endoplasmic reticulum, but its biological functions were not fully understood. Rather than a ribosomal receptor, LRRC59 is now considered a nuclear translocator for the growth factor FGF1 endocytosed by cells, which occurs in concert with KPNB1[35]. I found that the nuclear translocation of KHK-A is fructose-dependently driven by the LRRC59-KPNB1 complex. In this process, fructose plays an essential role in forming the trimeric complex of KHK-A, LRRC59, and KPNB1. The precise role of fructose in this interaction remains an open question. It is speculated that fructose may change the conformation of KHK-A to a structure favorable to interaction with LRRC59 and KPNB1.

The YWHA (or 14-3-3) family is composed of seven members (β, γ, ε, σ, ζ, τ, and η) and is widely expressed in all eukaryotic cells. The family members are phosphorylated by their upstream kinases and then bind to the phospho-serine/threonine motifs of their downstream effectors. Therefore, they

are regarded as the adaptors that mediate the protein kinase signaling pathways. As part of apoptosis, c-Jun N-terminal kinase (JNK) phosphorylates 14-3-3ζ and β at Ser186 or 14-3-3σ at Ser184. This phosphorylation dissociates the 14-3-3 proteins from BAX, and the free BAX then enters the mitochondrion to induce apoptosis by releasing cytochrome c [42]. Under GM-CSF stimulation, Src kinase phosphorylates 14-3-3ζ at Tyr179, and the phospho-14-3-3ζ activates phosphoinositide 3-kinase (PI3K) to increase the survival potential[43]. Aside from the aforementioned functions, the 14-3-3 proteins are believed to be involved in diverse cellular processes. In this work, I identified a phosphorylation site (Ser25) in 14-3-3η (YWHAH). Surprisingly, the upstream kinase for 14-3-3η is a metabolic enzyme, KHK-A, and the downstream effector of 14-3-3η is the transcription repressor SLUG. Among many functions, 14-3-3 proteins may act as transcriptional adaptors to modulate gene expression.

Within the YWHA family, five members have been reported to interact with the RXXXpS/TXP motifs in the SNAG and ZF (zinc finger) domains of SNAIL, and recruit SNAIL to the E-box element in the *CDH1* promoter[41]. SLUG, which is alternatively named SNAIL2, also has two putative 14-3-3 binding motifs, which are highly homologous with the RXXXpS/TXP motifs. As expected, I found that SLUG interacts with YWHAH. Interestingly, it is only after being phosphorylated at Ser25 by KHK-A that YWHAH acquires binding affinity to SLUG. As a consequence, YWHAH guides SLUG to gain access to the *CDH1* promoter. By contrast, SNAIL and YWHAH were found to be

constantly associated regardless of fructose stimulation or the phosphorylation of YWHAH. Given these results, it is suggested that SNAIL controls the basal level of CDH1, but SLUG takes part in the dynamic regulation of CDH1 expression in response to fructose stimulation. The molecular dynamics must be further investigated to elucidate how S25 phosphorylation permits YWHAH to interact with SLUG.

In conclusion, I observed that KHK-A promotes breast cancer metastasis upon fructose stimulation and also demonstrated a signaling pathway responsible for fructose-induced metastasis. This work provides a reasonable mechanism supporting the clinical evidence for fructose-induced cancer aggravation. Based on the results, high intake of fructose should be restricted in cancer patients to reduce the risk of metastasis. From a therapeutic perspective, the KHK-A signaling pathway could be a potential target to prevent cancer metastasis.

REFERENCES

1. Hess J, Latulippe ME, Ayoob K, Slavin J. The confusing world of dietary sugars: definitions, intakes, food sources and international dietary recommendations. *Food Funct* **3**, 477-486 (2012).

2. Bantle JP. Dietary fructose and metabolic syndrome and diabetes. *J Nutr* **139**, 1263S-1268S (2009).

3. Basciano H, Federico L, Adeli K. Fructose, insulin resistance, and metabolic dyslipidemia. *Nutr Metab (Lond)* **2**, 5 (2005).

4. Jegatheesan P, De Bandt JP. Fructose and NAFLD: The Multifaceted Aspects of Fructose Metabolism. *Nutrients* **9**, (2017).

5. Inoue-Choi M, Robien K, Mariani A, Cerhan JR, Anderson KE. Sugar-sweetened beverage intake and the risk of type I and type II endometrial cancer among postmenopausal women. *Cancer Epidemiol Biomarkers Prev* **22**, 2384-2394 (2013).

6. Chandran U, *et al.* Intake of energy-dense foods, fast foods, sugary drinks, and breast cancer risk in African American and European American women. *Nutr Cancer* **66**, 1187-1199 (2014).

7. Tasevska N, *et al.* Sugars in diet and risk of cancer in the NIH-AARP Diet and Health Study. *Int J Cancer* **130**, 159-169 (2012).

8. Michaud DS, Fuchs CS, Liu S, Willett WC, Colditz GA, Giovannucci E. Dietary glycemic load, carbohydrate, sugar, and colorectal cancer risk in men and women. *Cancer Epidemiol Biomarkers Prev* **14**, 138-147 (2005).

9. Bu P, *et al.* Aldolase B-Mediated Fructose Metabolism Drives Metabolic Reprogramming of Colon Cancer Liver Metastasis. *Cell Metab* **27**, 1249-1262 e1244 (2018).

10. Nomura K, Yamanouchi T. The role of fructose-enriched diets in mechanisms of nonalcoholic fatty liver disease. *J Nutr Biochem* **23**, 203-208 (2012).

11. Softic S, Cohen DE, Kahn CR. Role of Dietary Fructose and Hepatic De Novo Lipogenesis in Fatty Liver Disease. *Dig Dis Sci* **61**, 1282-1293 (2016).

12. Liu H, Huang D, McArthur DL, Boros LG, Nissen N, Heaney AP. Fructose induces transketolase flux to promote pancreatic cancer growth. *Cancer Res* **70**, 6368-6376 (2010).

13. Fan X, Liu H, Liu M, Wang Y, Qiu L, Cui Y. Increased utilization of fructose has a positive effect on the development of breast cancer. *PeerJ* **5**, e3804 (2017).

14. Gao W, Li N, Li Z, Xu J, Su C. Ketohexokinase is involved in fructose utilization and promotes tumor progression in glioma. *Biochem Biophys Res Commun* **503**, 1298-1306 (2018).

15. Jiang Y, *et al.* A Sucrose-Enriched Diet Promotes Tumorigenesis in Mammary Gland in Part through the 12-Lipoxygenase Pathway. *Cancer Res* **76**, 24-29 (2016).

16. Monzavi-Karbassi B, *et al.* Fructose as a carbon source induces an aggressive phenotype in MDA-MB-468 breast tumor cells. *Int J Oncol* **37**, 615-622 (2010).

17. Trinh CH, Asipu A, Bonthron DT, Phillips SE. Structures of alternatively spliced isoforms of human ketohexokinase. *Acta Crystallogr D Biol Crystallogr* **65**, 201-211 (2009).

18. Ishimoto T, *et al.* Opposing effects of fructokinase C and A isoforms on fructose-induced metabolic syndrome in mice. *Proc Natl Acad Sci U S A* **109**, 4320-4325 (2012).

19. Lanaspa MA, *et al.* Ketohexokinase C blockade ameliorates fructose-induced metabolic dysfunction in fructose-sensitive mice. *J Clin Invest* **128**, 2226-2238 (2018).

20. Asipu A, Hayward BE, O'Reilly J, Bonthron DT. Properties of normal and mutant recombinant human ketohexokinases and implications for the pathogenesis of essential fructosuria. *Diabetes* **52**, 2426-2432 (2003).

21. Hayward BE, Bonthron DT. Structure and alternative splicing of the ketohexokinase gene. *Eur J Biochem* **257**, 85-91 (1998).

22. Li X, *et al.* A splicing switch from ketohexokinase-C to ketohexokinase-A drives hepatocellular carcinoma formation. *Nat Cell Biol* **18**, 561-571 (2016).

23. Zamora-Leon SP, *et al.* Expression of the fructose transporter GLUT5 in human breast cancer. *Proc Natl Acad Sci U S A* **93**, 1847-1852 (1996).

24. Chun YS, *et al.* Zinc induces the accumulation of hypoxia-inducible factor (HIF)-1alpha, but inhibits the nuclear translocation of HIF-1beta, causing HIF-1 inactivation. *Biochem Biophys Res Commun* **268**, 652-656 (2000).

25. Yang X, *et al.* Structural basis for protein-protein interactions in the 14-3-3 protein family. *Proc Natl Acad Sci U S A* **103**, 17237-17242 (2006).

26. Ritchie DW, Kemp GJL. Protein docking using spherical polar Fourier correlations. *Proteins* **39**, 178-194 (2000).

27. Kabsch W, Sander C. Dictionary of Protein Secondary Structure - Pattern-Recognition of Hydrogen-Bonded and Geometrical Features. *Biopolymers* **22**, 2577-2637 (1983).

28. Abraham MJ, *et al.* GROMACS: High performance molecular simulations through multi-level parallelism from laptops to supercomputers. *Softwarex* **1-2**, 19-25 (2015).

29. Huang J, MacKerell AD, Jr. CHARMM36 all-atom additive protein force field: validation based on comparison to NMR data. *J Comput Chem* **34**, 2135-2145 (2013).

30. Bussi G, Donadio D, Parrinello M. Canonical sampling through velocity rescaling. *J Chem Phys* **126**, (2007).

31. Parrinello M, Rahman A. Polymorphic Transitions in Single-Crystals - a New Molecular-Dynamics Method. *J Appl Phys* **52**, 7182-7190 (1981).

32. Kumar S, Bouzida D, Swendsen RH, Kollman PA, Rosenberg JM. The Weighted Histogram Analysis Method for Free-Energy Calculations on Biomolecules .1. The Method. *Journal of Computational Chemistry* **13**, 1011-1021 (1992).

33. Han J, *et al.* Glucose promotes cell proliferation, glucose uptake and invasion in endometrial cancer cells via AMPK/mTOR/S6 and MAPK signaling. *Gynecol Oncol* **138**, 668-675 (2015).

34. Sun S, Sun Y, Rong X, Bai L. High glucose promotes breast cancer proliferation and metastasis by impairing angiotensinogen expression. *Biosci Rep* **39**, (2019).

35. Zhen Y, *et al.* Nuclear import of exogenous FGF1 requires the ER-protein LRRC59 and the importins Kpnalpha1 and Kpnbeta1. *Traffic* **13**, 650-664 (2012).

36. Xu D, *et al.* The protein kinase activity of fructokinase A specifies the antioxidant responses of tumor cells by phosphorylating p62. *Sci Adv* **5**, eaav4570 (2019).

37. Lemkul JA, Bevan DR. Assessing the Stability of Alzheimer's Amyloid Protofibrils Using Molecular Dynamics. *J Phys Chem B* **114**, 1652-1660 (2010).

38. Patey GN, Valleau JP. Free-Energy of Spheres with Dipoles - Monte-Carlo with Multistage Sampling. *Chem Phys Lett* **21**, 297-300 (1973).

39. Valiev M, Yang J, Adams JA, Taylor SS, Weare JH. Phosphorylation reaction in cAPK protein kinase-free energy quantum mechanical/molecular mechanics simulations. *J Phys Chem B* **111**, 13455-13464 (2007).

40. Zhou B, Wong CF. A computational study of the phosphorylation mechanism of the insulin receptor tyrosine kinase. *J Phys Chem A* **113**, 5144-5150 (2009).

41. Hou Z, *et al.* 14-3-3 binding sites in the snail protein are essential for snail-mediated transcriptional repression and epithelial-mesenchymal differentiation. *Cancer Res* **70**, 4385-4393 (2010).

42. Tsuruta F, *et al.* JNK promotes Bax translocation to mitochondria through phosphorylation of 14-3-3 proteins. *EMBO J* **23**, 1889-1899 (2004).

43. Barry EF, *et al.* 14-3-3:Shc scaffolds integrate phosphoserine and phosphotyrosine signaling to regulate phosphatidylinositol 3-kinase activation and cell survival. *J Biol Chem* **284**, 12080-12090 (2009).

44. Broad Institute of MIT and Harvard. *Broad Institute TCGA Genome Data Analysis Center*, Firehose stddata_2016_01_28 run. doi:10.7908/C11G0KM9 (2016).

국문 초록

현대 사회에서 식습관의 서구화로 인하여 과당의 섭취가 늘어났으며 그에 따라 비만, 당뇨, 지방간을 악화시킨다고 보고되어 있다. 이 외에도 과당의 섭취는 유방, 소장, 및 대장암을 포함한 다양한 암의 발병과 전이에 관련이 있다는 것이 역학적으로 보고되었다.

암 대사는 다량의 포도당을 소비하도록 Reprogramming이 일어나며, 포도당이 고갈되어 있는 암세포는 과당을 대체에너지원으로 이용한다. 췌장암과 대장암에서 과당 대사 경로의 활성화로 인해 암의 증식과 전이가 촉진된다는 것이 보고되어 있지만, 이 현상을 뒷받침하는 기전은 보고된 바가 없다.

Ketohexokinase는 fructose를 fructose-1-phosphate로 전환하는 효소이다. KHK는 alternative splicing을 통해 조직 특이적으로 KHK-A와 KHK-C를 발현한다. 과당의 F-1-P 로의 분해는 간, 신장에서 KHK-C에 의해 일어나며, 반면 KHK-A는 과당에 대한 효소 활성도가 매우 낮아 과당의 대사에 기여하지 않는 것으로 여겨졌다. 그럼에도 불구하고 KHK-A는 대부분의 조직에서 발현하기 때문에 에너지 대사 이외의 생물학적 기능을 가지고 있다는 의견이 제기되었다.

유방암 세포는 정상 유방세포 대비, 과당 수용체인 GLUT5의 발현양이 높고, 과당 처리 시, 세포의 형태가 mesenchymal 하게 변한다는 것이 알려져 있다. 하지만 그 분자 메커니즘에 대해서는 알려진 바가 없다.

먼저 유방암 세포주를 포함한 암세포주에 과당 처리 후 이동능의 증가를 확인하였고, 간, 신장 유래 암세포를 제외하고는 모두 KHK-A가 우세하게 발현하는 것을 확인하였다. 따라서 유방암 세포주에서 Fructose에 의한 암 전이과정에 KHK-A가 관여되어 있을 것이라는 가설을 세웠다. 마우스 xenograft model을 이용하여 과당 공급 시 KHK-A를 발현하는 유방암 세포주가 폐로 전이됨을 확인하였고, 유방암 세포주에서 과당 존재 시, KHK-A가 공통적으로 결합하고 있는 단백질을 선정하였다. LRRC59는 과당이 존재할 때, KPNB1과 결합하여 KHK-A를 세포질에서 세포핵으로 이동시키며, 핵으로 들어간 KHK-A는 YWHAH (14-3-3 eta)의 25번 Serine잔기를 인산화 시키는 것을 확인하였다. 인산화된 YWHAH는 Slug와 결합하고 *CDH1*의 전사를 억제함으로써 유방암 세포주의 상피간엽이행을 유도하여, 결과적으로는 암 전이에 기여하는 것을 확인하였다. YWHAH의 인산화는 유방암 xenograft 모델에서 폐를 포함하여 뇌, 비장, 간 등 다양한 주요 장기로의 전이를 촉진하였다. 유방암 환자 조직에서 nuclear KHK-A와

YWHAH-pSer25의 발현이 서로 양의 상관관계를 보이며, 유방암 예후와 연관되어 있음을 보여줌으로써 상기 기전을 확인하였다.

그런데 왜 KHK-A는 과당은 인산화 시키지 못하는 것일까? 본 연구에서는 2016년도에 KHK-A의 기질로 보고된 PRPS1과의 비교연구를 통하여, KHK-A는 아미노산 DDMA로 이루어진 모티프를 인식하여 기질 단백질과 결합, 인산화 시킴을 확인하였다. 따라서 위의 물음에 대하여 KHK-A는 과당 인산화효소가 아닌 Serine/Threonine 인산화 효소이기 때문이다. 라는 해답을 제시하였다.

이러한 연구 결과는 KHK-A가 과당에 의한 암 전이 과정에서 KHK-A가 결정적인 스위치 조절자라는 새로운 기전을 규명하였으며, 나아가 KHK-A-YWHAH-CDH1 기전이 과당에 의한 암의 전이를 억제하는 새로운 치료 표적이 될 가능성을 제시하였다. 또한 우리가 간과하기 쉬운 식습관의 중요성을 다시금 일깨우는 메시지를 제공하고 있다. 그 메시지는 암환자가 영양보충을 하고자 과당을 많이 섭취하는 것은 좋지 못한 결정이라는 것이다.

주요어: 유방암, 전이, 과당, KHK-A, serine/threonine 인산화 효소.
학번: 2014-25057